Simulation study of packing of fine particles under electric fields

Author:
Yang, Siyuan Eric

Publication Date:
2015

DOI:
https://doi.org/10.26190/unsworks/17317

Simulation Study of Packing of Fine Particles under Electric Fields

---

YANG, Siyuan Eric

B.Sc. Hons. (The University of New South Wales, 2010)

A thesis in fulfilment of the requirements for the degree of

Doctor of Philosophy

at the

School of Materials Science & Engineering

of the

University of New South Wales

Sydney, Australia

ABSTRACT

Electrostatic precipitation processes have been widely applied to remove particulate matter from flue gases in coal-fired power stations. A high negative voltage is usually applied to a discharge electrode so that the gases are ionised in such processes. When the suspended particles in flue gases enter the ionised space, they are electrically charged and deposited on collection walls to form a layer of particle packing. Essentially, the underlying working principle of electrostatic precipitation processes is the packing of fine particles under electric fields. Despite the possibility of achieving high collection efficiencies of the precipitation processes through careful tuning of the electrical and aerodynamic conditions, improvements on the removal of fine particulate matter, such as PM2.5 have not been achieved. Understanding the formation process of particle packing under electric fields is the key to improve the collection efficiency of fine particulate matter. Yet, it is mostly impossible to carry out a study on packings of fine particles through practical experiments.

In this thesis, we have developed a numerical model based on the discrete element method to simulate packings of fine particles under various electric fields. Both the formed packings under uniform and non-uniform electric fields are comprehensively examined. For the packings under uniform electric fields, the packing structures are characterised in terms of the packing fraction, coordination number, radial distribution function, and Voronoi tessellations. Our results indicate that the particle diameter and electric field are the two important parameters that determine the structure of the formed packings under electric fields. Such observations can be explained by the competition between the electric-field-induced electrostatic interactions and the interparticle van der Waals interactions during the formation of stable packings.

For the packings under non-uniform electric fields, special emphasis is given to the elliptical-shaped packing structural profiles commonly observed in electrostatic precipitation processes. The results have demonstrated that non-uniform packing structures are formed as a result of the imposed non-uniform electric fields. Despite the non-uniformity of the overall structural profile, the local packing structures are correlated to the local electric fields in terms of packing fraction and coordination

number. These findings may lead to better controls of the formed packings under various electric fields.

In addition, a novel numerical method to evaluate electrical transport in the formed packings under electric fields is presented. Both the electrical potential and electric current on each and every particle in a packing are numerically solved to obtain the effective electrical conductivity of the packing. Here, the focus is given to the contacts between particles. Our results have shown that the three variables, the material properties of particles, the contact area between particles and packing structures all have determining effects on the effective conductivity. Furthermore, analyses on the electric current network and contact force network have revealed that the electric current flow is significantly influenced by the contact force distribution in a packing.

Lastly, two mathematical models, that are applicable to industrial electrostatic precipitation processes, have been developed to predict the effective conductivity of the formed packings under electric fields. Conventional models predicting the effective conductivity require the use of the structural parameters of packings, such as the packing fraction, coordination number and contact diameter. However, such information is difficult to obtain in industrial applications. In contrast, based on the previously established relations, we have modelled the effective conductivity of packings using only the particle diameter, electric field and packing depth, which are all controllable parameters. Hence, the desirable electrical transport properties of the formed packings under electric fields can be achieved through changing the controllable parameters. Our findings may lead to better design and controls of electrostatic precipitation processes.

ACKNOWLEDGEMENT

I am greatly indebted my supervisor Prof. Aibing Yu, who inspires and teaches me to always give of my best in order to realise my full potential. Without his kind guidance and encouragement I would have unable to complete this project. I am also grateful to my co-supervisor Dr. Kejun Dong for his dedication and support throughout my studies.

I would like to express my appreciation to Dr. Ruiping Zou and Dr. Rohana Chandratilleke for their patient assistance in editing and proofing this manuscript. Dr. Baoyu Guo deserves special mention for countless insightful discussions. I also wish to thank Dr. Albert Yuen at Fujian Longking Co. Ltd. for sharing his perceptive field experience that resulted in two filed patents.

I wish to thank A. Prof. Runyu Yang, Dr. Zongyan Zou, Dr. Jeffrey Yue, Dr. Tomo Shiozawa, Dr. Komiyama Keisuke, Dr. Amir Esfandiary and all the other members of Laboratory for Simulation and Modelling of Particulate Systems.

I would also like to acknowledge Australian Research Council and Fujian Longking Co. Ltd. for their financial support for this APA-Industry project. Additional research support was provided by the University of New South Wales.

Lastly, I am always grateful to my families and friends for their endless love for me.

Contents

LIST OF FIGURES

LIST OF TABLES

LIST OF ACHIEVEMENTS

Journals

S. Yang, K. Dong, R. Zou, A. Yu and J. Guo, "Packing of fine particles in an electrical field", *Granular Matter*, vol. 15, pp 467-476 (2013)

B. Guo, S. Yang, X. Mao, K. Dong, A. Yu and J. Guo, "Toward the development of an integrated multiscale model for electrostatic precipitation", *Industrial & Engineering Chemistry Research*, vol. 52, pp 11282-11293 (2014)

S. Yang, K. Dong, A. Yu and J. Guo, "Numerical study of the packing of fine particles under uniform electric fields", *to be submitted* (2014)

S. Yang, A. Yu and J. Guo, "Evaluation of the effective electrical conductivity of packings under electric fields", *to be submitted* (2014)

S. Yang, A. Yu and J. Guo, "Modelling of the effective electrical conductivity of packings under electric fields", *to be submitted* (2014)

Conferences

S. Yang, K. Dong and A. Yu, "Discrete element simulation of cake formation in electrostatic precipitation processes", *22nd International Symposium on Chemical Reaction Engineering, ISCRE 22*, Maastricht, The Netherlands, 2-5 September (2012)

S. Yang, K. Dong, R. Zou and A. Yu, "Random packing of charged particles in non-uniform electric fields", *Powders and Grains 2013*, Sydney, Australia, 8-12 July (2013)

Patents

B. Guo, S. Yang, K. Dong, A. Yu, J. Guo and L. Li, "ESP system simulation methods", publication number: CN103218486A, application number: CN201310118012, filing data: 7 April 2013

J. Guo, S. Yang, K. Dong, A. Yu, Y. Su, X. Ye and L. Li, "ESP dust deposition and cake generation discrete element test methods", in application, 2014

CHAPTER 1. INTRODUCTION

1.1. Electrostatic precipitation

Industrialisation in developing countries has prompted a rapid expansion of power industries since the late 20th century. For instance, the total electricity production in China has almost tripled over the last decade [1]. In contrast to the increasing use of renewable energy in developed countries, power generations in developing countries are still largely dependent on coal as a major energy source due to economic reasons. Consequently, the air pollution associated with burning coal is a serious problem. High levels of air pollution in Beijing and Shanghai are illustrated in Figure 1.1 [2, 3]. The severe pollution not only is putting pressure on the global and local environment but also threatens human health [3-7]. Regarding to the health impacts, recent study has demonstrated that fine particulates, such as PM2.5, increases the chance that people will suffer heart attacks, not to mention, negative impacts on lungs. Hence, proper management of the emission of particulate matter is of great significance.

Figure 1.1: Polluted air in major cities in China (a) Beijing (b) Shanghai.

Electrostatic precipitation process is one of the most frequently applied methods to capture particulate matter in power industries. In this process, the fine particles released from burning coal are electrically charged and collected so that the cleaned flue gases will be released into the atmosphere (see Figure 1.2). There are several factors influencing the efficiency of the precipitation process, such as electric fields, gas flows, particle properties etc. While the optimisation of the electric fields and gas flows has been intensively studied over the last few decades, the effect of particles is usually neglected because of the difficulties in experimental examinations of the particles [8]. However, the basic problem in the design of electrostatic precipitation processes in recent years has been the need to collect fine particles, especially PM2.5. An accurate knowledge of the behaviour of particles is of fundamental importance to improve the collection of fine particles.

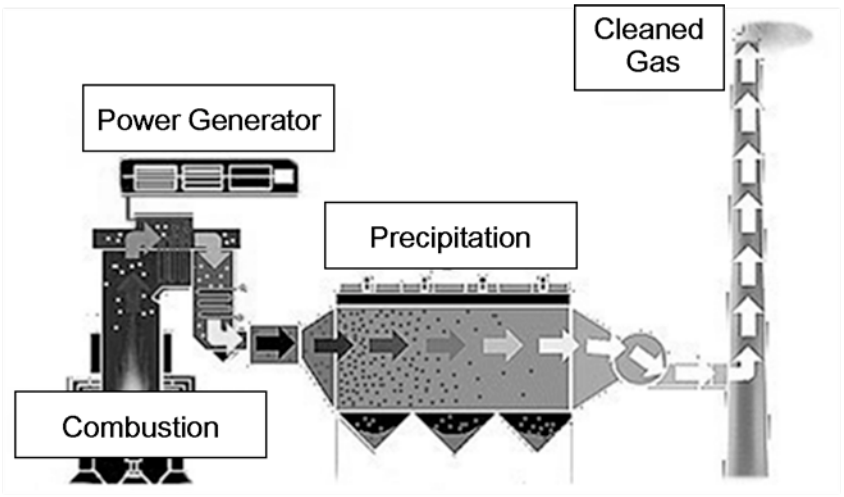

Figure 1.2: Electrostatic precipitation process in power plants [9].

The essential components of electrostatic precipitation processes are outlined in Figure 1.3. When high voltage is applied to a discharge electrode, the ionised gas molecules, usually negative ions, are produced by corona discharge. When fine particles enter the ionised gas space, they are electrically charged by the negative ions. Under the influence of electrostatic interactions, the charged particles are deposited to form a layer of particle packing on a collection wall. In essence, the underlying physical principle of this precipitation process is the formation of the particle packing under electric field, which is a dynamics process controlled by the imposed electric and gas flow. In this thesis, as the

simulated zone is close to the collection plate where the gas flow is weak, the effect of gas flow is not considered in the model. Nevertheless, the key nderlying physical principle of this precipitation process is the formation of particle packing under electric fields, and therefore, more advantage can be made from such a study of particle packing.

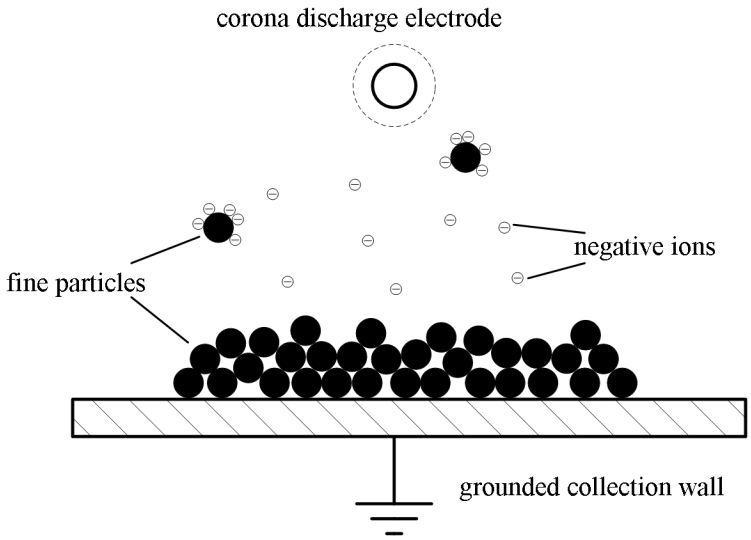

Figure 1.3: The essential components of electrostatic precipitation processes.

1.2. Particle packing

Particle packing is frequently encountered in nature, in industry and in everyday life. Some examples of the particle packing are: sands, minerals, soils, pharmaceuticals, ceramics, nuclear fuels, cereals, coffee beans, etc (see Figure 1.1). Most packings are random as far as one can see, and subsequently, the physical properties are diffcult to determine. The study of particle packing is an important research subject in many areas of science and engineering.

Early studies of particle packing focus on the problems of achieving the densest possible structure. One of such problems is the Kepler conjecture which states the highest packing fraction possible for a packing of uniform spherical particles is $\pi/3\sqrt{2}$. Another example is finding the maximum possible number of uniform spherical particles can be packed around an equivalent particle. Gregory and Newton famously

reached different answers that are either 12 or 13 touching particles are possible. Now, we know that they are both correct. While it is possible to fit 13 touching particles, only 12 touching particles are achievable in a stable packing.

Figure 1.4: Random packings in nature, in industry and in our daily life.

Systematic studies of particle packing did not start until 1960s. In attempts to model amorphous systems, that are simple liquid and metallic glass, Bernal and Scott experimentally characterised the structure of packings in terms of packing fraction and coordination number [10, 11]. Two interesting states of particle packing were identified: random dense packing and random loose packing, which represent the packing fraction of the unconsolidated and consolidated packings respectively. More recently, numerical simulations have been increasingly applied in the studies of particle packing [12-14]. In particular, the use of numerical simulations, such as the discrete element method, has advanced our understanding of the packings found in a wide range of industrial applications, such as agricultural, chemical, pharmaceutical, mining, civil, oil and gas industries [15, 16].

In this thesis, we are interested in packings of fine particles under electric fields, which is essential to industrial electrostatic precipitation processes as mentioned earlier. In addition, solving this problem is beneficial to a range of other applications, such as

electrophotographic process, powder spray coating, electrofluidized bed, electric arc furnace, etc [17-20]. The aims of this thesis are:

1. To develop a numerical model based on the discrete element method to simulate packings of fine particles under various electric fields;
2. To investigate the structure of the formed packings under electric fields with special emphasis on the effect of electrostatic interactions;
3. To study the electrical transport properties, in particular, the effective electrical conductivity of the packings.

A better understanding of the structural and electrical properties of the formed packings under electric fields may lead to improvements on the design and operations of electrostatic precipitation processes.

1.3. Synopsis

This thesis is arranged into seven chapters:

Chapter 1 provides a brief introduction to the study of particle packing associated with electric fields highlighting its importance to industrial electrostatic precipitation processes.

In Chapter 2, a detailed review of the numerical simulations, structural characterisations and electrical transport analysis in the study of particle packing is presented. Particular importance is attached to the incorporation of electrostatic interactions in the discrete element method. Also, various experimental and numerical methods to characterise the structure of a packing are included. The chapter concludes with a discussion of the recent literature on the evaluation of effective electrical conductivity from a packing structure. It is our intention to provide a broad introduction to this research subject.

Chapter 3 presents the newly developed numerical model based on the discrete element method to simulate packings of fine particles under electric fields. The basic governing equations for a charged particle under an imposed electric field are discussed. As the

first attempt, the structure of the simulated packings is characterised in terms of packing fraction, coordination number, radial distribution function and Voronoi properties. The effects of particle diameter and electric field on the packing structure are comprehensively examined. Also, the importance of the electrostatic and van der Waals interactions is discussed in this chapter.

In Chapter 4, the formed packings under various non-uniform electric fields are considered. In particular, we focus on the elliptical-shaped packing structures, which are commonly observed in electrostatic precipitation processes. In general, the non-uniform packing structure is the result of the imposed non-uniform electric field. Analysis of the localised structure in packings has revealed that the packing fraction and coordination number are determined by the particle diameter and electric field in the localised regions. These observations are in good agreement with the previously established relations in literature.

Chapter 5 concentrates on finding the effective electrical conductivity of the formed packing structures under various electric fields. In these packings, the electric current is carried mostly through the interconnecting particles, therefore the continuum electrical equations do not apply at the interface between the particle and the interstitial gas. Here, the effective conductivity of the packings is numerically determined by solving for the electrical potential and electric current on each particle. Our results have demonstrated that the particle properties, contact area between particles and packing structure all have significant effect on the effective conductivity. In addition, comparisons are made between the contact force network and electric current network to highlight the importance of the exerting forces on particles to the electrical tranport properties of the resultant packings.

The object of Chapter 6 is to model the effective electrical conductivity of the formed packings under various electric fields. The previously established models in literature usually require microscopic characters of packing, such as coordination number and contact diameter. These characters are difficult to measure in practical experiments, and therefore, it is impossible to apply them to electrostatic electrostatic precipitation processes. In this chapter, we have firstly modelled the microscopic characters of the

formed packings using the easily controllable particle diameter, electric field and packing depth. Then, two newly proposed models predicting the effective electrical conductivity are presented. These models give better predictions for the effective conductivity comparing to the predictions by the previous model. Our findings could be applied to achieve the desirable effective electrical conductivity of a packing under various electric fields by adjusting the controllable parameters. This may lead to a better design and operations of electrostatic precipitation processes.

Finally, Chapter 7 summarizes the important findings of this thesis, and some suggestions of future research are also included.

References

[1] EIA, "EIA report on China," *U.S. Energy Information Administration,* 2014.

[2] L. Y. Guan, "Smog in China boost the development of new energy vehicles," *China Southern Daily,* 2014.

[3] J. Marshall, "PM 2.5," *Proceedings of the National Academy of Sciences,* vol. 110, p. 8756, 2013.

[4] R. A. Kerr, "Soot is warming the world even more than thought," *Science,* vol. 339, p. 382, January 25, 2013.

[5] M. Patience, "Beijing smog: when growth trumps life in China," *BBC Magazine,* January 27, 2013.

[6] J. Rockström, *et al.*, "A safe operating space for humanity," *Nature,* vol. 461, pp. 472-475, 2009.

[7] M. Cone, "Hearts and air pollution: 5 deadly air pollutants measured on 5 continents," *Scientific American,* February 15, 2012.

[8] H. J. White, *Industrial electrostatic precipitation*: Addison-Wesley Pub. Co., 1963.

[9] Neundorfer-Inc., "Introduction to Precipitators," *Electrostatic Precipitator Knowledge Base*.

[10] J. D. Bernal and J. Mason, "Co-ordination of random packed spheres," *Nature,* vol. 188, pp. 910-911, 1960.

[11] G. D. Scott, "Packing of equal spheres," *Nature,* vol. 188, pp. 908-909, 1960.

[12] J. L. Finney, "Random Packings and the Structure of Simple Liquids. I. The Geometry of Random Close Packing," *Proceedings of the Royal Society of London. A. Mathematical and Physical Sciences,* vol. 319, pp. 479-493, November 10, 1970 1970.

[13] L. Oger, et. al., "Voronoi tessellation of packings of spheres: topological correlation and statistics," *Philosophical Magazine B,* vol. 74, pp. 177-197, 1996.

[14] R. Y. Yang, R. P. Zou, and A. B. Yu, "Computer simulation of the packing of fine particles," *Physical Review E,* vol. 62, p. 3900, 2000.

[15] H. Zhu, et. al., "Discrete particle simulation of particulate systems: A review of major applications and findings," *Chemical Engineering Science,* vol. 63, pp. 5728-5770, 2008.

[16] H. P. Zhu, et. al., "Discrete particle simulation of particulate systems: Theoretical developments," *Chemical Engineering Science,* vol. 62, pp. 3378-3396, 2007.

[17] J. Q. Feng and D. A. Hays, "A finite-element analysis of the electrostatic force on a uniformly charged dielectric sphere resting on a dielectric-coated electrode in a detaching electric field," *Industry Applications, IEEE Transactions on,* vol. 34, pp. 84-91, 1998.

[18] M. Xiangbo and et al., "The characteristics of particle charging and deposition during powder coating processes with ultrafine powder," *Journal of Physics D: Applied Physics,* vol. 42, p. 065201, 2009.

[19] P. W. Dietz and J. R. Melcher, "Interparticle electrical forces in packed and fluidized-beds," *Industrial & Engineering Chemistry Fundamentals,* vol. 17, pp. 28-32, 1978.

[20] P. Eidem, et. al., "Effect of Contact Resistance on Bulk Resistivity of Dry Coke Beds," *Metallurgical and Materials Transactions B,* vol. 40, pp. 388-396, 2009.

CHAPTER 2. LITERATURE REVIEW

2.1. Introduction

Previous works on particle packing are reviewed comprehensively in this chapter. There are three main topics. First of all, the numerical simulations of particle packing are presented with emphasis on the electrostatic interactions. Secondly, various methods to characterise a packing structure are summarised. The structural characterisation of particle packing is of paramount importance to its transport properties. Lastly, the evaluation of the effective electrical conductivity of packings is discussed in details.

2.2. Numerical Modelling of Particle Packing

2.2.1. Overview

In recent decades, numerical simulations have become more and more popular in the studies of particle packing largely due to general availabilities of computers and advancements in the computational technologies. In literature, the numerical methods to simulate particle packing can be divided into four categories: collective rearrangement models, sequential deposition models, soft sphere discrete element methods and event driven granular dynamics [1, 2].

The collective rearrangement models start with random generation of particles with overlaps. Then, the particles follow certain algorithm to rearrange themselves to minimise the overlaps. For instance, two overlapping particles are allowed to move away from each other, or the overlapping particles are allowed to shrink or expand to eliminate the overlaps or gaps respectively. The simulation finishes with a stable packing with no overlap between particles and a maximum possible packing fraction.

In the sequential deposition models, particle packing is simulated as a dynamic process, and certain algorithm has to be defined to simulate the settling of particles. For example, gravitational potentials are defined for a packing under gravity. Randomly generated particles are always travelling towards the lowest potential level. Consequently, any

displacement and rotation that lowers the potential of a particle is allowed. Finally, the formed packing has a theoretically minimum potential sum.

In general, the collective rearrangement and sequential deposition models are considered as geometric models. The level of restructuring of a simulated packing is essential, because it determines the compactness of the resultant packing structure. On the other hand, the Newton's laws of motion are solved in the soft sphere discrete element methods and event driven granular dynamics.

In the soft sphere discrete element methods, particles are randomly generated and allowed to move according to the pre-defined physical forces, such as contact force, gravitational force etc. When a collision between two particles occurs, an overlap is allowed between the particles. The dissipative nature of the collision is determined by the overlaps as well as the particle properties. Finally, a stable packing is formed when the velocity of all particles is minimised.

In the event driven granular dynamics, particles are rigid and move undisturbed with its own momentum and energy before an event occurs. An event can be a particle collides with another particle or with a wall. When a collision occurs, there is no overlap between particles so that the interparticle contact is assumed to be instantaneous. This is fundamentally different from the discrete element methods. Momentum and energy dissipations are introduced through arbitrary coefficients of restitution. The simulation finishes when the minimum energy is achieved.

Overall, each simulation method has its own merits and shortcomings. The aim of this thesis is to simulate packings of fine particles under electric fields relating to the industrial electrostatic precipitation processes. The discrete element method is preferred over the geometric models, because the real forces are considered. The event driven granular dynamics focus on the kinetics of particles, for instance, shaking particles in a box [3]. However, the effect of interparticle forces, e.g., van der Waals interactions and electrostatic interactions, are difficult to incorporate in these models. Thus, we choose to apply the soft sphere discrete element method in the study of particle packing under electric fields. This simulation method is discussed in details in the following sections.

2.2.2. Discrete element method

In discrete element methods, the translational and rotational motions of particles are calculated according to the classical Newton's law of motion [4]:

$$m_i \frac{d\mathbf{v}_i}{dt} = \mathbf{F}_i \tag{2.1}$$

and

$$I_i \frac{d\boldsymbol{\omega}_i}{dt} = \mathbf{T}_i \tag{2.2}$$

where m_i is the mass, $\mathbf{v}_i$ is the translational velocity, t is the time, I_i is the moment of inertia, $\boldsymbol{\omega}_i$ is the angular velocity, $\mathbf{F}_i$ is the total force and $\mathbf{T}_i$ is the total torque. The forces and torques acting on particles depend on the specific simulated systems. For the formed packings under electric fields, we consider the contact forces, van der Waals interactions, electrostatic interactions and contact torques amongst particles. In the ensuing sections, the details of these forces and the subsequent incorporation in the discrete element method are summerized.

2.2.3. Contact forces

In the discrete element method, the most fundamental forces between any two contacting particles are mechanical contact forces. The commonly used model in the calculation of the contact forces is the spring-dashpot-slider model as depicted in Figure 2.1, which demonstrates the normal and tangential contact force which are perpendicular to and parallel to the contact surface respectively. The springs and dashpots accordingly represent the elastic and dissipative nature of the contact forces.

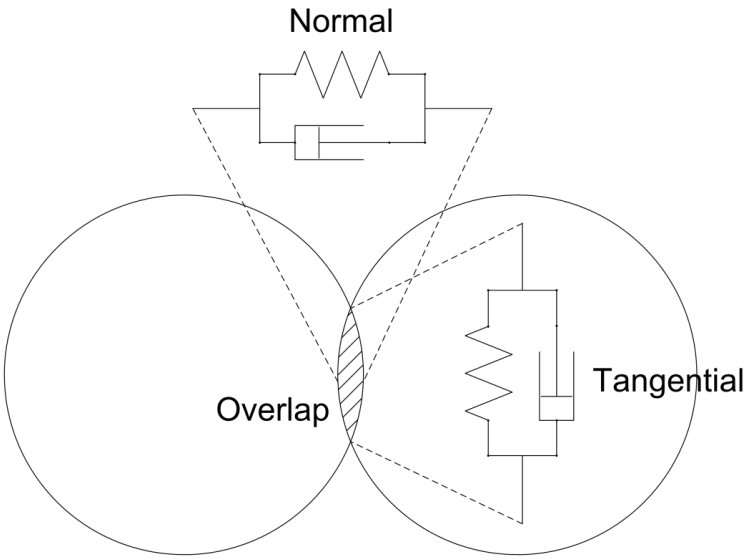

Figure 2.1: The schematic diagram of the spring-dashpot-slider model of the mechanical contact force between two contacting particles.

In the calculation of the contact forces, the nonlinear Hertz model is considered. When two particles collide, the normal contact force depends on the overlap between particles, which is given by [5, 6],

$$\mathbf{F}_{ij}^{n} = \left[\frac{2}{3}\frac{Y}{(1-\nu)^2}\sqrt{R_{eff}}\,\xi_n^{\frac{3}{2}} - \gamma_n \frac{Y}{(1-\nu)^2}\sqrt{R_{eff}}\sqrt{\xi_n}\left(\mathbf{v}_{ij}\cdot\hat{\mathbf{n}}_{ij}\right)\right]\hat{\mathbf{n}}_{ij} \tag{2.3}$$

where Y is the Young's modulus, ν is the Poisson's ratio, ξ_n is the overlap between particles, γ_n is the normal damping coefficient, $\mathbf{v}_{ij}$ is the difference in the particle velocities, $\mathbf{n}_{ij}$ is the unit vector in the direction between particles and R_{eff} is the effective radius, which is given by,

$$R_{eff} = \frac{R_i R_j}{R_i + R_j} \tag{2.4}$$

It is worth noting that the first term in Eq.2.3 accounts for the Hertzian elastic component of the normal contact force, while the second term represents the dissipative component. Also, all variables are dependent on the materials properties of particles and

the dynamics of a specific packing process, but the normal damping coefficient, which is always determined by the normal coefficient of restitution [7].

There is also a tangential contact force, which is given by [8, 9],

$$\mathbf{F}_{ij}^{s} = -\mathrm{sgn}(\xi_s)\mu\left|\mathbf{F}_{ij}^{n}\right|\left[1-\left(1-\frac{\min(\xi_s,\xi_{s,\max})}{\xi_{s,\max}}\right)^{\frac{3}{2}}\right] \tag{2.5}$$

where μ is the friction coefficient, ξ_s is the tangential displacement between particle. The maximum tangential displacement, $\xi_{s,\max}$, is the tangential displacement before gross sliding between particles occurs, which is,

$$\xi_{s,\max} = \mu\frac{2-\nu}{2(1-\nu)}\xi_n \tag{2.6}$$

Moreover, the tangential contact force is applied in the direction of the tangential displacement, and consequently, it takes the sign of ξ_s. Here, the first three terms in Eq.2.5 represent the Coulomb law of friction, while the other terms represent the dissipative nature of the tangential contact force. The choice of the friction coefficient is determined by the material property of particles.

2.2.4. van der Waals interactions

The van der Waals interactions are like the gravitational force acting between all particles. When two particles are in close contact with each other, the interparticle van der Waals interactions are significant especially for fine particles. In packings of coarse particles, the van der Waals interactions are sometimes neglected, because the magnitude of these interactions is much smaller than field forces, such as gravity. However, earlier study of the packing of fine particle has demonstrated that the van der Waals interactions dominate as the particle diameter decreases to less than about 100μm [10]. In this work, we shall include the van der Waals interactions.

on a nanoscale, the van der Waals interactions between two molecules are usually consisted of an attractive and a repulsive term. However, we are concerned about the van der Waals interactions between two macroscopic particles on a microscale. The so-called 'phenomenological' van der Waals interactions including only the attractive term are employed, and mathematically, these interactions are given by [11],

$$\mathbf{F}_{ij}^{vdw} = -\frac{H_a}{6} \times \frac{64 R_i^3 R_j^3 \left(h + R_i + R_j\right)}{\left(h^2 + 2R_i h + 2R_j h\right)^2 \left(h^2 + 2R_i h + 2R_j h + 4R_i R_j\right)^2} \hat{\mathbf{n}}_{ij} \qquad (2.7)$$

where H_a is the Hamaker's constant and h is the separating distance between particles. To avoid singular attraction at zero seperation, a minimum separation is set in the calculation of the van der Waals force. This treatment has been successfully applied in a range of studies dealing with fine particles [10, 12]. The same treatment is also applicable to the electrostatic interactions when the distance between two particles is very small. Nonetheless, the van der Waals interacitons are essential in packings of fine particles.

2.2.5. Electrostatic interactions

A review of electrostatic interactions experienced by the particles under electric fields is presented in this section. Fundamentals of the electrostatic interactions are comprehensively discussed. Emphasis is placed on the significance of these interactions to the formed packings under electric fields relating to electrostatic precipitation processes. The subsequent incorporation of these electrostatic interactions in the numerical simulations is also included.

It should be noted that the effect of electrically charged particles on the imposed electric field is weak, because the velocity of the charged particles is low comparing to that of the charged ions. As a result, the majority of the electric current between electrodes is contributed from the movement of the ions instead of that of the charged particles. Thus,

the effect of electrically charged particles on the imposed electric field is not considered in our simulations.

2.2.5.1. Electrical charging

A particle must be electrically charged to experience any electrostatic interaction under an imposed electric field. In classical physics, the electrical charging is essentially the process of transferring electrical charges so that the amount of positive and negative charges is no longer balanced. If there are excessive positive or negative charges on particle, then the particle is positively or negatively charged respectively.

There are various ways to electrically charge a particle. The suspended particles found in electrostatic precipitation processes are charged by attachments of the ionised gas molecules from corona discharges, typically the negative ions. There are two types of charging mechanisms for the corona discharge: ionic bombardment and ionic diffusion [13].

In the ionic bombardment, negative ions are driven by the imposed electric field. When suspended particles enter the ionised space, the ions attach to the particles. For instance, the electric field around an uncharged particle is depicted in Figure 2.2a. As the charging progresses, the attached ions on the particle interact with the electric field. As a result, the electric field around the particle is distorted (see Figure 2.2b). The rate of the ionic bombardment decreases until the saturation charge is reached, at which point the electric field completely bypasses the saturated particle. For a conductive particle, the saturation charge is given by [14, 15],

$$q_{\max} = ne = 3\mathbf{R}^2\mathbf{E} \tag{2.8}$$

where $\mathbf{E}$ is the applied electric field and $\mathbf{R}$ is the particle radius. For a dielectric particle, the saturation charge is corrected by the distortion induced by the unevenly attached ions, and that is:

$$q_{\max} = 4\pi\varepsilon_0 \left[2\left(\frac{k_p - 1}{k_p + 2} \right) + 1 \right] \mathbf{R}^2 \mathbf{E} \tag{2.9}$$

where k_p is the dielectric constant and ε_0 is the permittivity of space. Also, the complete charging process is expressed as:

$$q = q_{\max} \frac{t}{t + \tau} \tag{2.10}$$

where t is time in seconds, and τ is the charging time constant, that is given by,

$$\tau = \frac{1}{\pi N_0 e b} \tag{2.11}$$

where N_0 is the ion density, e is the electric charge and b is the ion mobility. We have estimated that the charging time for a typical particle in electrostatic precipitation processes is about 0.002 second using N_0=5x10^{8}ions/cm^3, b=660m^2/V·s and e=4.8x10^{-10}esu. In conventional electrostatic precipitation processes, the precipitation time is much greater than the charging time for a particle. Thus, it is acceptable to neglect the charging process, and the saturated charge is assumed. As seen in Eq.2.9, the saturation charge on a particle is related to the particle radius quadratically. This means the acquired amount of charge through the ionic bombardment sharply decreases with the particle radius. Hence, the changing of fine particles could be inefficient by the ionic bombardment, and the ionic diffusion shall be considered.

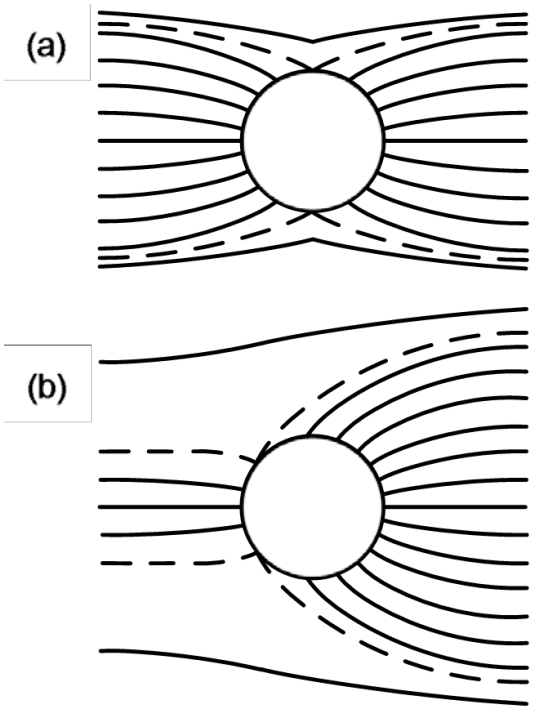

Figure 2.2: Electric field around (a) an uncharged and (b) a charged particle.

The dominant charging mechanism is the ionic diffusion for fine particles. According to laws of kinetic theory, the thermal motion of ions is always fuelled by the thermal energy. This means the ions are always diffusing through the ionised gases. When the collision between the ions and the suspended fine particles occurs, sometimes the ions will adhere to and electrically charge the particles. It should be noted that the ionic diffusion charging is continuous as long as the gas is ionized. Therefore, it is independent of the strength of the imposed electric field. Quantitatively, the charging rate can be derived from the time interval of ion-particle collisions,

$$q = \frac{4\pi\varepsilon_0 RkT_k}{e} \log\left(\frac{N_0 e^2 \bar{\mathbf{v}}_i R}{4\varepsilon_0 kT_k} t + 1\right) \tag{2.12}$$

where k is the Boltzmann constant, T_k is the temperature, and $\overline{v_i}$ is the averaged velocity of the ions. Typical values of the parameters relating to the ionic diffusion are listed in Table 2.1. In general, the ionic diffusion is only significant when the size of particles is less than 0.2μm. For the particles with a diameter of 1μm or larger found in electrostatic precipitation processes, the amount of charges acquired from the ionic

bombardment is several orders of magnitude higher than that from the ionic diffusion. In summary, we use the saturated charge from the ionic bombardment to model the electrical charging process (Eq.2.9).

Table 2.1: Parameters relating to the ionic diffusion charging mechanism.

Parameters	Values
Permittivity of space, ε_0	$8.854187817 \times 10^{-12}$ F/m
Boltzmann constant, k	$1.3806503 \times 10^{-23}$ m^2 kg s^{-2} K^{-1}
Elementary charge, e	$1.60217646 \times 10^{-19}$ C
Temperature, T_k	300 K
Ion concentration, N_0	$5x10^{14}$ ions/m^3
Ion velocity, $\bar{\mathbf{v}}_i$	1.17×10^{7} m/s

2.2.5.2. Coulomb's Force

The most fundamental electrostatic interaction between two electrically charged particles is the Coulomb's force. In 1785, French physicist Charles Coulomb demonstrated two charged particles experienced the repulsion or attraction forces using a torsion balance. Like charges repel each other, while opposite charges attract each other. Mathematically, the Coulomb's force $\mathbf{F}_{coulomb}$ is given by,

$$\mathbf{F}_{coulomb} = k_c \frac{q_i q_j}{\mathbf{r}^2} \hat{\mathbf{r}}_{ij} \tag{2.13}$$

where k_c is the Coulomb's constant, q is the electrical charge of particles, $\mathbf{r}$ is the vectorial distance between the particles. The Coulomb's force experienced by a charged particle under an imposed electric field is simply,

$$\mathbf{F}_{coulomb} = q\mathbf{E} \tag{2.14}$$

where **E** is the electric field. Using the saturated charge derived in the last chapter, the explicit form of the Coulomb's force exerting on a dielectric particle under an electric field is,

$$\mathbf{F}_{coulomb} = 4\pi\varepsilon_0\left[2\left(\frac{k_p - 1}{k_p + 2}\right) + 1\right]\mathbf{R}^2\mathbf{E}^2 \tag{2.15}$$

The charged particles in electrostatic precipitation processes are certainly under the influence of the Coulomb's force. In fact, it is the key working principle of this process. The charge distribution on a particle is considered to be uniform. This is valid considering the scale of electrostatic precipitation system is much greater than the particle diameter.

2.2.5.3. Electrical polarisation

On a particle scale, the charge distribution on a particle under electric fields is usually not uniform due to the finite size of the particle, and therefore, the electric-field-induced electrical polarisation need to be considered. For instance, when a particle is placed under an imposed electric field, the positive and negative charges are aligned with the electric field as depicted in Figure 2.3a. Such a particle is electrically polarised. In the simplest case of a single particle under a uniform electric field, an electrical dipole is usually sufficient to represent an electrically polarised particle as illustrated in Figure 2.3b. Under a steady state, the force and the torque on the electrical dipole are given by,

$$\mathbf{F}_{dipole} = \mathbf{p}\nabla\mathbf{E} \tag{2.16}$$

and

$$\mathbf{T}_{dipole} = \mathbf{p} \times \mathbf{E} \tag{2.17}$$

where **p** is the dipole moment. In more complicated situations, for instance three or more polarised particles, multipole expansions are applied to determine the multipole moment and the subsequent electrostatic interactions. It is worth noting that the electrical polarisation is fundamentally different from the molecular dipole van der Waals interactions. The van der Waals interactions are observable in the absence of an imposed electric field.

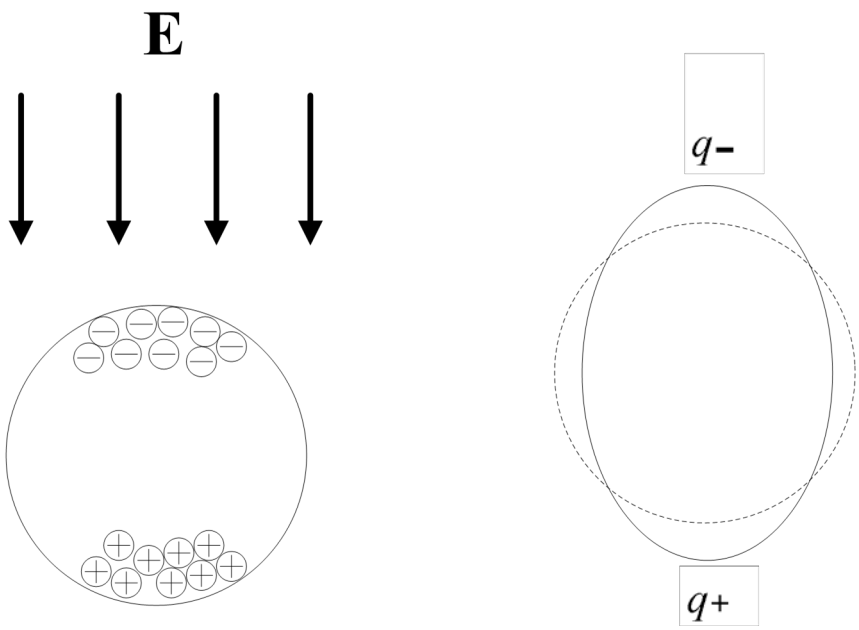

Figure 2.3: A polarised particle and the corresponding dipole moment under an imposed electric field.

Despite the existence of electrical polarisations, it is not included in our simulation for several reasons. First of all, the size of electrostatic precipitation system is much larger than the dimensions of a single particle as mentioned earlier. When a charged particle is suspended in the ionised gases, the Coulomb's force induced by the imposed electric field dominates. Thus, the effect of electrical polarisation is negligible. Secondly, when a layer of particle packing is precipitated on a collection plate, we have estimated that the electrostatic interactions on a particle due to the electrical polarisation of its immediate neighbours are much smaller than the interparticle van der Waals

interactions. A recent numerical study has extended the approximation of the electrostatic interaction caused by the electrical polarisation to include every charged particle in a packing using the boundary element method [16]. However, such a method is computational heavy, and therefore, its application is only limited to a small number of particles. Lastly, it is generally accepted that the electrical polarisation is weak when particles are randomly distributed in a packing, because the dipole interactions between two contacting particles is influenced by imposed electric fields and also the electric field generated by the surrounding charged particles [17]. Thus, the effect of electrical polarisation on particles is neglected in this work considering the Coulomb's force is dominant for suspended particles, while the van der Waals interactions are dominant for particles in a formed packing.

2.2.5.1. Boundary image force

Furthermore, when a charged particle approaches to any boundary, the particle experiences an additional attractive force due to the different electrical properties across the boundary. The exact electrostatic interaction between particles and boundaries is difficult to solve directly. Instead, the method of image is usually applied in electrostatics studies [18-20]. Mathematically, the attractive boundary image force is equivalent to the force imposed by an imaginary particle with the same amount of the opposite charges on the other side of the boundary (see Figure 2.4), which is given by,

$$\mathbf{F}_{image} = -\frac{q^2}{16\pi\varepsilon_0 h_d^2} \tag{2.18}$$

where h_d is the particle-wall separation. The explicit expression of the boundary image force for dielectric particles is,

$$\mathbf{F}_{image} = -\frac{\pi\varepsilon_0}{h_d^2}\left[2\left(\frac{k_p-1}{k_p+2}\right)\mathbf{R}^2\mathbf{E}+\mathbf{R}^2\mathbf{E}\right]^2 \tag{2.19}$$

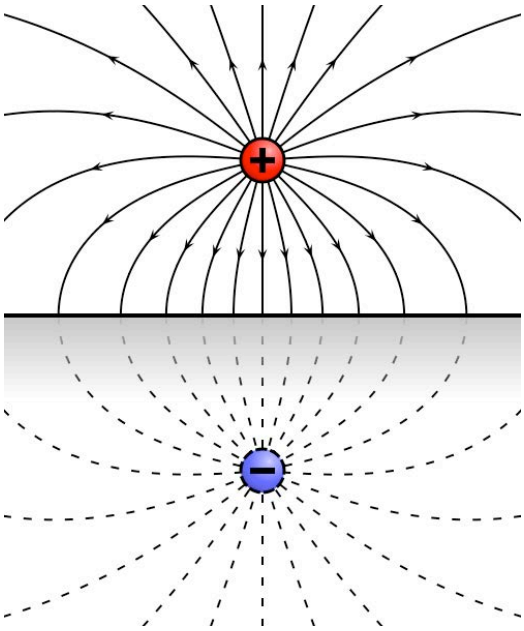

Figure 2.4: Schematic diagram of the image force experienced by a particle close to the grounded boundary.

In summary, the sum of the electrostatic interactions exerting on a charged particle under an imposed electric field is given by,

$$\mathbf{F}_e = q\mathbf{E} - \frac{q^2}{16\pi\varepsilon_0 h_d^{\,2}} \tag{2.20}$$

Using the saturated charges on a dielectric particle (Eq.2.9), the explicit form of the electrostatic interactions is,

$$\mathbf{F}_e = 4\pi\varepsilon_0 \left[2\left(\frac{k_p - 1}{k_p + 2} \right) + 1 \right] \mathbf{R}^2\mathbf{E}^2 - \frac{\pi\varepsilon_0}{h_d^{\,2}} \left[2\left(\frac{k_p - 1}{k_p + 2} \right) \mathbf{R}^2\mathbf{E} + \mathbf{R}^2\mathbf{E} \right]^2 \tag{2.21}$$

where q is the electrical charge, $\mathbf{E}$ is the electric field, ε_0 is the permittivity of space, h_d is the particle-wall separation, k_p is the dielectric constant and $\mathbf{R}$ is the particle radius. The electrostatic interactions will be applied on every particle under an imposed electric field in numerical simulations.

2.2.6. Contact torques

When two particles are in contact, it is understandable that torque is induced from the normal contact force. In contact mechanics, this torque is given by,

$$\mathbf{T}_i^s = \mathbf{R}_i \times \mathbf{F}_{ij}^s \tag{2.22}$$

where $\mathbf{R}_i$ is the vector from the centre to the point of contact. In addition, when rolling friction exists between two contacting particles, an additional torque induced by the rolling friction shall be considered. Mathematically, it is given by [21, 22],

$$\mathbf{T}_{ij}^r = -\mu_r R_i \left|\mathbf{F}_{ij}^n\right| \hat{\boldsymbol{\omega}}_i \tag{2.23}$$

where μ_r is the rolling friction. Thus, the total torque between two contacting particles can be expressed as,

$$\mathbf{T}_i = \sum \left(\mathbf{R}_i \times \mathbf{F}_{ij}^s + \mu_r \left|\mathbf{R}_i\right| \left|\mathbf{F}_{ij}^n\right| \frac{\boldsymbol{\omega}_i}{\left|\boldsymbol{\omega}_i\right|} \right) \tag{2.24}$$

The torque induced by the rolling friction is particularly important in providing the stability of the system, and therefore, achieving a stable unconfined packing.

2.2.7. Gravitational force

In this work, the gravitational force is not important to the formation of packings under electric field in electrostatic precipitation processes. Typical barbed electrostatic precipitation systems are illustrated in Figure 2.5 [23]. The barbed discharge electrodes and the collection walls are all vertically orientated. Therefore, the direction of the gravitational force is perpendicular to the direction of the packing formation on the collection walls. For this reason, the effect of the gravitational force is neglected in our simulation. It is worth noting that the gravitational force is important in dislodging a

layer of particle packing during mechanical rapping processes, but this is outside of the scope of this thesis.

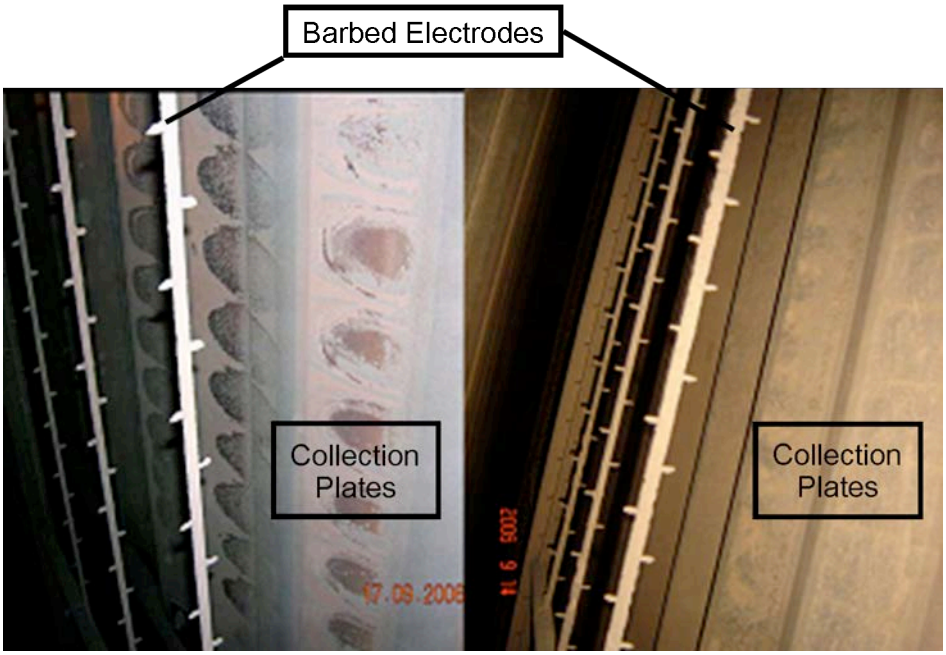

Figure 2.5: Photos taken inside two barbed electrostatic precipitation units installed at two power plants in China.

2.3. Structural Characterisation of Particle Packing

2.3.1. Overview

The structural characterization of particle packing is an important subject of study in many fields of technology, because almost all the packings encountered in nature and in industry are random. A range of techniques to characterise packing structures are summarised in this section.

2.3.2. Packing fraction

Packing fraction is the volume fraction of particles per unit volume of a packing,

$$\rho = \frac{V_p}{V_{total}} \tag{2.25}$$

where ρ is the packing fraction, V_p is the volume occupied by particles and V_{total} is the bulk volume of a packing. The reciprocal of packing fraction is porosity, which is given by

$$\phi = 1 - \rho \tag{2.26}$$

The packing fraction and the porosity are interchangeable.

Packing fraction is an important structural parameter in the study of particle packing. It is well established that the maximum possible packing fraction of a random structure is 0.60 before compaction and 0.64 after compaction, which are identified respectively as random loose packing and random dense packing [24-27]. More recently, it has been suggested that random close packing is not well-defined, and maximum random jamming state is proposed to replace the random close packing [28, 29]. It is argued that the particles in a jamming state are blocked in configurations far from equilibrium. This means that a packing is not entirely jammed except when the packing fraction is at the maximum random jamming state. Therefore, the maximum random jamming state can be seen as a second-order phase transition point, beyond which point order packings begin to form in local regions. In short, the packing fraction of a packing is a simple but robust structural parameter, although the detailed microscopic structural parameters are probably needed to comprehensively describe the packing structure.

There are several methods to measure packing fraction of a packing in practical experiments. For packings of coarse particles, the packing fraction can be obtained by counting the number of particles in a container. However, it is challenging to determine the packing fraction of packings of fine particles, such as pharmaceutical powders, filtered dusts. In addition, when the local packing structure is not uniform, it is difficult to determine changes of the local packing fraction in practical experiments. Recently, x-ray computed tomography is used to measure the detailed packing fraction as well as other structural parameters (see Figure 2.6) [9]. The spatial resolution of the x-ray

computed tomography can be up to several micron-meters and sometimes even nanometers. However, the cost of micro-CT increases significantly as the resolution is enhanced. Therefore, it is still impractical to apply to the packing of fine particles.

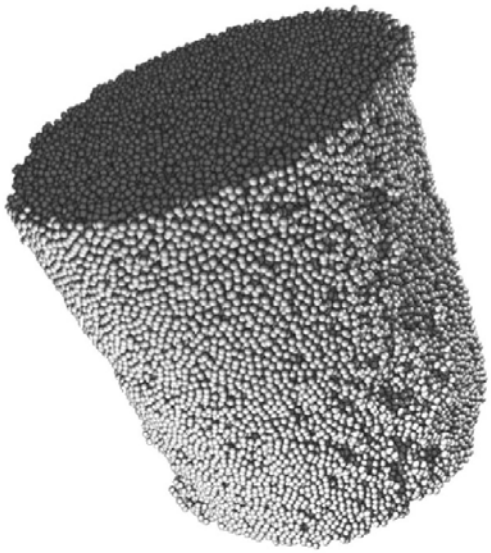

Figure 2.6: Processed image of the packing structure of 150000 spheres in a cylindrical container measured by x-ray tomography.

For the precipitated packings in electrostatic precipitation processes, the scanning electron microscopic has been applied to measure the areal packing fraction [30]. Firstly sophisticated preparation procedures must be applied to consolidate the packings made of fine particles because of their fragility [31]. Then, the cross-sectional area of the prepared packings is examined using the scanning electron microscopic to obtain qualitative areal packing fraction. The averaged areal packing fractions are included in Table 2.2. Obviously, the two dimensional measurements of the areal packing fraction of a three dimensional packing are only rough estimates. To explain these observations, it has been proposed that the precipitated packings under weak electric fields have dendrite-like structures [32]. In contrast, particles are rearranged during the process of packings under strong electric fields, and therefore, dense structures are formed. To our knowledge, there is no experimental proof for this hypothesis because of the limitation of practical measurements. Nonetheless, the experimental studies suggest that there could be a correlation between packing fraction and electric field.

Table 2.2: The averaged areal packing fraction of packings

Formed packings under strong electric fields	Formed packings under weak electric fields
0.25	0.12

Determinations of the packing fraction for packings of fine particles are mainly dependent on computer simulations. For instance, the packing fraction of simulated packings is readily available in the discrete element method, not to mention that the non-uniform local packing fraction is easily detectable if there is any. In addition, one of the most important advantages of simulation studies is that the force exerting on particle can be systematically analysed. It is revealed in the study of the packing of fine particles under gravity that packing fraction is closely related to the competition between the gravity and the cohesive interparticle forces, e.g., van der Waals interactions [10]. Similar results are found in the study of packings of wet particles [12]. Thus, it is expected that the electrostatic interactions play an important role in the formed packings under electric fields.

2.3.3. Coordination number

Coordination number of a particle represents the number of its contacting neighbours. The coordination number of ordered packings is trivial, for example, the coordination number is six for simple cubic packing, twelve for face centred cubic packing. In random packings, the coordination number of particles varies due to the random structure. For packings of coarse particles, the coordination number varies between three and ten [27]. For packings of fine particles, the coordination number has been found to be as low as two, which is corresponding to the lowest possible coordination number to support a stable packing. Chain-like structure with coordination number of 2 has been frequently observed in packings of nanoparticles [33].

The measurement of coordination number of a packing is challenging in practical experiments. Early experiments use rigid particles soaked in paint to mark the contacts between particles (see Figure 2.7) [25]. After breaking up the paint soaked packing, the contact spots should be paint free and the coordination number on each particle is then determined. Similar principle is applied using lead beads soaked in 20% acetic acid [34]. However, these methods are incapable of distinguish the near contact between particles. Whether two particles are in contact of in near contact has significant impact on the stress propagation, electrical conduction and thermal conduction between the particles. Such a difficulty is easily overcome by numerical simulations.

Figure 2.7: A packing is soaked in paint to reveal coordination number.

The coordination number of each particle in a packing can be effortlessly obtained in numerical simulations. To avoid the near contact between particles, a critical distance of separation is usually defined so that the neighbouring particles are defined in contact when the displacement between them is less than the critical separation [10]. Also, the distribution of coordination number in a packing is revealed with ease in numerical simulations. It has been revealed that two packings having the same averaged coordination number would have similar distributions of coordination number. Nevertheless, the coordination number distribution often gives better indications of the internal structure of a packing.

With the careful determination of coordination number, it has been discovered that the averaged coordination number is closely correlated with packing fraction. A list of

important and commonly applied empirical models is included in Table 2.3. Rumpf is the first to propose the correlation between coordination number and packing fraction [35]. The multiplicative inverse relation is simple to use, but it is limited to packings of coarse particles. According to the method of packing formations, the empirical numerator must be evaluated before its application. Then, the second order polynomial equation has been proposed to give better predictions for the relation between coordination number and packing fraction [36]. However, there is no physical meaning in the polynomial approximation. As a result, the packing fraction can be less than zero when the coordination number is approaching two. This is certainly physically impossible. On the other hand, a universal equation of coordination number and packing fraction has been developed in the numerical study of the packing of fine particles under gravity [10]. The success application of this model in both packings of coarse and fine particles is probably due to the highly reproducibility of the numerical simulations. Notably, the physical meaning of the empirical parameter is that z_0 is defined as the limiting coordination number, which is corresponding to the lowest coordination number needed to support a stable packing. Thus, when the packing fraction of a packing is approaching to zero, the coordination number is approach to z_0.

Table 2.3: Empirical equations relating coordination number with packing fraction.

$$\bar{z} = i/(1-\rho) \tag{2.27}$$

$$\rho = 1-\left(j + k\bar{z} + l\bar{z}^2\right) \tag{2.28}$$

$$\bar{z} = z_0 \frac{1+m\rho^4}{1+n\rho^4} \tag{2.29}$$

In short, coordination number is an important structural parameter indicating the connectivity of a packing, which in turn, affects the transport properties, such as electrical and thermal conductivity. The effect of coordination number on the electrical conductivity of a packing will be discussed in the latter sections.

2.3.4. Radial distribution function

Radial distribution function or sometimes called pair correlation function $g(r)$ is defined as the ratio of the probability to find another disk at a distance between r and $r+dr$ to the averaged number density [1], and $g(r)$ is expressed as

$$g(r) = \frac{dN(r)}{4\pi r^2 dr \rho_0} \tag{2.30}$$

where $dN(r)$ is the averaged number of particles within distance dr and ρ_0 is the averaged number of particles per unit volume.

The radial distribution function of a packing is studied experimentally using x-ray scattering based techniques. In 1970s, the radial distribution function of packings was intensively studied to model the structure of amorphous materials, such as metallic glasses and liquid metals [27, 37]. For packings of coarse particles, it has been revealed that the second peak in the radial distribution function is often split into two sub-peaks [27]. The difference between particle packing and liquid metals in terms of radial distribution function is that the second sub-peak is higher than the first one in packings, while the opposite is found in liquid metals [37].

In numerical studies, the radial distribution function of the simulated packings is effortlessly determined from the exact position of each particle. The radial distribution functions of two simulated packings are depicted in Figure 2.8. Noticeably, the radial distribution function of packings of fine particles shows no distinct peak, except for the first peak and the second peak corresponding to the immediate neighbours of a reference particle. In contrast, there is a distinct split in the second peak for packings of coarse particles, which suggested there are certain short ranged orders existing in these packings (see Figure 2.8b). The geometric representations of the split second peak in the radial distribution function are presented in Figure 2.8c. In essence, the radial distribution function as a statistical microscopic parameter of a packing gives qualitative descriptions of the packing structure. Comparing to packing fraction and coordination

number, the extent of the short and medium range order in the local region is revealed by examining the radial distribution function of a packing.

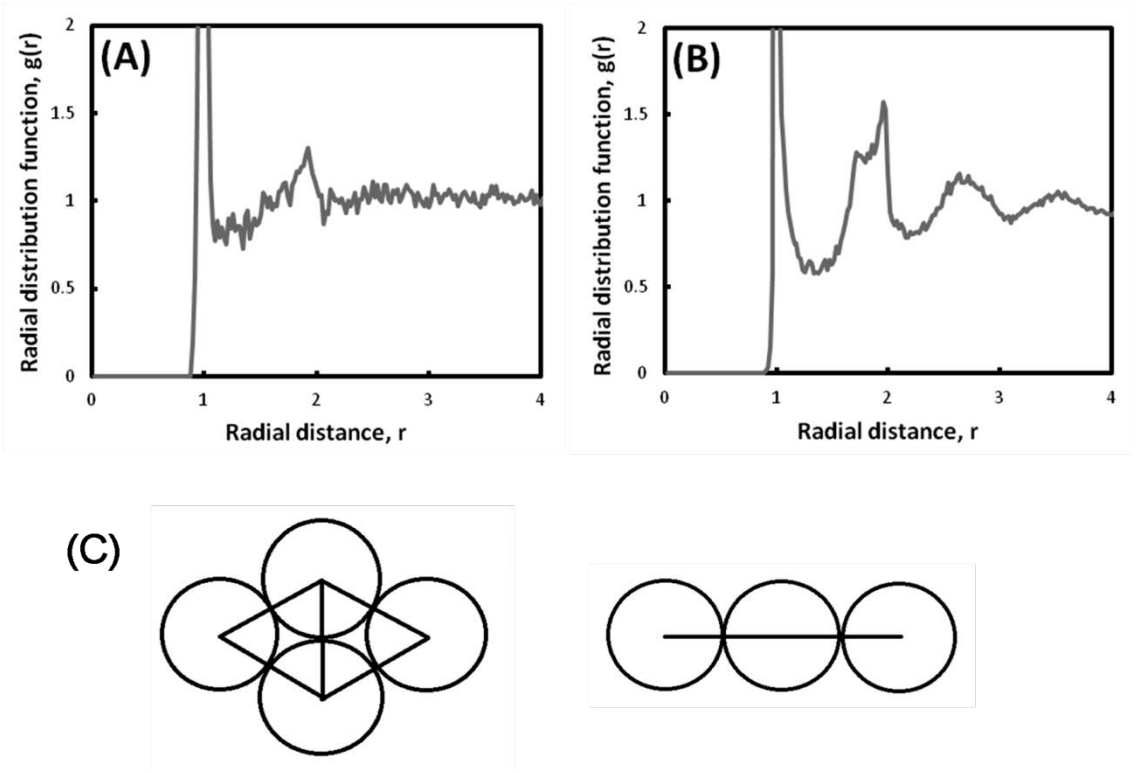

Figure 2.8: The radial distribution functions of (A) disordered and (B) ordered packings. (C) Two dimensional geometric representation of the split peak in radial distribution functions.

2.3.5. Voronoi tessellation

Voronoi tessellation is applied to quantify the spatial configuration of particles in a packing. Voronoi polyhedron is defined as the smallest polyhedron formed by perpendicularly bisecting the vectors between the particle centres in a packing. There is no further plane can cut through the enclosed space in the polyhedron. Mathematically, it is described as [38],

$$\mathbf{x} \in V_i \Leftrightarrow \left|x - x_i\right| < \left|x - x_j\right| \qquad \forall j \tag{2.31}$$

where **x** is the location vector. The voronoi diagram of 12 points in two-dimensional space is depicted in Figure 2.9. It should be noted that any point within a Voronoi cell is closer to its cell centre than any other cell centres.

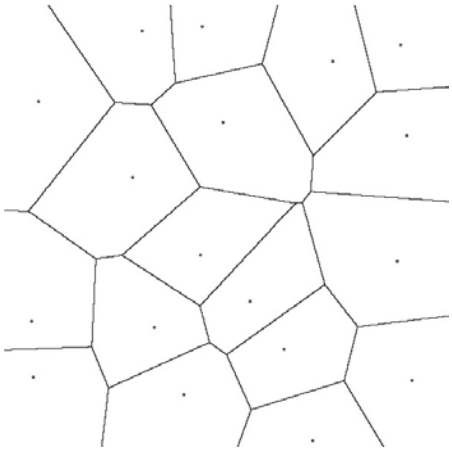

Figure 2.9: Voronoi tessellation of 12 points in two-dimensional space.

Voronoi analysis in the studies of particle packing was applied by Bernal dated back to early 1960s, though the aim is to study the structure of liquids [39]. Then, Finney extensively studied the Voronoi polyhedron cell, which provides a tool to solve the transport properties of a packing [27]. In computer simulation studies, Voronoi tessellation is commonly used to characterise packing structures [40-42]. It is revealed that certain metrical and topological properties of the polyhedra can be determined from the packing fraction. These relations are especially useful in application of Voronoi characters to determine transport properties of packings. For instance, Voronoi cell has been successfully applied in the study of thermal conduction through packed beds [43]. Voronoi tessellation of a three-dimensional packing is illustrated in Figure 2.10. It is shown that Voronoi tessellation gives statistical geometrical representation of a packing structure in real space.

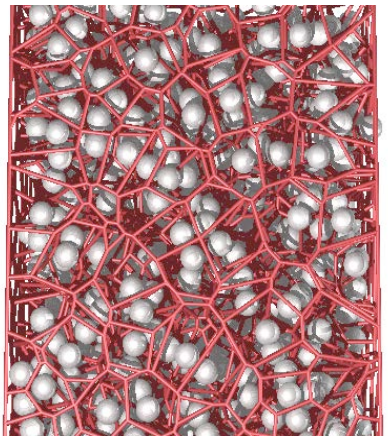

Figure 2.10: Voronoi tessellation of a simulated packing.

2.4. Effective Conductivity of Particle Packing

2.4.1. Overview

Fundamental and applied studies of particle packing regarding the transport phenomena have generated significant amount of interest over the last few decades because of the importance of particle packing in many areas of science and engineering, e.g., metallurgy, nuclear physics to chemical, petroleum engineering. Our focus is finding the effective electrical conductivity of a typical packing structure depicted in Figure 2.11, where two distinct phases are the solid particle phase and the interstitial gas phase. The electrical properties of such a structure in a steady state is described mathematically by the continuity equation and the Laplace's equation,

$$\nabla \mathbf{J} = 0 \tag{2.32}$$

$$\nabla^2 \varphi = 0 \tag{2.33}$$

where $\mathbf{J}$ is the electric current density and φ is the electrical potential. These conditions must be satisfied within the particle and gas phases as well as at the inter-phase boundaries. At the boundaries, we have,

$$\mathbf{n}\sigma_{gass}\nabla\varphi_{gas} = \mathbf{n}\sigma_{particle}\nabla\varphi_{particle} \tag{2.34}$$

where **n** is an unit vector pointing outwards on the surface of the particle, $\sigma_{particle}$ and σ_{gas} denote the conductivity of the particles and gases respectively. The analytical solution to these equations is impractical, especially for random packings due to its stochastic nature.

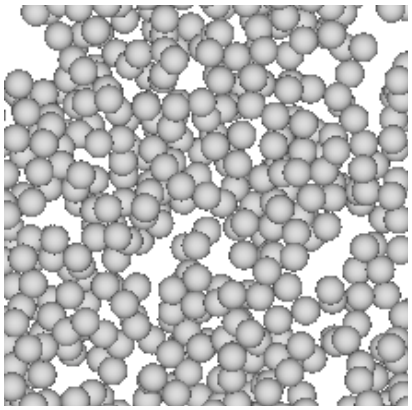

Figure 2.11: A typical packing made of solid particles and interstitial gases.

The effective electrical conductivity, σ_{eff}, is defined as,

$$<\mathbf{J}> = \sigma_{eff} <\mathbf{E}> \tag{2.35}$$

where <**J**> is the volume averaged current density and <**E**> is the volume averaged electric field applied to system. Note that the effective conductivity is treated as scalar vector because of isotropic packings.

Theoretical approaches to estimate the effective electrical conductivity in the studies of particle packing can be categorized into two major groups that are continuum mean field theories and discrete resistor network models. The continuum mean field theories involve the use of a simplified or idealised structure to represent a packing structure. As a result, the equations describing electrical conditions (Eq.2.35) is then solvable. This type of mathematically treatments is referred to the mean field theory. In contrast, a packing structure is discretised into an equivalent network of diverse resistors in the

discrete resistor network models. The effective conductivity of the packing is then found through analysing the connectivity of the resistor network, a concept originated from the percolation theory.

In this section, we attempt to present a review of the important literature on finding the effective electrical conductivity of packings, with emphasis on the effect of the structural parameters. The review concludes with the direction and challenge of applying different approaches in the discrete element method.

2.4.2. Continuum mean field theories

2.4.2.1. Maxwell's approaches

For a simply cubic packing of particles embedded in a medium, Lord Rayleigh derived an analytical expression for the effective electrical conductivity as [44],

$$\sigma_{eff} = \sigma_m \left(1 + \frac{3\beta\rho_p}{1 - \beta\rho_p - 0.525\left(\frac{\alpha - 1}{\alpha + 4/3}\right)\beta\rho^{10/3}} \right) \tag{2.36}$$

and

$$\beta = \frac{\sigma_p - \sigma_m}{\sigma_p + 2\sigma_m}\ ,\ \alpha = \frac{\sigma_p}{\sigma_m}$$

where ρ_p is the packing fraction, σ_m and σ_p are the bulk electrical conductivity of the medium and particle respectively. The term β is sometimes referred as the polarisability which represents the induced flux through the medium with particle inclusions relative to the flux without particle inclusions. For other ordered structures or random structures, analytical solution to the effective conductivity is usually not available. Even for the Rayleigh's expression, it still fails to predict the effective conductivity for the structure made of the particle and medium with very differing conductivities [45].

For disordered packing structure, the problem of finding the effective conductivity was firstly studied by Maxwell in 1873 [46]. Maxwell assumed that the distance between particles was large enough to ignore any interactions between the particles. Then, the equation for the effective conductivity was derived by integrating over the electrical potential at the particle surface and in its surroundings,

$$\sigma_{eff} = \sigma_m \frac{1 + 2\beta\rho_p}{1 - \beta\rho_p} \tag{2.37}$$

Based on the Maxwell's equation, Jeffrey included the particle interactions to the second order of packing fraction and found that [47],

$$\sigma_{eff} = \sigma_m \left(1 + 3\beta\rho_p + 3\beta\rho_p^2\Sigma\right) \tag{2.38}$$

where Σ depends on both β and α. The Maxwell's type expressions predicting the effective conductivity with higher order of packing fraction are also available in literature. However, the problem with these types of expression is that the summation of high order expressions converges slowly. For instance, the Σ term in Eq.2.38 requires over 100 terms before the convergence of the first three decimal points. Thus, Σ is usually empirically determined in practical experiments.

In general, the Maxwell's approach only applies to the structure with a low packing fraction, in other words, particle inclusions must be loosely dispersed. However, it has been shown that the Maxwell's equation (Eq.2.37) provides accurate predictions for the effective conductivity, even for the packing with packing fraction of 0.6 when the ratio of the bulk conductivity between particle and medium is moderate [48]. For cases with α is greater than 10, the Maxwell's equation significantly underestimate the effective conductivity. This is caused by the electrical conditions are no longer continuous at the boundary between the particle and medium, the interparticle contact plays an important role in this situation. In short, the Maxwell's approach is usually limited to small α.

2.4.2.2. Effective medium approaches

The effective medium approach is originated from the study of the electrical conductivity of composite material by Bruggeman [49]. For a composite material made of an equal amount of two different phases, finding the exact electrical conductivity could be difficult if the structure is disordered. Two simple structures are depicted in Figure 2.12. Assuming the exact arrangement of the two phases is not important, the electrical conductivity of the structure is the lowest, when the phases are arranged perpendicular to the direction of electric current (see Figure 2.12a). The effective conductivity of the corresponding structure is,

$$\sigma_{eff} = \sigma_m \rho_m + \sigma_p \rho_p \tag{2.39}$$

On the other hand, the electrical conductivity is the highest when the phases are arranged in parallel to the current flow (see Figure 2.12b), and the effective conductivity is then expressed as,

$$\sigma_{eff} = \frac{\sigma_m \sigma_p}{\sigma_m \rho_p + \sigma_p \rho_m} \tag{2.40}$$

The conductivity of any unknown structure with an equal amount of two phases must be bounded by these limits. In this case, two extreme structures are applied to roughly approximate the effective conductivity.

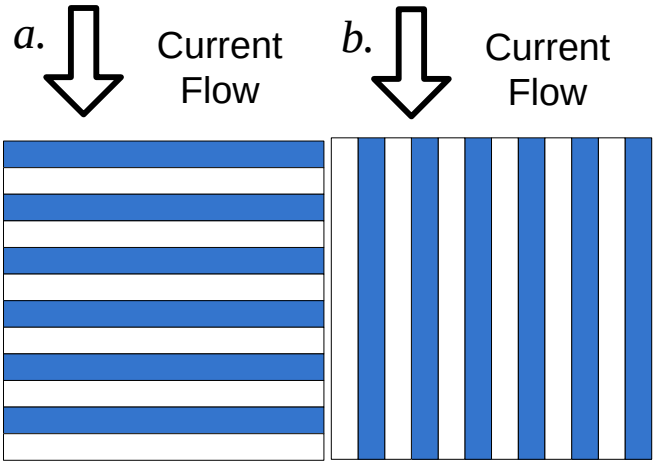

Figure 2.12: Two basic limiting structures of composite materials.

Using the variational principle, Hashin and Shtrikman improved the limiting bound for the effective conductivity of the structure made of two phases. These bounds are exceptionally useful in many engineering applications. Assuming the potential energy and the complementary energy must be minimised, the effective conductivity of the system is now bounded by,

$$\sigma_L \leq \sigma_{eff} \leq \sigma_U \tag{2.41}$$

where

$$\sigma_L = \left(\rho_m\sigma_m + \rho_p\sigma_p\right) - \frac{\rho_m\rho_p\left(\sigma_p - \sigma_m\right)^2}{\left(\rho_p + 2\right)\sigma_m + \rho_m\sigma_p} \tag{2.42}$$

$$\sigma_U = \left(\rho_m\sigma_m + \rho_p\sigma_p\right) - \frac{\rho_m\rho_p\left(\sigma_p - \sigma_m\right)^2}{\rho_p\sigma_m + \left(\rho_m + 2\right)\sigma_p} \tag{2.43}$$

Note that the particle and the medium phase are interchangeable to give the upper and lower bounds. The physical meaning of the lower bound is that the effective conductivity is lowered when the electric current must flow around particle inclusions. Also, it is possible that some isolated particles are not contributing the overall conduction, and as a result, the effective conductivity decreases.

In fact, the effective medium approach is applied in the Maxwell's calculation of the effective conductivity described in the previous section. In the original Maxwell's equation, it is assumed that there is no interaction between particles embedded in the medium. In essence, the structure with a single inclusion is used to represent the structure with dilute inclusions.

For symmetric structure or the structure with interchangeable phases, self consistent effective medium approximation has shown to provide reasonable prediction on the effective conductivity,

$$\sigma_{eff} = \frac{\sigma_p(3\rho_p - 1) + \sigma_m(3\rho_m - 1) + \sqrt{(\sigma_p(3\rho_p - 1) + \sigma_m(3\rho_m - 1))^2 + 8\rho_p\rho_m}}{4} \quad (2.44)$$

Furthermore, differential effective medium approximation is derived based on the fact that the incremental changes in the packing fraction of a packing would cause the incremental changes in its effective conductivity. For instance, if we know the effective conductivity of a packing with known packing fraction, then the effective conductivity of a similar packing with packing fraction of $\rho_p+\delta\rho_p$ can be calculated.

$$\frac{\sigma_p - \sigma_{eff}}{\sigma_p - \sigma_m}\left(\frac{\sigma_m}{\sigma_{eff}}\right)^{\frac{1}{3}} = 1 - \rho_p \quad (2.45)$$

Obviously, the limitation of such an approximation is the difference in the packing fraction of two structures must be small. When the conductivity of particle is zero, the formula is reduced to,

$$\sigma_{eff} = \sigma_m \rho_m^{\frac{3}{2}} = \sigma_m(1 - \rho_p)^{\frac{3}{2}} \quad (2.46)$$

This is consistent with the empirical formula developed in the study of electrical conduction through fluid filled sediment packings [50].

$$\sigma_{eff} = \sigma_p \left(1 - \rho_p\right)^m \tag{2.47}$$

The uncertainty in the value of the exponent is probably caused by the fact that the only structural parameter used is the packing fraction. The experimental observations highlight that the structure is a key parameter that determines the effective conductivity of a packing. Nevertheless, it has been widely applied in the studies on soils, rocks and oil reservoir characteristics to give qualitatively predictions for the effective conductivity.

In some cases, the analytical solution to the effective conductivity of a binary medium is found using the n-point probability function in the statistical mechanics. For the structure made of the phases with similar electrical conductivity, the effective conductivity is given by [51],

$$\sigma_{eff} = \sigma_m \frac{1 + 2\rho_p\beta - 3\rho_m\zeta\beta^2}{1 - \rho_p\beta - 2\rho_m\zeta\beta^2} \tag{2.48}$$

ζ is called the three point parameter, which is expressed in terms of ρ_p in Taylor series. Using the first order approximation, ζ is,

$$\zeta = 0.5615\rho_p \tag{2.49}$$

The explicit form of three point parameter ζ can be found elsewhere [51]. It should be noted that the determination of the three point parameter requires a precise structural characterisation, which is often difficult in practical experiments.

The effective medium approach is frequently used in the study of the effective conductivity, because only simple structural information, e.g., packing fraction, is required in most situations. The key concept of the effective medium approach is to estimate the conductivity of disordered structure using the conductivity of some known structures. When the appropriate representative structure is found, it is easy to give reasonable predictions for the effective conductivity. It is worth noting that when the

difference in the conductivity of each phase in a packing is large, the effective medium approaches often fail due to the discontinuity of the electrical conditions across the inter-phase boundary. Nevertheless, the effective medium approach is popular due to its simplicity and gives good qualitative results.

2.4.3. Discrete resistor network models

2.4.3.1. Numerical calculations

Over the last few decades, numerical approaches have been frequently applied in the studies of particle packing regarding to the effective electrical conductivity due to rapid advancements in computer technology. In numerical approaches, by solving for the electrical potential and electric current, the effective electrical conductivity is found as,

$$\sigma_{eff} = \frac{I \cdot H}{A \cdot \Delta V} = \frac{J \cdot H}{\Delta V} \tag{2.50}$$

where I is the electric current, H and A are the height and the cross-sectional area of the packing, ΔV is the applied electrical potential difference, and J is the electric current density.

To apply Eq.2.50, the electrical potential and current on each particle in a packing must be firstly solved. In the discrete resistor network models, a packing structure is represented by an equivalent network of resistors. The resistors will have a diverse range of electrical properties depending on the structure. The effective electrical conductivity can then be derived by solving the electrical circuit law. As a result, the effective conductivity is determined by the connectivity of the network. The detailed method of finding the electrical properties on each particle is included in Appendix I. Hence, the effective conductivity is solved explicitly from the numerical models.

In a packing of conductive particles, the electric current is carried mainly through the interconnecting particles. As a result, the effective electrical conductivity is determined by the contact conductivity between particles, and therefore, the interparticle contact

area plays a key role. As mentioned in the previous section, the contact area between particles in the discrete element method is described by the Hertz contact theory. However, it is common practice to use a reduced simulated Young's modulus to represent the real Young's modulus in order to increase the computational efficiency [52]. Thus, a correction factor must be introduced to account for the contact radius affected by the reduced Young's modulus,

$$r_c^* = r_c\left(\frac{Y_{sim}}{Y_{real}}\right)^{\frac{1}{5}} \tag{2.51}$$

where Y_{sim} and Y_{real} are the simulated and the real Young's modulus respectively. Then the contact electrical conductance between particles is found as [53],

$$G_c = \frac{\rho_p}{2r_c^*} \tag{2.52}$$

Considering the size of the contact between particles, the contact conductance is always several orders of magnitude lower than the materials conductance of particle. Consequently, the majority of the resistance to the electric current flow across a packing exists at the vicinity of the contact between particles, and the effective conductivity is determined by the contact conductance between particles.

2.4.3.2. Theoretical models

The discrete resistor network models are particularly useful when the local equilibrium assumption is invalid. When the difference in the electrical properties of solid particle and interstitial gas is large, the electric current and potential across the particle-gas boundary is no longer continuous. Such a problem is difficult to handle by the effective medium theory. In contrast, when the solid particle phase and the interstitial gas phase are converted into equivalent resistors, continuity is not necessary between the two phases. Then the electrical conditions in each phase are described as,

$$< J >= \frac{1}{V}\int_{V_m} J \cdot dV + \frac{1}{V}\int_{V_p} J \cdot dV = -\frac{\sigma_m}{V}\int_{V_m} \nabla\phi \cdot dV - \frac{\sigma_p}{V}\int_{V_p} \nabla\phi \cdot dV \tag{2.53}$$

where V is the volume of a packing. For ordered simple cubic packings, analytical solution for the effective conductivity is available [54, 55],

$$\sigma_{eff} = \sigma_p \frac{d_c}{d} \tag{2.54}$$

where d_c is the contact diameter and d is particle diameter. For random packings, Batchelor and O'Brien formulated the equation for the effective conductivity when the electric current is mainly conducted by the particles as [56],

$$\sigma_{eff} = \sigma_p \frac{d_c \rho z}{\pi d} \tag{2.55}$$

where z is the coordination number. It should be noted that the microscopic coordination number determines the connectivity of a packing, and therefore, impact on its effective conductivity. As the coordination number varies in a random structure, it is difficult to obtain the coordination number distribution in practical experiments. Thus, the averaged coordination number is used in the application of such a model.

To avoid the use of microscopic coordination number, Kendall has developed a model to predict the effective electrical conductivity of packings using the concept from the study of the elasticity of particles in packings [57]. Using the relation between the effective Young's modulus and the structural parameters, an expression for the effective conductivity is derived as,

$$\sigma_{eff} = \sigma_p \times 32.3\rho^4 \left[\Gamma\left(1-\nu^2\right)/Yd\right]^{\frac{1}{3}} \tag{2.56}$$

where Γ is the interfacial energy which is required to separate two adhesive surfaces, ν is the Poisson's ratio, Y is the Young's modulus. Now finding the effective Young's

modulus is an analogue of finding the effective conductivity. When a hexagonal close packing is under external stress, there is a pair of particles is on the load bearing direction and another four pairs are at 60 degrees angle. Comparing to a simple cubic packing, there are three times more particles contributing to the external load. It is assumed that packing fraction and coordination number are the only two factors influencing the effective properties. Then the contribution of coordination number to the effective Young's modulus in a hexagonal close packing is 3.78 times of it in a simple cubic packing, because the packing fraction of the hexagonal close packing is $(\rho_{cubic}/\rho_{hcp})^{2/3}$=0.794 times that of the simple cubic packing. Now, there is no way to determine these structural properties for most packing structures. The ρ^4 relation is found to be 13.3 by empirically fitting the effective Young's modulus for ordered and disordered packings. Using a $\rho^4=(\rho_{random}/\rho_{cubic})^4$ relation, the effective electrical conductivity is given by,

$$\sigma_{eff} = \sigma_p \frac{13.3 d_c \rho^4}{d} \tag{2.57}$$

Using ρ as the only measurement of packing structure, the model has successfully predicted the electrical conductivity of ceramic powders.

2.4.4. Electrostatic precipitation processes

The effective electrical conductivity of a layer of particle packing plays an important role in electrostatic precipitation processes. Air is usually an insulting medium, but the ionised air in electrostatic precipitation is capable of conducting electricity. When a high voltage is applied on a discharge electrode, the ionised gas molecules are produced and this process is called the corona discharging (see Figure 2.13). The negative polarity is usually applied to the electrode to produce negative ions, because a negative corona supports a higher voltage. The conductivity of ionised gases is given by [58-60],

$$\sigma_m = \frac{J}{E} = \rho_{ion} b \tag{2.58}$$

where ρ_{ion} is the space charge density and b is the ion mobility. Without the presence of particle packing on the collection plate, the conductivity of the ionised gases is approximately $1x10^{-9}$S/m. Fine particles passing through the ionised regions are firstly electrically charged through the attachment of ionised gas molecules, and then, they are precipitated on a collecting wall to form a packing of fine particles (see Figure 2.13). When a layer of particle packing is present, electric current must be conducted through the packing to establish a complete electrical circuit between the discharge electrode and the collecting wall. Almost all of the ionised gas molecules are attached to the particles before reaching the wall, and therefore, the ion concentration of the interstitial gases is low. Thus, the electrical conductivity of the interstitial gases is much smaller than that of the particles in the packing. As a result, electrical properties of precipitated packings determines the electrical conditions in electrostatic precipitation processes.

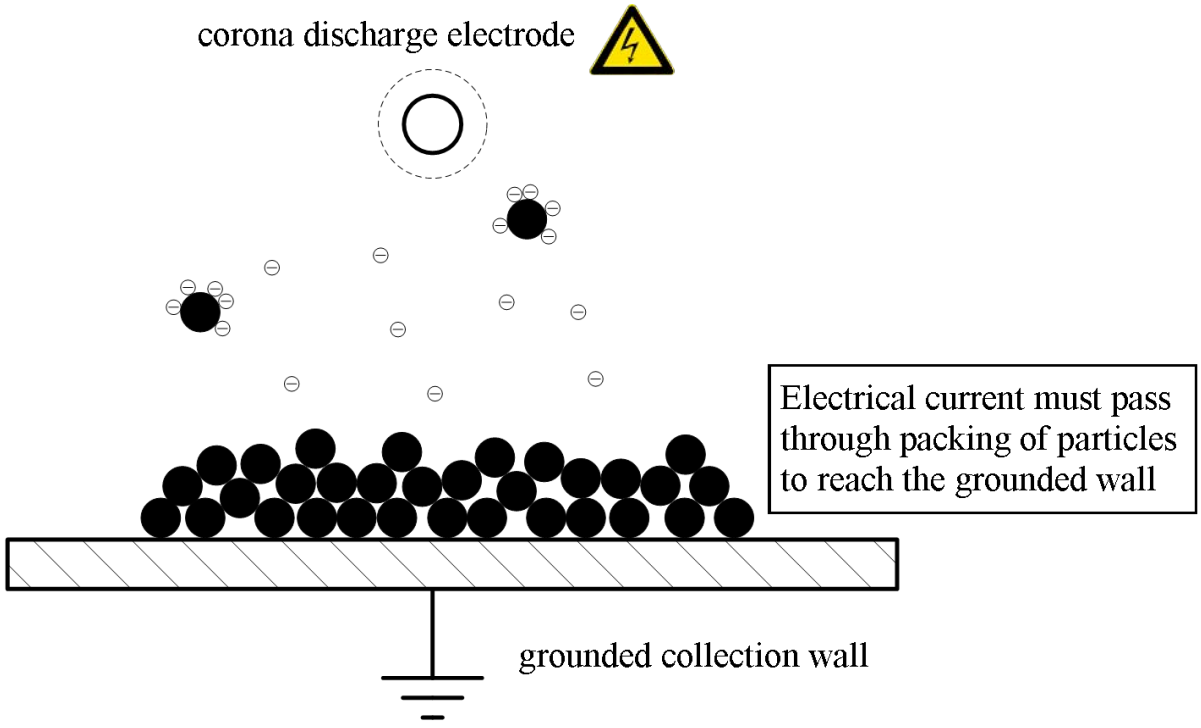

Figure 2.13: The schematic diagram of a packing formation and the electrical conditions in electrostatic precipitation processes.

Experimental studies on the effective electrical conductivity of packings are limited. This is due to the difficulty in characterisations of a packing in practical experiments. Masuda studied the effect of temperature on the effective electrical conductivity [61]. It was found that the temperature impact on the conductivity through changing the contributions from the surface and the volume conductivity of particles. When the temperature is lowered, there are always layers of water vapour adsorbed on the particles. The water vapour positively contributes to the surface conductivity of particles. As the temperature increases, the water vapour evaporates and therefore, the conductivity of the particles decreases. However, when all the adsorbed water vapour is evaporated at high temperature, further increasing the temperature causes the conductivity of particles to increases again. This is rationalised by the fact that the volume conductivity of the particles increases with the temperature. Thus, both the surface and volume conductivity of particles must be considered in the model for the effective electrical conductivity of a packing.

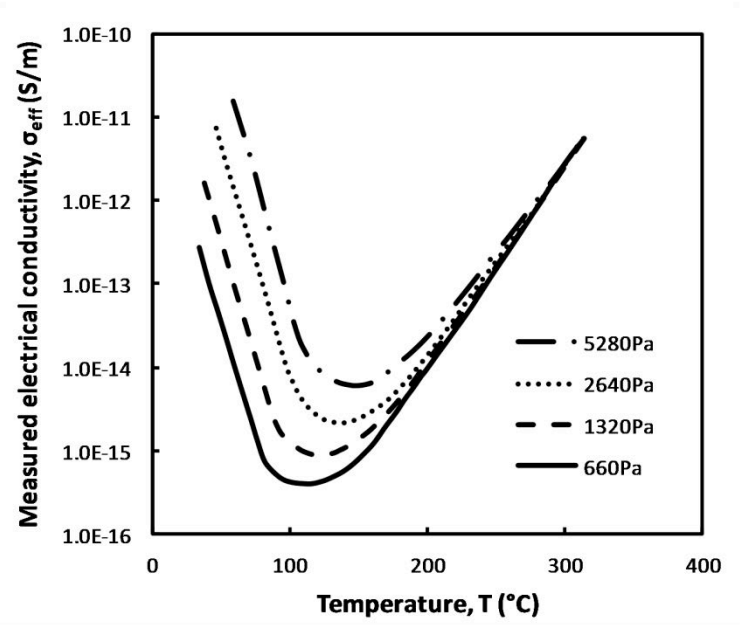

Figure 2.14: The effect of temperature on effective conductivity.

A previous parametric study of industrial electrostatic precipitators has revealed that the performance of the system deteriorates as the packing height increases (see Figure 2.15) [62]. From this study, we notice that the importance of the effective conductivity of precipitated packings in electrostatic precipitation is unquestionable. Amongst all the

factors determining the efficiency of electrostatic precipitators, the effect of gas flow and electric conditions have been intensely studied in literature [63]. The effect of the precipitated packings is difficult to study due to the limitation of practical experiments. In contrast, the characters of a packing can be readily examined in numerical simulations. Thus, we attempt to firstly simulate packings of fine particles under electric fields using the discrete element method and then examine the structure and the effective electrical conductivity of the simulated packings. This may lead to better understanding and subsequently design of electrostatic precipitation processes.

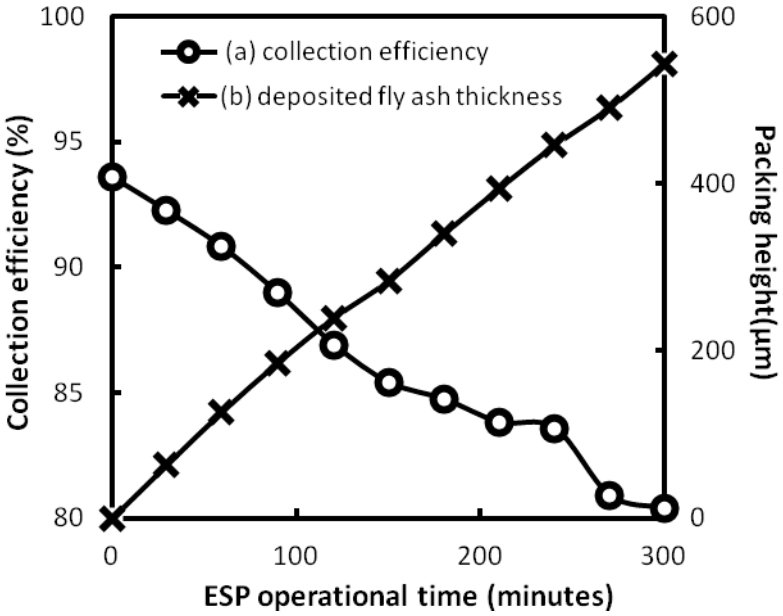

Figure 2.15: Experimental observations of the collection efficiency deteriorating along with the increasing packing height in electrostatic precipitation processes.

Nomenclature

m = mass

$\mathbf{v}$ = velocity

t = time

I = moment of inertia

$\mathbf{F}$ = force

T = torque

R = particle radius

Y = Young's modulus

n = unit vector

H_a = Hamaker constant

h = interparticle separation

E = electric field

k_p = dielectric constant

q = electrical charge

N_0 = ion density

b = ion mobility

k = Boltzmann constant

T_k = temperature

e = elementary charge

k_c = Coulomb’s constant

r = vectorial distance

p = dipole moment

h_d = particle-wall separation

d = particle diameter

V = volume

z = coordination number

x = location vector

J = electric current density

I = electric current

H = packing height

A = cross-sectional area

ΔV = electrical potential difference

r_c = contact radius

d_c = contact diameter

G_c = contact conductance

Greek Letters

$\boldsymbol{\omega}$ = angular velocity

ν = Poisson's ratio

ξ = the overlap between particles during collisions

γ = damping coefficient

μ = friction

ε_0 = vacuum permittivity

τ =charging time constant

ρ = packing fraction

Φ = porosity

φ = electrical potential

σ = conductivity

ζ = three point parameter

Γ = interfacial energy

Subscript

i, j = ith particle, jth particle

n = normal direction

s = tangential direction

r = rolling friction

e = electrical

p = particle phase

m = medium or gas phase

References

[1] D. Bideau and A. Hansen, *Disorder and Granular Media*: North-Holland, 1993.

[2] T. Pöschel and T. Schwager, *Computational granular dynamics*: Springer, 2005.

[3] D. C. Hong, *et al.*, "Reverse Brazil nut problem: competition between percolation and condensation," *Physical Review Letters,* vol. 86, p. 3423, 2001.

[4] P. Cundall and O. Strack, "A discrete numerical model for granular assemblies," ed: Dames and Moore London, England, 1979.

[5] N. V. Brilliantov, *et al.*, "Model for collisions in granular gases," *Physical Review E,* vol. 53, p. 5382, 1996.

[6] T. Schwager and T. Pöschel, "Coefficient of normal restitution of viscous particles and cooling rate of granular gases," *Physical Review E,* vol. 57, pp. 650-654, 1998.

[7] F. G. Bridges, *et al.*, "Structure, stability and evolution of Saturn's rings," 1984.

[8] P. A. Langston, *et al.*, "Discrete element simulation of granular flow in 2D and 3D hoppers: Dependence of discharge rate and wall stress on particle interactions," *Chemical Engineering Science,* vol. 50, pp. 967-987, 1995.

[9] R. D. Mindlin and H. Deresiewicz, "Timoshenko's shear coefficient for flexural vibrations of beams," *J. Appl. Mech.,* vol. 20, 1953.

[10] R. Y. Yang, *et al.*, "Computer simulation of the packing of fine particles," *Physical Review E,* vol. 62, p. 3900, 2000.

[11] J. N. Israelachvili, *Intermolecular and surface forces: revised third edition*: Academic press, 2011.

[12] K. J. Dong, *et al.*, "Settling of particles in liquids: Effects of material properties," *AIChE Journal,* vol. 58, pp. 1409-1421, 2012.

[13] K. J. McLean, "Electrostatic precipitators," *Iee Proceedings-a-Science Measurement and Technology,* vol. 135, pp. 347-361, 1988.

[14] H. J. White, "Particle charging in electrostatic precipitation," *American Institute of Electrical Engineers, Transactions of the,* vol. 70, pp. 1186-1191, 1951.

[15] W. Strauss, *Air pollution control, part I*: Wiley-Interscience, 1971.

[16] G. Liu, *et al.*, "Discrete-element method for particle capture by a body in an electrostatic field," *International Journal for Numerical Methods in Engineering,* vol. 84, pp. 1589-1612, 2010.

[17] R. Landauer, "Electrical conductivity in inhomogeneous media," *AIP Conference Proceedings,* vol. 40, pp. 2-45, 1978.

[18] M. Soltani, *et al.*, "Direct simulation of charged particle deposition in a turbulent flow," *International Journal of Multiphase Flow,* vol. 24, pp. 77-92, 1998.

[19] A. Li and G. Ahmadi, "Aerosol -particle deposition with electrostatic attraction in a turbulent channel flow," *Journal of Colloid and Interface Science,* vol. 158, pp. 476-482, 1993.

[20] D. W. Cooper, *et al.*, "Predicted deposition of submicrometer particles due to diffusion and electrostatics in viscous axisymmetric stagnation-point flow," *Aerosol Science and Technology,* vol. 11, pp. 133-143, 1989.

[21] N. V. Brilliantov and T. Pöschel, "Rolling friction of a viscous sphere on a hard plane," *Europhysics Letters,* vol. 42, p. 511, 1998.

[22] F. Beer, *et al.*, *Vector Mechanics for Engineers: Statics and Dynamics*, 6th Edition ed.: McGraw Hill, 2001.

[23] A. M. Yuen, "Collector current density and dust collection in wire-plate electrostatic precipitators," Ph.D thesis, School of Materials Science and Engineering, University of New South Wales, 2006.

[24] G. D. Scott, "Packing of spheres: packing of equal spheres," *Nature,* vol. 188, pp. 908-909, 1960.

[25] J. D. Bernal and J. Mason, "Coordination of randomly packed spheres," *Nature,* vol. 188, pp. 910-911, 1960.

[26] G. D. Scott, "Packing of equal spheres," *Nature,* vol. 188, pp. 908-909, 1960.

[27] J. L. Finney, "Random packings and the structure of simple liquids. I. The geometry of random close packing," *Proceedings of the Royal Society of London. A. Mathematical and Physical Sciences,* vol. 319, pp. 479-493, 1970.

[28] S. Torquato, *et al.*, "Is random close packing of spheres well defined?," *Physical Review Letters,* vol. 84, pp. 2064-2067, 2000.

[29] C. S. O'Hern, *et al.*, "Random packings of frictionless particles," *Physical Review Letters,* vol. 88, 2002.

[30] J. Miller, *et al.*, "Local deposition of particles in a laboratory scale electrostatic precipitator with barbed discharge electrodes," in *Sixth International Conference on Electrostatic Precipitation*, Budapest, 1996, pp. 325-334.

[31] E. Schmidt and F. Loffler, "Preparation of dust cakes for microscopic examination," *Powder Technology,* vol. 60, pp. 173-177, 1990.

[32] D. Blanchard, *et al.*, "Correlation between current density and layer structure for fine particle deposition in a laboratory electrostatic precipitator," *Ieee Transactions on Industry Applications,* vol. 38, pp. 832-839, 2002.

[33] M. Mizuno, *et al.*, "The estimation of packing characteristics by centrifugal compaction of ultrafine particles," *KONA Powder and Particle Journal,* vol. 9, pp. 19-27, 1991.

[34] W. Smith, *et al.*, "Packing of homogeneous spheres," *Physical Review,* vol. 34, p. 1271, 1929.

[35] H. Rumpf, "Grundlagen und methoden des granulierens," *Chemie Ingenieur Technik,* vol. 30, pp. 144-158, 1958.

[36] K. Ridgway and K. Tarbuck, "Random packing of spheres," *British Chemical Engineering,* vol. 12, p. 384, 1967.

[37] G. S. Cargill, "Dense random packing of hard spheres as a structural model for noncrystalline metallic solids," *Journal of Applied Physics,* vol. 41, pp. 2248-2250, 1970.

[38] G. F. Voronoi, "Nouvelles applications des paramètres continus à la théorie des formes quadratiques.," *Journal für die reine und angewandte Mathematik* vol. 134, p. 198, 1908.

[39] J. D. Bernal, "The Bakerian lecture, 1962. The structure of liquids," *Proceedings of the Royal Society of London. Series A, Mathematical and Physical Sciences,* pp. 299-322, 1964.

[40] R. Y. Yang, *et al.*, "Voronoi tessellation of the packing of fine uniform spheres," *Physical Review E,* vol. 65, p. 041302, 2002.

[41] L. Oger, *et al.*, "Voronoï tessellation of packings of equal spheres," *Powders and grains,* vol. 97, pp. 287-290, 1997.

[42] L. Oger, *et al.*, "Voronoi tessellation of packings of spheres: topological correlation and statistics," *Philosophical Magazine B,* vol. 74, pp. 177-197, 1996.

[43] G. J. Cheng, *et al.*, "Evaluation of effective thermal conductivity from the structure of a packed bed," *Chemical Engineering Science,* vol. 54, pp. 4199-4209, 1999.

[44] L. Rayleigh, "On the influence of obstacles arranged in rectangular order upon the properties of a medium," *Philosophical Magazine Series 5,* vol. 34, pp. 481-502, 1892.

[45] J. C. Garland and D. B. Tanner, "Electrical transport and optical properties of inhomogeneous media," American Institute of Physics, New York1978.

[46] J. C. Maxwell, *A treatise on electricity and magnetism* vol. 1: Clarendon Press, 1881.

[47] D. J. Jeffrey, "Conduction through a random suspension of spheres," *Proceedings of the Royal Society of London. A. Mathematical and Physical Sciences,* vol. 335, pp. 355-367, 1973.

[48] J. C. R. Turner, "Two-phase conductivity : The electrical conductance of liquid-fluidized beds of spheres," *Chemical Engineering Science,* vol. 31, pp. 487-492, 1976.

[49] D. A. G. Bruggeman, "Calculation of various physics constants in heterogenous substances I Dielectricity constants and conductivity of mixed bodies from isotropic substances," *Annalen Der Physik,* vol. 24, pp. 636-664, Nov 1935.

[50] G. E. Archie, "The electrical resistivity log as an aid in determining some reservoir characteristics," *Transactions of the American Institute of Mining and Metallurgical Engineers,* vol. 146, pp. 54-61, 1942.

[51] S. Torquato, "Effective electrical conductivity of two phase disordered composite media," *Journal of Applied Physics,* vol. 58, pp. 3790-3797, 1985.

[52] Z. Y. Zhou, *et al.*, "A new computational method for studying heat transfer in fluid bed reactors," *Powder Technology,* vol. 197, pp. 102-110, 2010.

[53] R. Holm, *Electric contacts theory and application*. New York: Springer-Verlag, 1967.

[54] G. B. Moslehi and S. A. Self, "Current flow across a sphere with volume and surface conduction," *Journal of Electrostatics,* vol. 14, pp. 7-17, 1983.

[55] G. B. Moslehi and S. A. Self, "Electromechanics of precipitated particulate layers," *Ieee Transactions on Industry Applications,* vol. 20, pp. 1598-1606, 1984.

[56] G. K. Batchelor and R. W. O'Brien, "Thermal or electrical conduction through a granular material," *Proceedings of the Royal Society of London. Series A, Mathematical and Physical Sciences,* vol. 355, pp. 313-333, 1977.

[57] K. Kendall, "Electrical conductivity of ceramic powders and pigments," *Powder Technology,* vol. 62, pp. 147-154, 1990.

[58] H. E. Rose and A. J. Wood, *An introduction to electrostatic precipitation in theory and practice*: Constable, 1966.

[59] H. J. White, "Industrial electrostatic precipitation," in *Industrial electrostatic precipitation,* ed: Addison-Wesley, 1963.

[60] K. Parker, *Electrical operation of electrostatic precipitators*: IET, 2003.

[61] S. Masuda, "Effects of temperature and humidity on the apparent conductivity of high resistivity dust," *Electrotech journal, Japan,* vol. 7, p. 108, 1962.

[62] S. H. Kim and K. W. Lee, "Experimental study of electrostatic precipitator performance and comparison with existing theoretical prediction models," *Journal of Electrostatics,* vol. 48, pp. 3-25, 1999.

[63] A. Jaworek, *et al.*, "Modern electrostatic devices and methods for exhaust gas cleaning: A brief review," *Journal of Electrostatics*, vol. 65, pp. 133-155, 2007.

CHAPTER 3. NUMERICAL STUDY OF THE PACKING OF FINE PARTICLES UNDER UNIFORM ELECTRIC FIELDS

Abstract

A numerical model based on the discrete element method is developed to investigate packings of fine particles under uniform electric fields relating to electrostatic precipitation processes. The simulated particles are electrically charged and deposited to form a stable packing under the influence of the electrostatic interactions induced by the imposed electric fields. Our results reveal that increasing either the particle diameter or electric field will cause the packing fraction of a packing to increase until it reaches a limiting packing fraction that approximately equals to the packing fraction of random loose packing. The corresponding structural changes are analysed in terms of coordination number, radial distribution function and other topological and metric properties generated from the Voronoi tessellation. The results indicate that the changes in packing structures according to packing fraction are similar to those found in the packings under gravity. The similarities are rationalised by the competition between the cohesive force between particles and the field force that forms the stable packings. In particular, we demonstrate that by replacing the gravitational force with the electrostatic interactions, the existing correlation between packing fraction and the rario of the cohesive force to the field force is still applicable in the case of the packing of fine particles under electric fields.

3.1. Introduction

Electrostatic precipitation process is one of the most commonly used methods to clean flue gas in industrial processes, such as coal power plants, incineration plants and pulp mills etc. In this process, the fine particles in flue gas are electrically charged during the flight, and then deposited on collection walls to form a layer of particle packing by the electrostatic interactions induced by the imposed electric field [1]. Recent environmental regulations have renewed research interests on the improvement of electrostatic precipitation processes in order to meet stricter air pollution standards [2].

Early experimental studies have determined that the collection efficiency of electrostatic precipitation processes is influenced by the factors, e.g., inlet pressure, material resistivity, particulate load, interelectrode distance etc, which are relating to the operational condictions, the geometry of electrodes and the material properties of particles in the systems [3-5]. However, it has been difficult to gain insightful information about the in situ behaviour of particles due to the high voltage environment. Theoretical and numerical studies have mainly focused on the optimisation of the gas flow and the electrical conditions of the process [6-8]. The effectiveness of these approaches is usually limited to specific geometric configurations, because of the lack of the fundamental understanding of the particle collection process, particularly, the precipitated packings on collection walls and the subsequent effects on the electrical and flow conditions. Particle packing is in fact essential to electrostatic precipitation processes [9, 10]. For example, the overall collection efficiency has been observed to deteriorate with the growth of a layer of particle packing on collection walls [11, 12]. The formation of a packing provides additional resistance to the flow of electric current between electrodes, and therefore, negatively impact on the electrical conditions in the process. In general, the electrical properties of a packing structure is dependent on its structure. Thus, it is important to understand the formation and the consequent structure of the formed packings in electrostatic precipitation processes.

To address these issues, process simulation on a computer, in particular, by the discrete element method provides an effective alternative [13]. As a state of the art numerical technique, the discrete element method has shown its validity and wide applications in the research of particle packing [14]. In the past, it has been successfully applied in the study of the formed packings under gravity, in sedimentation etc [15, 16]. One of the advantages of the discrete element method is the dynamics process of packing formation is simulated, where the forces exerting on every particle are considered. The use of the first principle ensures that the simulation results are more comparable with the experimental observations than those from the models that geometrically determine the interaction between particles [17]. Also, the detailed structural and force analysis is readily available in the discrete element method, and consequently, the mechanism of the packing formation can be better understood. Thus, the discrete element method has increasingly been applied in the studies of particle packing. However, to our knowledge,

little has been done on packings of particles under electric fields, where the electrostatic interactions are included.

In this work, we study packings of fine particles under electric fields using the discrete element method. The effects of the particle diameter and electric field on the packing structure are quantified in terms of packing fraction, and microscopic parameters, such as coordination number, radial distribution function and other properties from Voronoi tessellations. The role of the interparticle forces in the packings is explored, which may lead to a better understanding of the formation mechanism of particle packing under electric fields.

3.2. Numerical Model

In the discrete element method, the translational and rotational motions of particle i are described by the following equations:

$$m_i \frac{d\mathbf{v}_i}{dt} = \mathbf{F}_i \tag{3.1}$$

and

$$I_i \frac{d\boldsymbol{\omega}_i}{dt} = \mathbf{T}_i \tag{3.2}$$

where m_i is the mass, $\mathbf{v}_i$ is the translational velocity, I_i is the moment of inertia, $\boldsymbol{\omega}_i$ is the angular velocity. $\mathbf{F}_i$ is the total force on the particle and $\mathbf{T}_i$ is the torque induced from the interaction of the particle with its neighbours, which are respectively given by:

$$\mathbf{F}_i = \sum \left(\mathbf{F}_{ij}^{n} + \mathbf{F}_{ij}^{s} + \mathbf{F}_{ij}^{vdw} \right) + \mathbf{F}_i^{e} \tag{3.3}$$

and

$$\mathbf{T}_i = \sum \left(\mathbf{R}_i \times \mathbf{F}_{ij}^s + \mathbf{T}_{ij}^r \right) \tag{3.4}$$

$\mathbf{F}_{ij}^n$, $\mathbf{F}_{ij}^s$ and are respectively the normal and tangential contact forces, $\mathbf{F}_{ij}^{vdw}$ is the van der Waals interactions between particle i and j, $\mathbf{F}_i^e$ represents the electrostatic interactions, and $\mathbf{T}_{ij}^r = -\mu_r R_i |\mathbf{F}_{ij}^n| \hat{\boldsymbol{\omega}}_i$ is the torque caused by the rolling friction between particle i and j, where $\hat{\boldsymbol{\omega}}_i = \boldsymbol{\omega}_i / |\boldsymbol{\omega}_i|$. The detailed equations to calculate these forces are listed in Table 3.1. The normal contact force on particle i from its contacting neighbour particle j consists of an elastic component and a viscous dissipative component. The elastic component is based on the Hertz model, and depends on $\bar{R} = R_i R_j / (R_i + R_j)$, the overlap or deformation between two particles ξ_n , and the effective modulus $Y' = Y/(1-\nu^2)$, where Y and ν are the Young's modulus and the Poisson's ratio. The second term of the normal contact force equation represents the damping component, where $\mathbf{v}_{ij} = \mathbf{v}_j - \mathbf{v}_i$, and γ_n is the normal damping coefficient, which is directly related to the normal coefficient of restitution [18, 19]. The tangential contact force acting on the contacting particles depends on the normal contact force. ξ_s is the tangential displacement and there exists a maximum tangential displacement $\xi_{s,\max} = \mu_s [(2-\nu)/2(1-\nu)] \xi_n$, beyond which the sliding between particles occurs [20, 21]. ξ_s is the unit vector of the tangential displacement, and μ_s is the sliding friction coefficient. $\hat{\mathbf{n}}_{ij}$ is the unit vector in the direction between the centers of particles i and j.

Table 3.1: The forces exerting on particle in the simulation.

Forces	**Equations**
Normal contact force	$\mathbf{F}_{ij}^{n} = \left[\frac{2}{3}Y'\sqrt{\overline{R}}\xi_n^{\frac{3}{2}} - \gamma_n Y'\sqrt{\overline{R}}\sqrt{\xi_n}\left(\mathbf{v}_{ij}\cdot\hat{\mathbf{n}}_{ij}\right)\right]\hat{\mathbf{n}}_{ij}$
Tangential contact force	$\mathbf{F}_{ij}^{s} = -\mu_s\left\|\mathbf{F}_{ij}^{n}\right\|\left[1-\left(1-\frac{\min\left(\xi_s,\xi_{s,\max}\right)}{\xi_{s,\max}}\right)^{\frac{3}{2}}\right]\hat{\xi}_s$
van der Waals interactions	$\mathbf{F}_{ij}^{vdw} = -\frac{H_a}{6}\times\frac{64R_i^3R_j^3\left(h+R_i+R_j\right)}{\left(h^2+2R_ih+2R_jh\right)^2\left(h^2+2R_ih+2R_jh+4R_iR_j\right)^2}\hat{\mathbf{n}}_{ij}$
Electrostatic interactions	$\mathbf{F}_i^e=(q\mathbf{E}+q^2/16\pi\varepsilon_0 {h_d}^2)\hat{\mathbf{n}}_E$

The van der Waals interactions is included in our simulation, because early study indicates it is significant when particle diameter is less than 100μm [22]. H_a is the Hamaker constant, and h is the separation between the neighbouring particle surfaces. There is a minimum separation h_{min} in the present study to represent the repulsive force when the separate h is zero to avoid singular attractions [23]. Note that the gravitational force is not considered here because charged particles are driven to form a layer of particle packing on the collection walls in electrostatic precipitation processes under the electrostatic interactions that are perpendicular to the walls. Conversely, the gravitational force acts parallel to the walls, and hence, contributes little to the packing formation.

$\mathbf{F}_i^e$ represents the collective electric-field-induced electrostatic interactions, which is given by,

$$\mathbf{F}_i^e=(q\mathbf{E}+q^2/16\pi\varepsilon_0 {h_d}^2)\hat{\mathbf{n}}_e \tag{3.5}$$

where $\mathbf{E}$ is the electric field; $\hat{\mathbf{n}}_e$ is the unit vector along the direction of the electric field, ε_0 is the vacuum permittivity, h_d is the particle-wall separation, and q is the amount of

charge on the particle. The first term in Eq.3.5 represents the Coulomb's force; and the second term represents the boundary image force between particle and wall. The charging time is usually much smaller than the precipitation time in electrostatic precipitation systems. Therefore, the electrical charging process is assumed as an instantaneous process, and we apply the maximum charge on a dielectric particles, which is given by [24]:

$$q = 16\pi\varepsilon_0 \left[2\left(k_p - 1\right)/\left(k_p + 2\right) + 1\right] d^2 \mathbf{E} \tag{3.6}$$

where k_p is the dielectric constant of the particle. It should be noted that the discharging process is also neglected, because the charging process is continuous and the conductivity of dielectric particles are generally poor. Also, we only consider uniform electric fields, and packings of fine particles under non-uniform electric fields will be discussed in the next chapter.

Despite the fact that the electrical charged particles in a packing may experience the electrostatic interactions induced by their neighbouring charged particles, they are not included in the present model for several reasons. First of all, we estimate that the electrostatic interactions induced by the neighbouring particles are extremely small comparing to the van der Waals interactions between particles. For example, the electric dipole interaction between two charged particles in an external electric field is given by:

$$\mathbf{F}_{dipole} = \frac{3\pi}{8}\left(\frac{\varepsilon_r - 1}{\varepsilon_r + 2}\right)^2 \varepsilon_0 d^2 \mathbf{E}^2 \tag{3.7}$$

where ε_r is the relative permittivity [25]. Hence, the electric dipole interaction between two silica particles of diameter 10^{-6} to 10^{-3}m under an external electric field of 10^6V/m is in the range of 10^{-14} to 10^{-8}N, which is a few orders of magnitude smaller than the van der Waals interactions in the range of 10^{-9} to 10^{-6}N. When there are more than two particles, the electrostatic interaction induced by the multipole moments is even weaker than the dipole interaction. Secondly, the exact charge distribution on each particle in the packing must be determined in order to calculate the electrostatic interactions

induced by the neighbouring particles. However, these calculations are impractical to simulate using the current computer technology. Thirdly, when a small current is passing through a packing structure, an electrical clamping force is experimentally observed on the macroscopic scale [26, 27]. However, the exact nature of such a force is never fully understood on the microscopic scale. The possible effect of the electrostatic interactions between the neighbouring particles due to the electrical clamping force may have to be studied in the future. Therefore, the negligence of the electrostatic interaction induced by the neighbouring particles is justified for the time being.

The packing of fine particles under electric fields is a dynamic process whose features must be considered carefully. In this work, a typical simulation starts with random generation of particles above an imaginary collection wall, while periodic boundaries are applied to the side walls as illustrated in Figure 3.1. It is worthy noting that all our simulations are conducted in 3D. The particles are generated in a set volume with an initial porosity of 0.919 to assure that they are dilutely dispersed, which is the same as the conditions in conventional electrostatic precipitation processes. Then, the particles are attracted to the collection wall in the presence of an imposed electric field, and consequently, a layer of particle packing starts to form. The simulation ends when all particles reached their stable positions with zero velocity.

In general, packing structures are formed under the influence of the Coulomb's force. However, in the regions close to the collection wall, the boundary image force plays an important role. The variations of the applied forces on each particle in a packing with the packing height above the collection wall is revealed in Figure 3.2. The results indicate that the boundary image force increases dramatically when the particle is approaching the collection wall. The findings are consistent with Eq.3.5. Under the simulation conditions, when the particle-wall distance is more than two particle diameter, the contribution of the image force to the total electrostatic interactions is insignificant. The majority of the particles, in particular, the particles at the centre of the packing are only influenced by the Coulomb's force. Thus, we only examine the Coulomb's force in the force analysis of the results section.

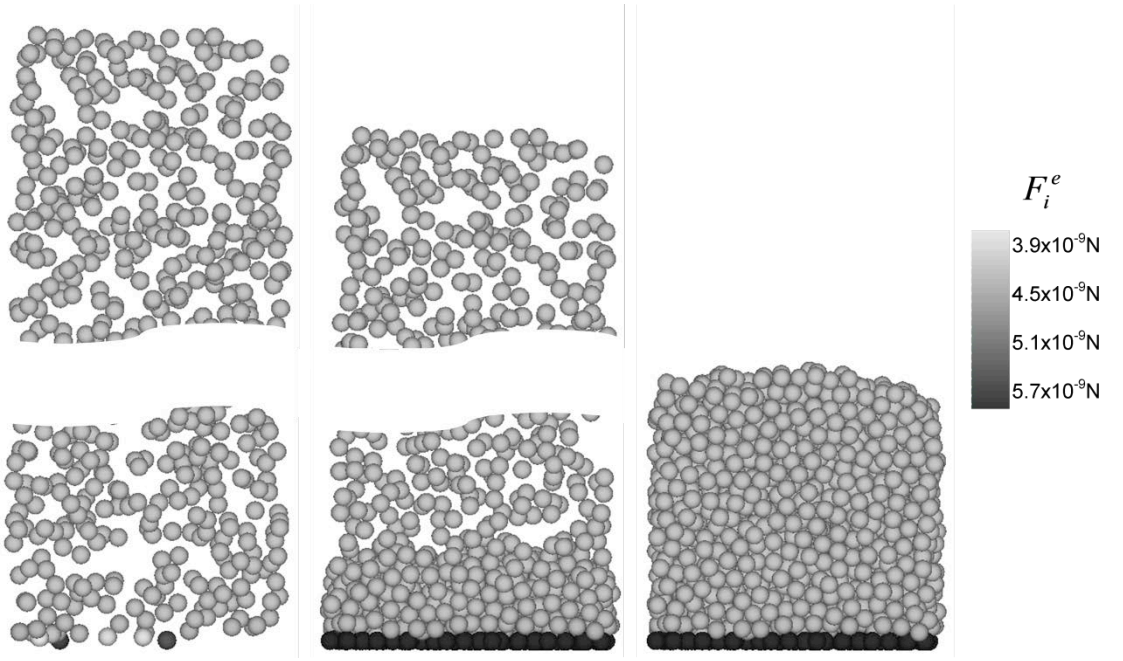

Figure 3.1: The snapshots showing the formation of a typical packing. The particles are coloured according to the magnitude of the electric interactions (from left to right: *t*=0s, 0.06s, 0.1s).

The present study focuses on the effects of two important variables, i.e., particle diameter and electric field. These effects are investigated by changing one variable while the other is kept constant as listed in Table 3.2. The parameters selected for the simulations are largely based on SiO_2 which is the main component of the fly ashes collected in the electrostatic precipitation process at coal-fired power stations.

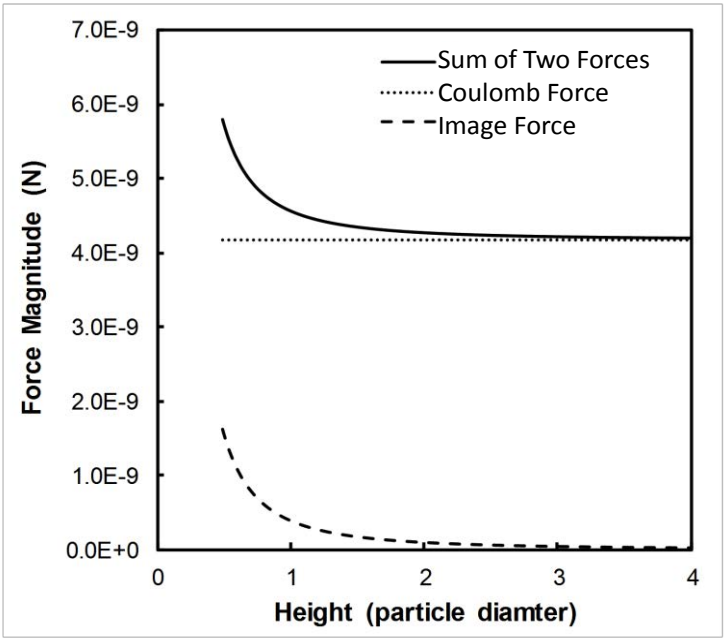

Figure 3.2: The comparisons of the electrostatic interactions at various heights.

Table 3.2: Parameters used in simulation.

Number of particles	3500
Particle diameter, d	*1 μm - 1 mm*
Electric field, **E**	$1x10^{4}$-$1x10^{6}$ *V/m*
Mass density, ρ_m	2500 kg/m^{-3}
Young's modulus, Y	1 x 10^{7} Pa
Poisson's ratio, v	0.29
Sliding friction coefficient, μ_s	0.4
Rolling friction coefficient, μ_r	0.02
Hamaker's constant, H_a	6.5 x 10^{-20} J
Initial porosity, ϕ_0	0.918551
Dielectric constant, k_p	2
Vacuum permittivity, ε_0	8.854x10^{-12} F/m

3.3. Results and Discussion

3.3.1. Model validation

To validate the developed model, our simulation results are quantitatively compared with the experimental measurements by Zhu et al, who have investigated the effect of electrode-wall spacings on the performance of an electrostatic precipitation system [28]. Based on their data, we have theoretically estimated the imposed electric fields according to the different electrode-wall spacings [29], which are then applied in our simulations. The packing fraction of the resultant packing structures are compared with the experimental measurements (see Table 3.3). A reasonable agreement between the predicted and measured results under various electric fields confirms the validity of the proposed model.

Table 3.3: The comparison of packing fraction in simulated and experimental packings.

E (V/m)	ρ (simulated)	ρ (experimental)
2.874×10^5	0.5415	0.5278
3.677×10^5	0.5611	0.5222
3.542×10^5	0.5550	0.5500
2.865×10^5	0.5392	0.5222

3.3.2. Macroscopic analysis

The effects of particle diameter and electric field on the structure of the packings under uniform electric fields are firstly examined in terms of packing fraction. Early study of packings of particles under gravity has demonstrated that the packing fraction decreases significantly with the particle diameter [30]. It has been suggested that the interparticle van der Waals interactions dominate when the particle diameter is reduced to below 100μm, and consequently, the packing fraction decreases with the diameter. Figure 3.3a

demonstrates that the packing fraction of the simulated packings also decreases with the particle diameter. However, the degree of the change in the packing fraction with the particle diameter varies according to the imposed electric field. This is because the electrostatic interactions acting as the driving force in the packing formations vary with the electric field. The simulations show that the formed packings under weak electric fields are loose, while dense packings are formed under strong electric fields. It can be seen that the packing fraction of small particles decreases more significantly with the decrease of electric field than that of large particles. This is due to that the ratio of cohesion to the electric force is larger for smaller particles under the same electric field strength, similar to the packing of fine particles under gravity [32]. With the increased electric field, the effect of cohesion becomes negligible and the packing fraction of particles of different sizes all approached to about 0.61, which is also consistent with the value of random loose packing obtained under gravity. Such results also explain that the effect of electric field is less significant for large particles as compared to small particles. Figure 3.3b directly shows that the packing fraction decreases with the electric field for various packings. It can be seen that the effect of electric field is more significant for smaller particles. Nevertheless, these trends are qualitatively consistent with the experimental observations in literature [9, 31].

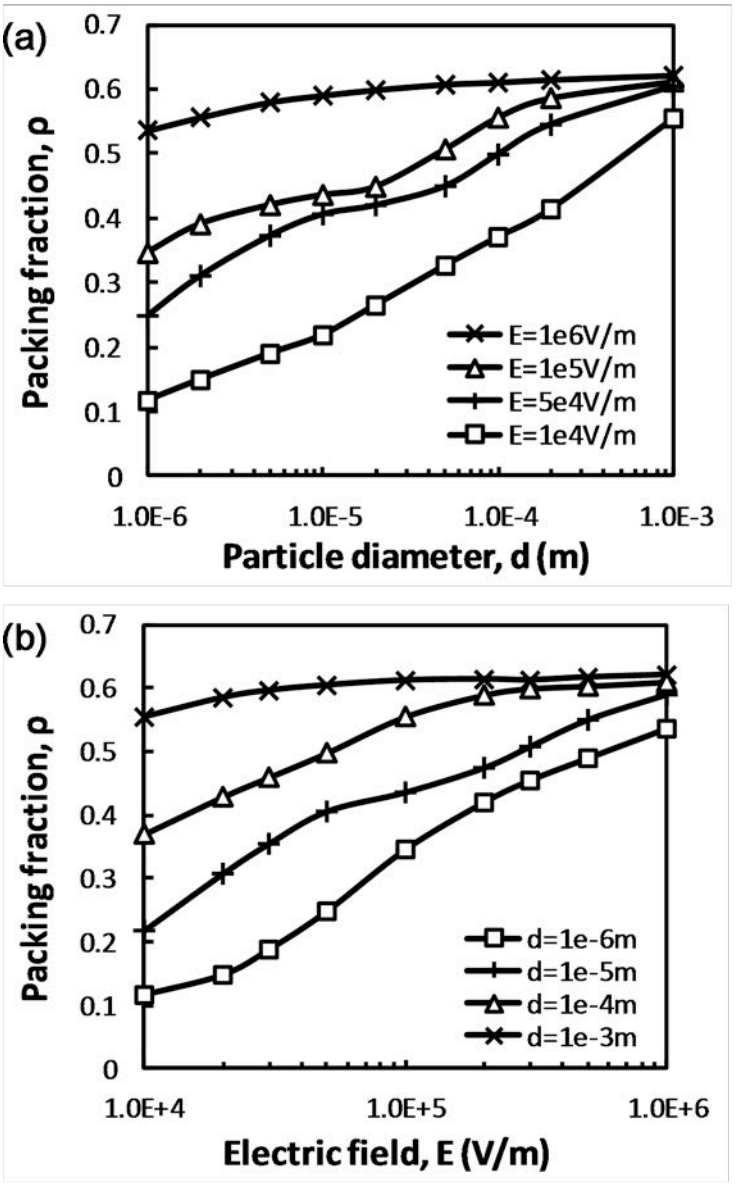

Figure 3.3: The increase of the packing fraction with the increase of: (a) the particle diameter under various electric fields; and (b) the imposed electric field for a range of particle diameters.

3.3.3. Microscopic structures

The simulations are not only capable of giving packing fraction, but are also capable of producing detailed packing structures. Figure 3.4 shows that the packing structure changes from loose chain-like to dense tetrahedron packing as the packing fraction

increases. In the following sections, we examine the resulting packing structures generated under different conditions in terms of coordination number, radial distribution function and other properties from the established Voronoi tessellation.

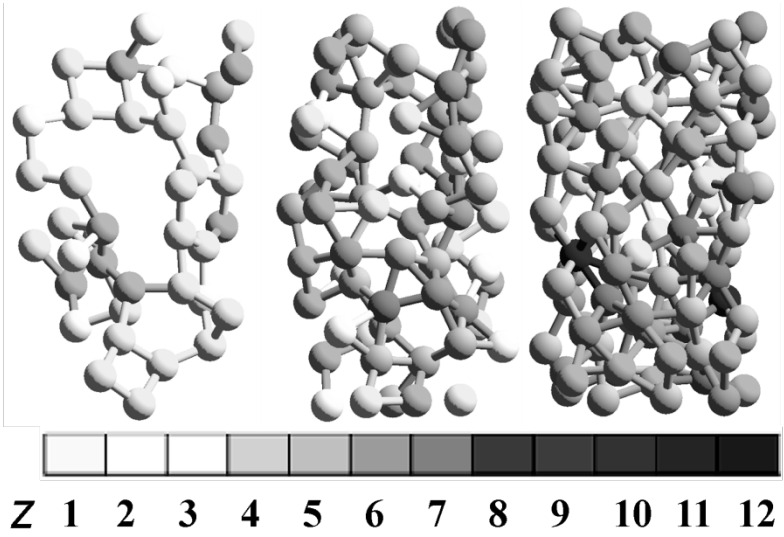

Figure 3.4: Formed structures under an electric field of 50,000 V/m: left, d=1μm and ρ=0.248; middle, d=10μm and ρ=0.406; and right, d=1000μm and ρ=0.604. Spheres represent particle, and sticks represents the contact between particles. The particles are coloured according to their coordination number.

Figure 3.5a illustrates that the distribution of coordination number in the various formed packings under different conditions. First of all, the peak of the distribution shifts to the left when the packing fraction of the packing decreases. Secondly, the distribution of coordination number are very similar for the packings with similar packing fractions. These findings are in good ment with the so called quasi-universality for the packings under gravity [23]. In addition, our results demonstrate that the averaged coordination number of the formed packings under electric fields can be correlated with the packing fraction regardless of the different particle diameters and electric fields (see Figure 3.5b). The correlation is consistent with that derived from the study of the packing of fine particles under gravity. Such observations strongly suggest that the correlation between coordination number and packing fraction of packing is independent of the method of packing [23, 32].

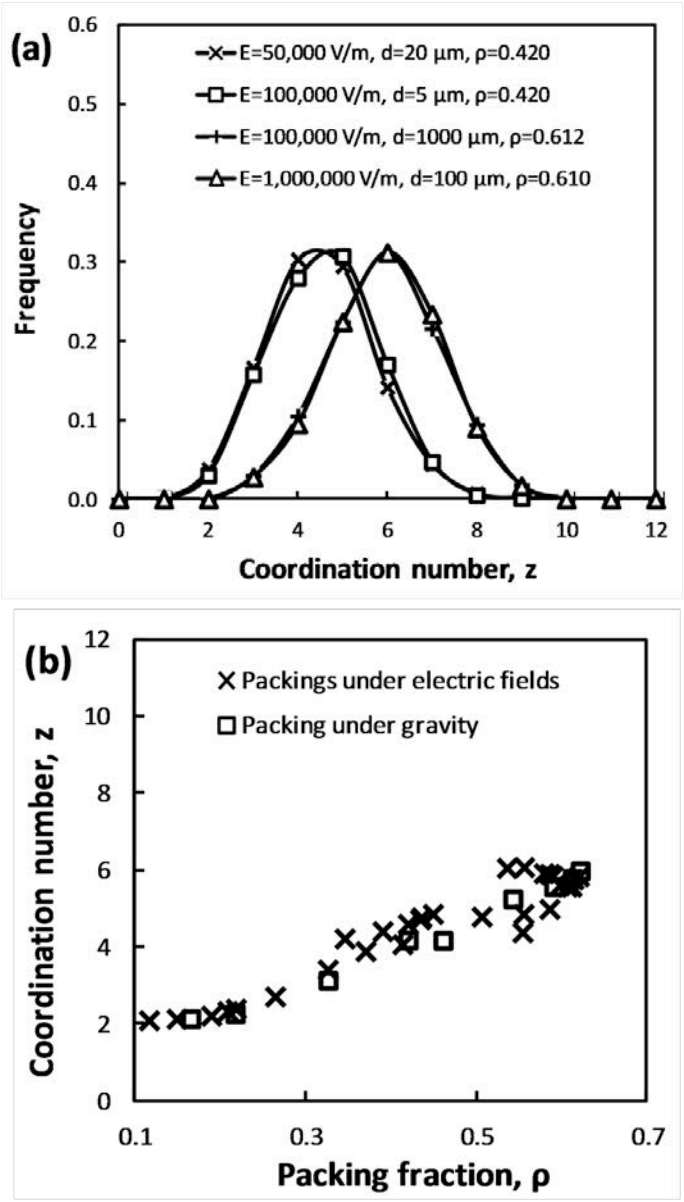

Figure 3.5: (a) The comparison of the coordination number distribution of the formed packings under various electric fields using a wide range of particle diameters. (b) Variations of the averaged coordination number with the packing fraction of the packing under electric fields and gravity.

Next, we analyse the simulated packing structures using the radial distribution function, that quantifies the probability of finding a particle at a certain distance from a reference particle. As shown in Figure 3.6, the number of peaks of the radial distribution function and their magnitude decrease with both the particle diameter (see Figure 3.6a) and the electric field (see Figure 3.6b). Noticeably, the split of the second peak in the radial distribution function of the relatively dense packings suggests the presence of short

range order in their structure. The findings are consistent with the observations from packings of non-cohesive particles [32]. Furthermore, as the particle diameter decreases, the second peak becomes weaker, which implies a more amorphous packing. The similar trend is observed when the electric field becomes smaller while the particle diameter remains the same (see Figure 3.6b).

The packing structure is further quantified in terms of the properties of Voronoi cells through the process of Voronoi tessellation, which partitions the packing space using non-overlapping polyhedra. As a result, more detailed local structural information is revealed for both particles and interstitial pores. The method has been found to be helpful in modelling transport properties through a packing, i.e., electrical and thermal conductivities [33, 34]. The exact method of Voronoi tessellation can be found in the previous chapter.

The Voronoi tessellation is carried out for all the simulated packings, and two types of properties are obtained:

(i) topological properties, e.g. the averaged number of faces per polyhedron, and the averaged number of edges per polyhedron face;
(ii) metric properties, e.g. the averaged perimeter and area per polyhedron face, the averaged surface area and sphericity ψ per polyhedron.

The results have been compared with the experimental or numerical data from the studies of packings of cohesionless and cohesive particles [35, 36].

Figure 3.7 shows that both the averaged number of faces per polyhedron and the averaged number of edges per polyhedron face increase with the packing fraction. The results are consistent with the previous findings. It is worth noting that the values of the packing fraction in the present study cover a wider range, compared to the data in the literature.

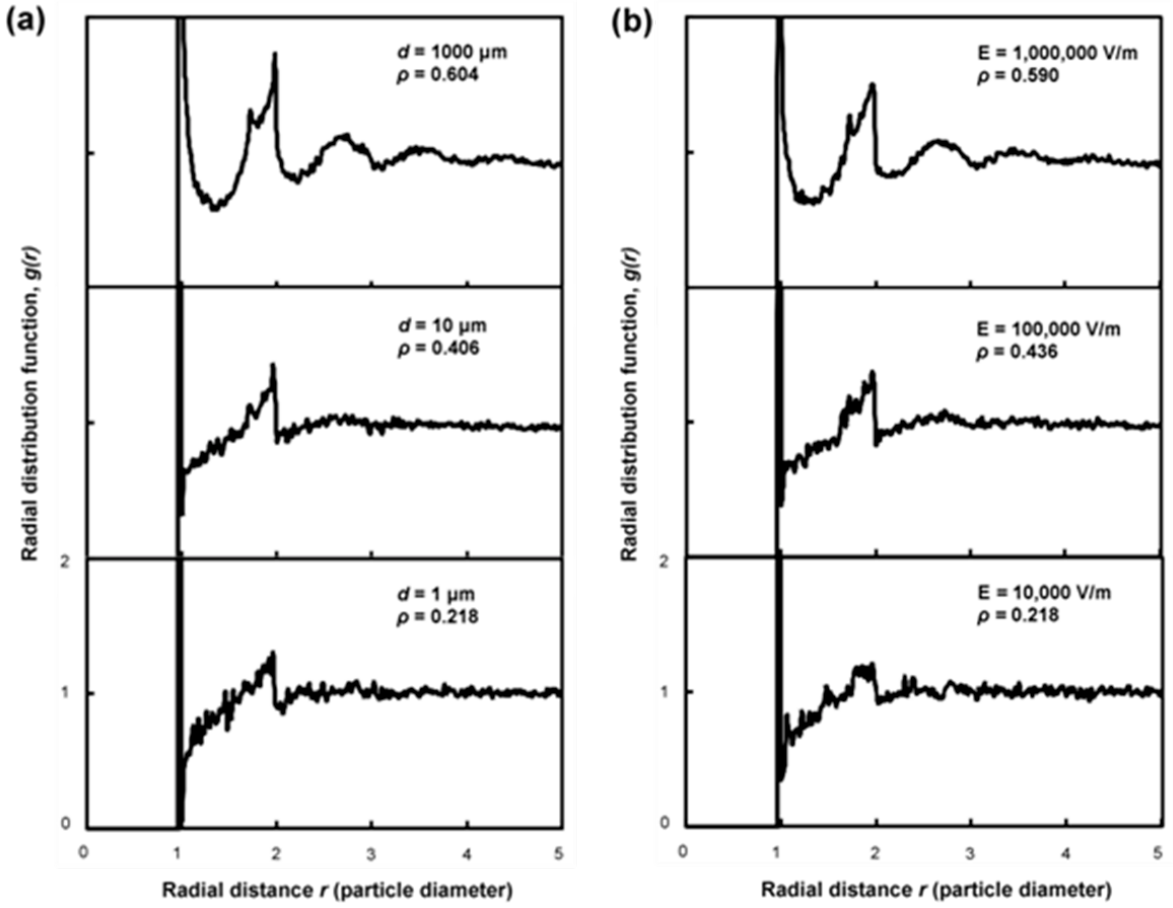

Figure 3.6: Variations of the radial distribution function with the packing fraction. The packings are formed (a) under an electric field of 50,000V/m; (b) with 10µm particles.

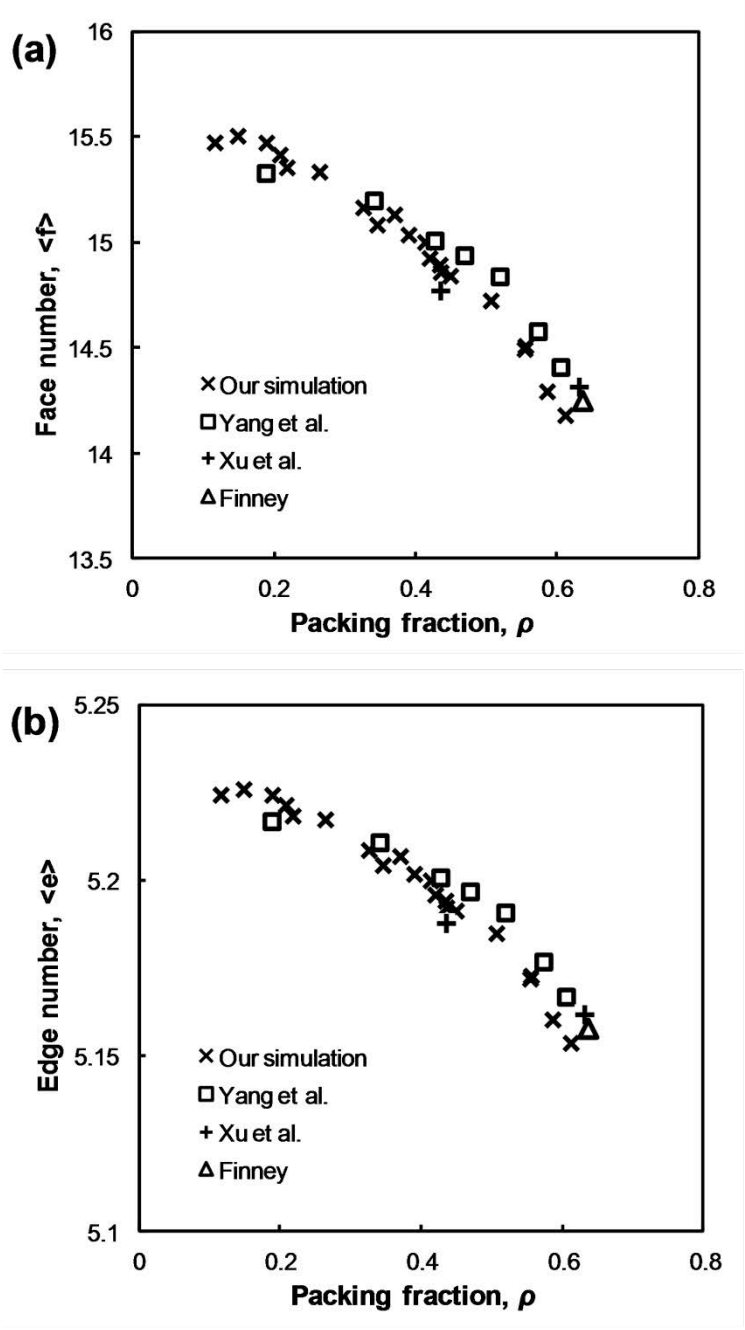

Figure 3.7: Topological properties of Voronoi polyhedra (a) the averaged number of faces <*f*>; (b) the averaged number edge in a polyhedron <*e*> are plotted against the packing fraction.

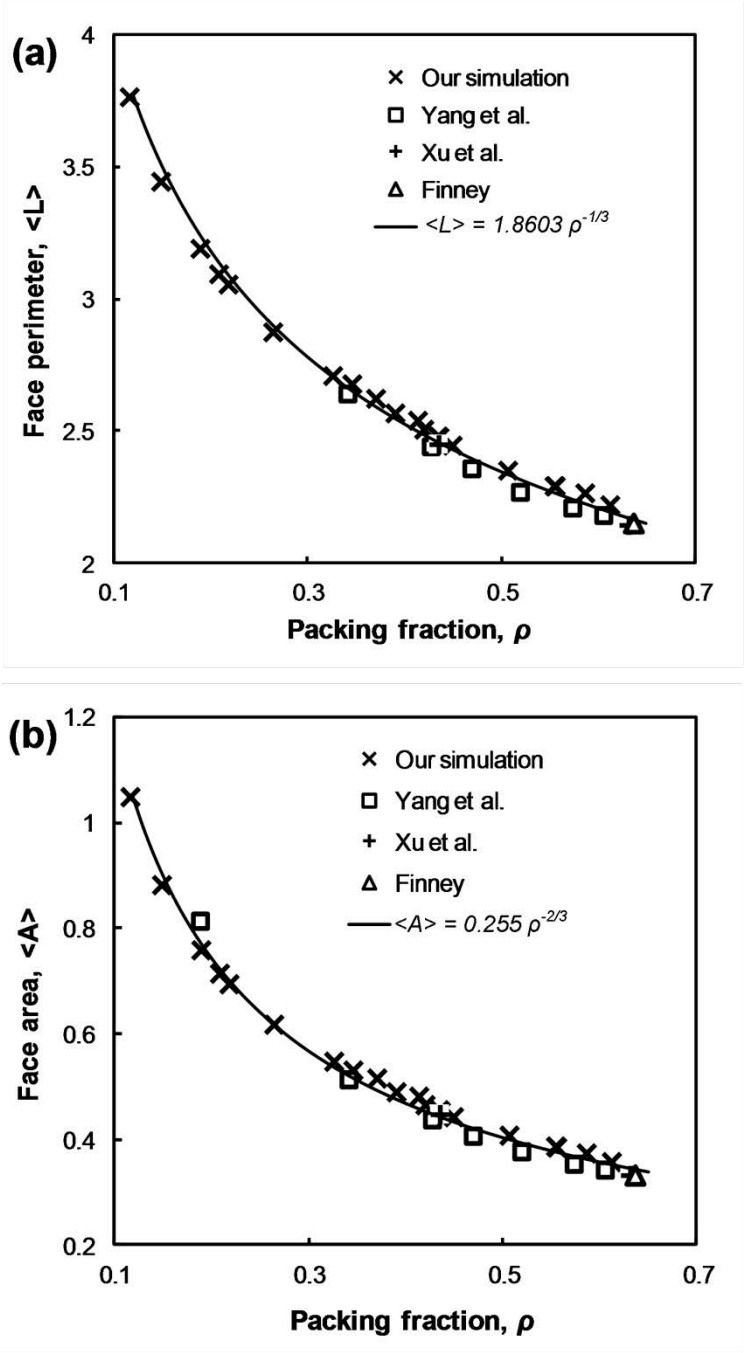

Figure 3.8: Metric properties of Voronoi polyhedra, (a) the averaged face perimeter $<L>$ and (b) the averaged face area of polyhedra $<A>$, as a function of packing fraction.

In terms of the metric properties, i.e., the averaged face perimeter and the averaged face area of polyhedra also vary with the packing fraction. The face properties are found to be inversely proportional to the number of touching particles. The trendlines of these

properties show that the averaged face perimeter and the averaged face area of polyhedra are proportional to $\rho^{-1/3}$ and $\rho^{-2/3}$ respectively (see Figure 3.8), and thus confirming previously established relations [37]. At low packing densities, there are less touching particles and hence resulting in a longer face perimeter and a larger face area. Furthermore, Figure 3.9 demonstrates that the surface area of polyhedra increases and the Voronoi polyhedra are less spherical with a decease in the packing fraction. Geometrically speaking, a large Voronoi surface area and less sphericity infer a loose packing structure. Again, our findings are in good agreement with the previous experimental and numerical results. These agreements further confirm the existence of some general relationships between mcrosscopic and macroscopic packing properties; and the latter is usually represented by the packing fraction.

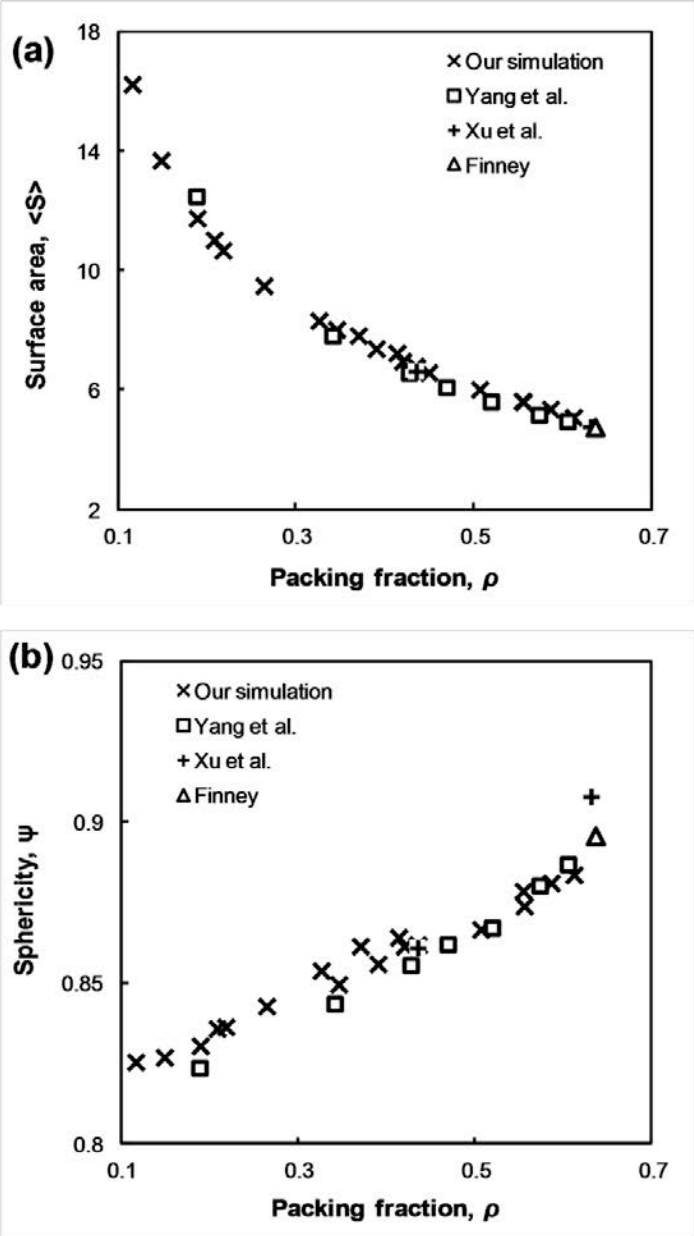

Figure 3.9: Metric properties of Voronoi polyhedra, (a) the averaged surface area of a polyhedron $<S>$, (b) the sphericity of polyhedra Ψ, as a function of packing fraction.

3.3.4. Force analysis

So far, we have demonstrated that different packing fractions result in different microscopic structural properties of packing. It is important to understand the underlying mechanisms in order to control the formation of a packing. To this end, the

forces involved in the formation of packing are considered to play major roles and thus are analysed in this section.

One of the major advantages of the discrete element method is that the forces on each particle can be readily obtained, and consequently the mechanisms governing the formation of a packing can be assessed in terms of the forces. For instance, the effects of particle and/or liquid properties are understood better from the force analysis [23, 32]. For these packings, it has been found that the packing fraction can be related to the ratio of the interparticle van der Waals interactions, to the effective gravity. The effective gravity is the total driving force to densify a packing, which may include the gravity, the liquid-particle forces and the impact induced pressure $\mathbf{F}_i^{IIP}$ under different packing conditions as discussed elsewhere [23]. The cohensive force, on the other hand, hinders the re-arrangement of particles so that loose packing structures are often formed. In this study, we use the electrostatic interactions to replace the gravitational force in the calculation of the force ratio,

$$\chi_i = \left| \sum_j \mathbf{F}_{ij}^{vdw} \right| / \left(\left| \mathbf{F}_i^e \right| + F_i^{IIP} \right) \tag{3.8}$$

and

$$\mathbf{F}_i^{IIP} = K \frac{m_i v^{imp}}{\sqrt{d / \Delta a}} = K \mathbf{F}_i^e \sqrt{\overline{H} / d} \tag{3.9}$$

where K is the fitting parameter, m_i is the particle mass, v^{imp} is the impact velocity, a is the particle acceleration, and $\overline{H}$ is the averaged initial height of particles. Note that here we treat the forces as scalar quantities. There are other forces in a packing, including the normal contact forces and friction forces. However, they are always regarded as passive forces balancing the active ones such as the electrostatic interactions and van der Waals interactions. Consequently, they are not involved in the calculation of the force ratio. Moreover, the effect of sliding and rolling frictions have been studied in details in the previous study of packing of fine particles [38]. It has been revealed that the effect of

friction is insignificant when the sliding friction coefficient is larger than 0.02 and the rolling friction coefficient is larger than 0.01.

Finally, the relationship between ρ and χ_i are described in early studies as,

$$\rho = \rho_0 \left(1 - \exp\left(\alpha \langle \chi_i \rangle^{\beta}\right)\right) \tag{3.10}$$

where α and β are the empirical fitting parameters, ρ_0 is sometimes referred as the initial packing fraction. They have the values of ρ_0 = 0.616, α = -2.78, β = -0.195, and K in Eq.3.9 is 4.35. By using the definition of the force ratio in Eq.3.8, our results indicate that the Eq.3.10 is still applicable to packings of fine particles under electric fields (see Figure 3.10).

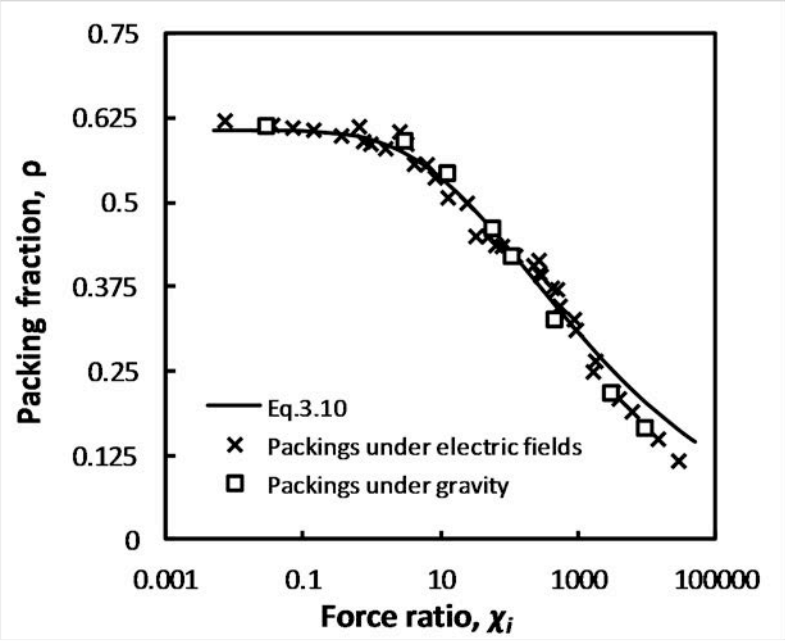

Figure 3.10: Packing fraction are expressed in terms of the force ratio between cohesive force and field force.

In addition, Eq.3.10 confirms the effects of the particle diameter and electric field on the packing fraction of the formed packings under electric fields. For instance, Figure 3.11 demonstrates when the electric field increases, the van der Waals interactions remain unchanged while the electrostatic interactions increase, and subsquently the force ratio

decreases. As a result, an increase in the packing fraction with the electric field is observed in Figure 3.3. The effect of the interparticle van der Waals interactions become more dominant as the particle diameter decreases. Furthermore, the effect of the eletrostatic interations on packings under electric fields is the same as the effect of gravitational force on packings under gravity. Therefore, the outcomes of the packings are comparable. This consideration should apply to other field forces as well. It should be pointed out that in industrial electrostatic precipitation processes, the field forces may not be unform. This will generate non-uniform packing structures. The use of the discrete element method to simulate packings of fine particles under non-uniform electric fields will be included in the next chapter.

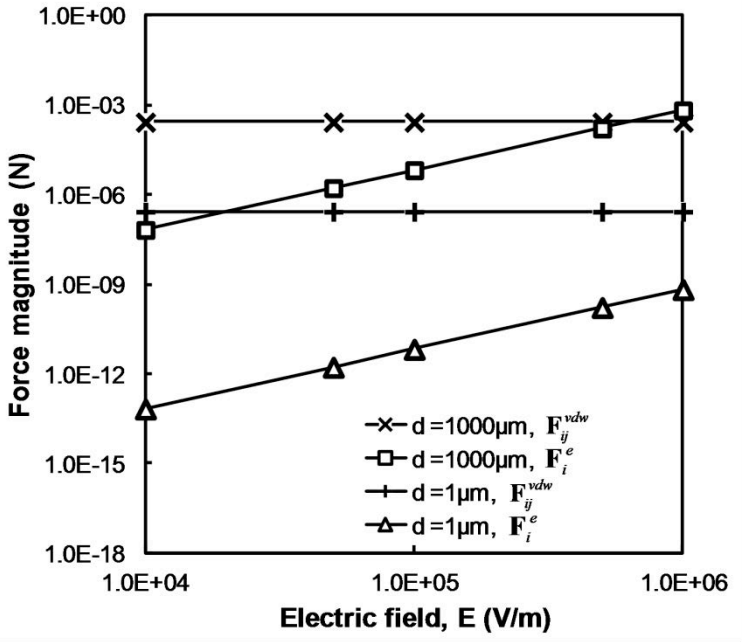

Figure 3.11: The electrostatic interactions $\mathbf{F}_i^e$ and the van der Waals interactions $\mathbf{F}_{ij}^{vdw}$ as a function of electric field on a typical particle.

3.4. Conclusions

Electrostatic interactions induced by external electric fields have been incorporated into the discrete element method to simulate packings of fine particles under uniform electric fields. The simulation conditions are relevant to electrostatic precipitation processes.

Our results show that the packing fraction of packing increases with an increase of either particle diameter or eletric field, and correspondingly, the packing structure varies. Furthermore, the structural variations with the packing fraction is consistent with the findings in the literature. The electric-field-induced electrostatic interactions are the driving forces in the packing formation, which is comparable to the role of the gravitational force for the packing formation under gravity. These results have been rationalised in terms of the competition between the cohesive force and the electrostatic interactions, in addition to other foces as given in Eq.3.8. The findings may lead to better understanding of the packing formation in electrostatic precipitation processes. In particular, the packing structual information, which is difficult to obtain experimentally, may potentially be applied to estimate the thermal, mechanical and electrical properties of packing. Such studies are included in the latter chapters.

Nomenclature

m = mass

$\mathbf{v}$ = velocity

t = time

$\mathbf{F}$ = force

I = moment of inertia

$\mathbf{T}$ = torque

$\mathbf{R}$ = particle radius

Y = Young's modulus

$\mathbf{n}$ = unit vector

H_a = Hamaker constant

h = interparticle separation

$\mathbf{E}$ = electric field

h_d = particle-wall separation

q = electrical charge

k_p = dielectric constant

d = particle diameter

a = acceleration

H = particle height

z = coordination number

Greek Letters

$\boldsymbol{\omega}$ = angular velocity

μ = friction

ξ = the overlap between particles during collisions

v = Poisson's ratio

γ = damping coefficient

ε_0 = vacuum permittivity

ε_r = relative permittivity

ρ_m = mass density

Φ_0 = initial porosity prior to packing formation

ρ = packing fraction

Ψ = sphericity

χ = force ratio

Subscript

i, j = ith particle, jth particle

n = normal direction

s = tangential direction

vdw = van der Waals

r = rolling friction

e = electrical

References

[1] K. R. Parker, *Applied electrostatic precipitation*: Springer, 1997.

[2] A. Jaworek, *et al.*, "Modern electrostatic devices and methods for exhaust gas cleaning: A brief review," *Journal of Electrostatics,* vol. 65, pp. 133-155, 2007.

[3] T. Ferge, *et al.*, "Particle collection efficiency and particle re-entrainment of an electrostatic precipitator in a sewage sludge incineration plant," *Environ. Sci. Technol,* vol. 38, pp. 1545-1553, 2004.

[4] R. Barranco, *et al.*, "The impact of fly ash resistivity and carbon content on electrostatic precipitator performance," *Fuel,* vol. 86, pp. 2521-2527, 2007.

[5] M. Jedrusik and A. Swierczok, "The influence of fly ash physical and chemical properties on electrostatic precipitation process," *Journal of Electrostatics,* vol. 67, pp. 105-109, 2009.

[6] A. Soldati, *et al.*, "Lagrangian simulation of turbulent particle dispersion in electrostatic precipitators," *Aiche Journal,* vol. 43, pp. 1403-1413, 1997.

[7] H. Fujishima, *et al.*, "Numerical simulation of three-dimensional electrohydrodynamics of spiked-electrode electrostatic precipitators," *Dielectrics and Electrical Insulation, IEEE Transactions on,* vol. 13, pp. 160-167, 2006.

[8] N. Farnoosh, *et al.*, "3-D numerical analysis of EHD turbulent flow and mono-disperse charged particle transport and collection in a wire-plate ESP," *Journal of Electrostatics,* vol. 68, pp. 513-522, 2010.

[9] D. Blanchard, *et al.*, "Correlation between current density and layer structure for fine particle deposition in a laboratory electrostatic precipitator," *Ieee Transactions on Industry Applications,* vol. 38, pp. 832-839, 2002.

[10] N. Neimarlija, *et al.*, "Finite volume method for calculation of electrostatic fields in electrostatic precipitators," *Journal of Electrostatics,* vol. 67, pp. 37-47, 2009.

[11] S. H. Kim and K. W. Lee, "Experimental study of electrostatic precipitator performance and comparison with existing theoretical prediction models," *Journal of Electrostatics,* vol. 48, pp. 3-25, 1999.

[12] K. McLean and R. Kahane, "Electrical performance diagram for a pilot scale electrostatic precipitator," *Proceedings of the International Clean Air Conference,* p. 207, 1978.

[13] H. P. Zhu, *et al.*, "Discrete particle simulation of particulate systems: Theoretical developments," *Chemical Engineering Science,* vol. 62, pp. 3378-3396, 2007.

[14] H. Zhu, *et al.*, "Discrete particle simulation of particulate systems: A review of major applications and findings," *Chemical Engineering Science,* vol. 63, pp. 5728-5770, 2008.

[15] J. P. Latham and A. Munjiza, "The modelling of particle systems with real shapes," *Philosophical Transactions of the Royal Society of London. Series A: Mathematical, Physical and Engineering Sciences,* vol. 362, p. 1953, 2004.

[16] K. J. Dong, *et al.*, "DEM simulation of cake formation in sedimentation and filtration," *Minerals Engineering,* vol. 22, pp. 921-930, 2009.

[17] P. Cundall and O. Strack, "A discrete numerical model for granular assemblies," ed: Dames and Moore London, England, 1979.

[18] N. V. Brilliantov, *et al.*, "Model for collisions in granular gases," *Physical Review E,* vol. 53, p. 5382, 1996.

[19] K. Parker, *Electrical operation of electrostatic precipitators*: IET, 2003.

[20] P. A. Langston, *et al.*, "Discrete element simulation of granular flow in 2D and 3D hoppers: Dependence of discharge rate and wall stress on particle interactions," *Chemical Engineering Science,* vol. 50, pp. 967-987, 1995.

[21] G. S. Cargill, "Dense random packing of hard spheres as a structural model for noncrystalline metallic solids," *Journal of Applied Physics,* vol. 41, pp. 2248-2250, 1970.

[22] G. F. Voronoi, "Nouvelles applications des paramètres continus à la théorie des formes quadratiques.," *Journal für die reine und angewandte Mathematik* vol. 134, p. 198, 1908.

[23] K. J. Dong, *et al.*, "Settling of particles in liquids: Effects of material properties," *AIChE Journal,* vol. 58, pp. 1409-1421, 2012.

[24] H. J. White, "Particle charging in electrostatic precipitation," *American Institute of Electrical Engineers, Transactions of the,* vol. 70, pp. 1186-1191, 1951.

[25] T. B. Jones, *Electromechanics of particles*. Cambridge: Cambridge University Press, 1995.

[26] M. Ghadiri, *et al.*, "Evaluation of the single contact electrical clamping force," *Chemical Engineering Science,* vol. 61, pp. 2290-2300, 2006.

[27] K. J. McLean, "Cohesion of precipitated dust layer in electrostatic precipitators," *Journal of the Air Pollution Control Association,* vol. 27, pp. 1100-1103, 1977.

[28] J. B. Zhu, *et al.*, "Characteristics of collected dust layer in a laboratory electrostatic precipitator," *Review of Science & Technology,* vol. 26, pp. 30-33, 2008.

[29] C. Riehle, "Basic and theoretical operation of ESPs," in *Applied electrostatic precipitation*, K. Parker, Ed., ed: Springer, 1997.

[30] K. J. Dong, *et al.*, "Role of Interparticle Forces in the Formation of Random Loose Packing," *Physical Review Letters*, vol. 96, p. 145505, 2006.

[31] J. Miller, *et al.*, "Local deposition of particles in a laboratory scale electrostatic precipitator with barbed discharge electrodes," in *Sixth International Conference on Electrostatic Precipitation*, Budapest, 1996, pp. 325-334.

[32] R. Y. Yang, *et al.*, "Computer simulation of the packing of fine particles," *Physical Review E*, vol. 62, p. 3900, 2000.

[33] G. K. Batchelor and R. W. O'Brien, "Thermal or electrical conduction through a granular material," *Proceedings of the Royal Society of London. Series A, Mathematical and Physical Sciences*, vol. 355, pp. 313-333, 1977.

[34] Z. Zhou, *et al.*, "Particle scale study of heat transfer in packed and bubbling fluidized beds," *Aiche Journal*, vol. 55, pp. 868-884, 2009.

[35] J. L. Finney, "Random packings and the structure of simple liquids. I. The geometry of random close packing," *Proceedings of the Royal Society of London. A. Mathematical and Physical Sciences*, vol. 319, pp. 479-493, 1970.

[36] J. Xu, *et al.*, "Analysis of the packing structure of wet spheres by Voronoi–Delaunay tessellation," *Granular Matter*, vol. 9, pp. 455-463, 2007.

[37] R. Y. Yang, *et al.*, "Voronoi tessellation of the packing of fine uniform spheres," *Physical Review E*, vol. 65, p. 041302, 2002.

[38] R. Y. Yang, *et al.*, "Effect of material properties on the packing of fine particles," *Journal of Applied Physics*, vol. 94, pp. 3025-3034, 2003.

CHAPTER 4. NUMERICAL STUDY OF THE PACKING OF FINE PARTICLES UNDER NON-UNIFORM ELECTRIC FIELDS

Abstract

This paper presents a numerical study of the packing of fine particles under non-uniform electric fields using the discrete element method with special emphasis on electrostatic interactions. In particular, the elliptical shaped electric field distributions commonly observed in electrostatic precipitation processes are studied. Our results indicate the resultant packing structures are highly non-uniform, which are caused by the non-uniformity of the imposed electric fields. Thus, it is difficult to characterize the packing structure as a whole.

Instead, we examine structures of the formed packings in the local regions where the local electric fields are approximately uniform. The local packing structure is characterised in terms of the packing fraction and coordination number, and we found that the local properties are in good agreement with previous findings of the study of the packing of fine particles under uniform electric fields. Furthermore, the analysis of forces on particles during the packing formation reveals that both the electrostatic interactions and interparticle van der Waals interactions have significant effects on the final packing structures. The findings may lead to better control of the formed packings under non-uniform electric fields, which results in improved electrical transport properties in the future.

4.1. Introduction

Randomly packed particles are found in many physical, chemical and engineering processes. It is generally accepted that both long-range field forces and short-range interparticle forces influence the process of the packing, and therefore, the resultant packing structure [1-3]. In literature, many efforts have been made in the studies of the packing of coarse, fine, wet particles, but little has been done for packings of charged particles under the influence of electric fields [4, 5]. Such a packing is essential to industrial applications including electrostatic precipitation processes, which are widely

used in power stations, paper mills, steelworks, tunnels, even in extra-terrestrial environments [6-8].

Understanding packings of fine particles under electric fields is of particular importance in the design of the electrostatic precipitation process because of the effect that the packing can have on the process. The structure of packing determines its electrical transport properties, which, in turn, impact on the collection efficiency of the precipitation process [9-11].

Experimental studies on the precipitated packings in electrostatic precipitation processes show that the packing structure is dense at the centres and loose at edges [12]. To date, there has been no direct explanation for such a packing structural profile. Despite the importance of these observations, they have been ignored in the studies on electrostatic precipitation processes, the reason perhaps being the difficulties in measuring the structural and electrical properties of a structurally vulnerable packing experimentally [7]. These difficulties can be overcome by numerical simulations, which provide robust alternatives for studying particle packing. In last chapter, we have studied the formed packings under uniform electric fields [13]. The results have revealed that the electric-field-induced electrostatic interactions play an important role in the packing formation processes.

The aim of this research is to study packings of fine particles under non-uniform electric fields using the discrete element method. Special emphasis is given here to the effect of elliptical shaped electric field distributions that are commonly observed in electrostatic precipitation processes. The non-uniform electric fields is expected to influence the resultant packing structures. Due the non-uniformity of the packing structure, it is useful to characterise the local packing structure. Therefore, we investigate the dependence of the local packing structures on the imposed electric fields in the local region where the electric field is assumed to be quasi-uniform. The local packing structure is characterised in terms of packing fraction and coordination number. Also, we study the process of packing by examining both the electrostatic interactions and the interparticle van der Waals interactions on the particles. This may advance the understanding of

packings of fine particles under non-uniform electric fields, thus leading to design improvements of electrostatic precipitation processes.

4.2. Model descriptions

In this chapter, we use the discrete element method to study the formed packings under non-uniform electric fields. The electric-field-induced long-range electrostatic interactions are incorporated in the simulation code. In the discrete element method, the equations describing the translational and rotational motions of particle i are:

$$m_i \frac{d\mathbf{v}_i}{dt} = \sum \left(\mathbf{F}_{ij}^n + \mathbf{F}_{ij}^s + \mathbf{F}_{ij}^{vdw} \right) + \mathbf{F}_i^e \tag{4.1}$$

and

$$I_i \frac{d\boldsymbol{\omega}_i}{dt} = \sum \left(\mathbf{R}_i \times \mathbf{F}_{ij}^s + \mathbf{T}_{ij}^r \right) \tag{4.2}$$

where m_i is the mass of the particle, $\mathbf{v}_i$ is the translational velocity, t is the time, I_i is the moment of inertia, $\boldsymbol{\omega}_i$ is the angular velocity, $\mathbf{R}_i$ is the radius of particle i, $\mathbf{T}_{ij}^r$ is the torque caused by the rolling friction between particle i and j; $\mathbf{F}_{ij}^n$, $\mathbf{F}_{ij}^s$ and $\mathbf{F}_{ij}^{vdw}$ are, respectively, the normal contact force, the tangential contact force and the van der Waals interactions between particle i and its neighbouring particle j; and $\mathbf{F}_i^e$ represents the electric-field-induced electrostatic interactions. More detailed descriptions of all the forces considered in the simulation can be found in our previous study of the packing of fine particles under uniform electric field [13]. We use material properties and operational conditions of the conventional electrostatic precipitation processes at coal-fired power plants in our simulations (see Table 4.1).

Before a simulation starts, the non-uniform electric field distribution needs to be defined. We study here electric field distributions of three different shapes, i.e., circular, rectangular, and elliptical. For all shapes, the maximum electric field is defined at the

centre, and the electric field is gradually reduced to the minimum at the periphery. The mathematical equations defining the shapes of non-uniform electric fields are listed in Table 4.2 and the corresponding electric fields are depicted in Figure 4.1.

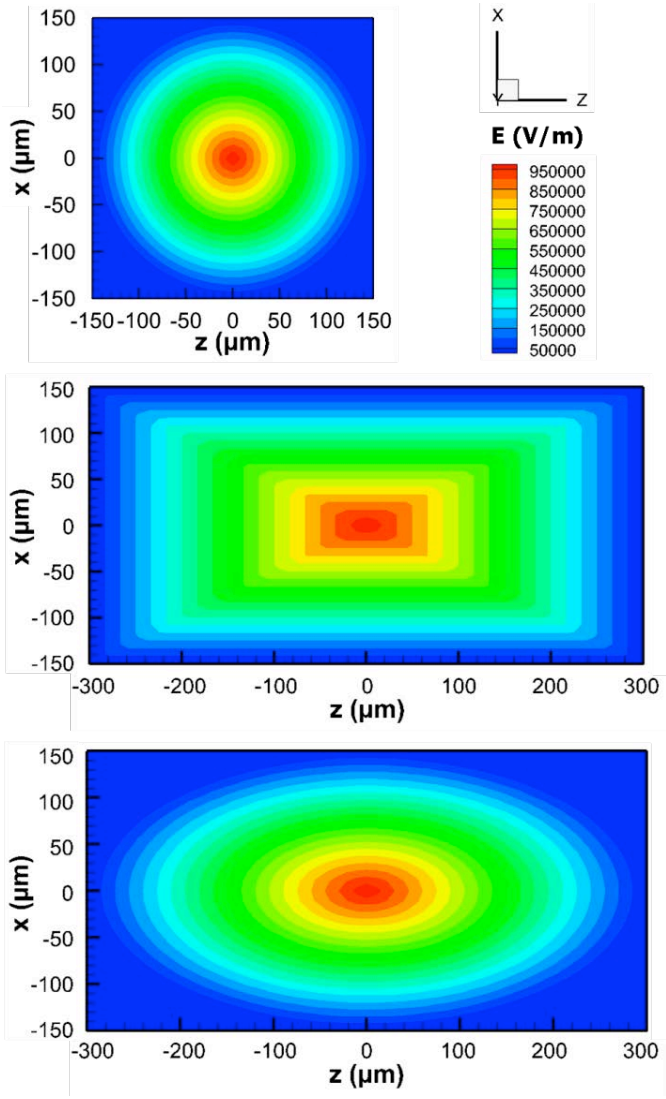

Figure 4.1: Contour maps of the three non-uniform electric fields. The electric field is 10^6V/m at the centre. Then, it is linearly reduced to zero at the periphery.

In addition to the shape of non-uniform electric fields, the spatial distribution is another important parameter, and therefore, it is considered here. One obvious way to characterise the spatial distribution is by the distance from the centre. The focus of this paper is the elliptical shaped electric field distributions, which are often observed in electrostatic precipitation processes. Such a shape can be characterised by its aspect ratio, which is the ratio of the major axis length to the minor axis length of ellipse. Here,

the distance from a given point to the centre is normalised by the major and the minor axes lengths. Mathematically, the normalised distance L is,

$$L = \left(\frac{dz}{a}\right)^2 + \left(\frac{dx}{b}\right)^2 \tag{4.3}$$

where a is the major axis, b is the minor axis of an ellipse, and dx and dz are the displacement from the elliptical centre along x-axis and z-axis respectively. Clearly, the value of L for any point in the ellipse is between 0 and 1, where 0 represents the elliptical centre and 1 represents the points at the periphery.

Table 4.1: Parameters used in our simulations.

Parameters	Values
Electric field, **E**	Up to 10^6 V/m
Mass density, ρ_m	2500 kg/m^{-3}
Young's modulus, Y	1 x 10^7 Pa
Poisson's ratio, v	0.29
Sliding friction coefficient, μ_s	0.4
Rolling friction coefficient, μ_r	0.02
Hamaker's constant, H_a	6.5 x 10^{-20} J
Dielectric constant, k_p	2

Thus, we now can define the electric field distributions according to the distance from the elliptical centre. For example, for an elliptical shape with the aspect ratio of 2:1, two non-uniform electric fields are defined according to the normalised distance (see Figure 4.2). In both cases, the electric field is at its maximum at the centre and gradually decreases to a minimum at the periphery [14, 15].

Table 4.2: Equations defining various non-uniform electric fields.

Shape	Equation	
Circular	$E = \left(1 - \frac{dx^2 + dz^2}{a^2}\right) E_{\max}$	if $dx^2 + dz^2 \le a^2$
	$E = 0$	if $dx^2 + dz^2 > a^2$
Rectangular	$E = \left(1 - \frac{dx}{a}\right) E_{\max}$	if $\left\|\frac{dx}{a}\right\| \ge \left\|\frac{dz}{b}\right\|$
	$E = \left(1 - \frac{dz}{b}\right) E_{\max}$	if $\left\|\frac{dx}{a}\right\| < \left\|\frac{dz}{b}\right\|$
Elliptical	$E = \left(1 - \frac{dx^2}{a^2} - \frac{dz^2}{b^2}\right) E_{\max}$	if $\frac{dx^2}{a^2} + \frac{dz^2}{b^2} \le 1$
	$E = 0$	if $\frac{dx^2}{a^2} + \frac{dz^2}{b^2} > 1$

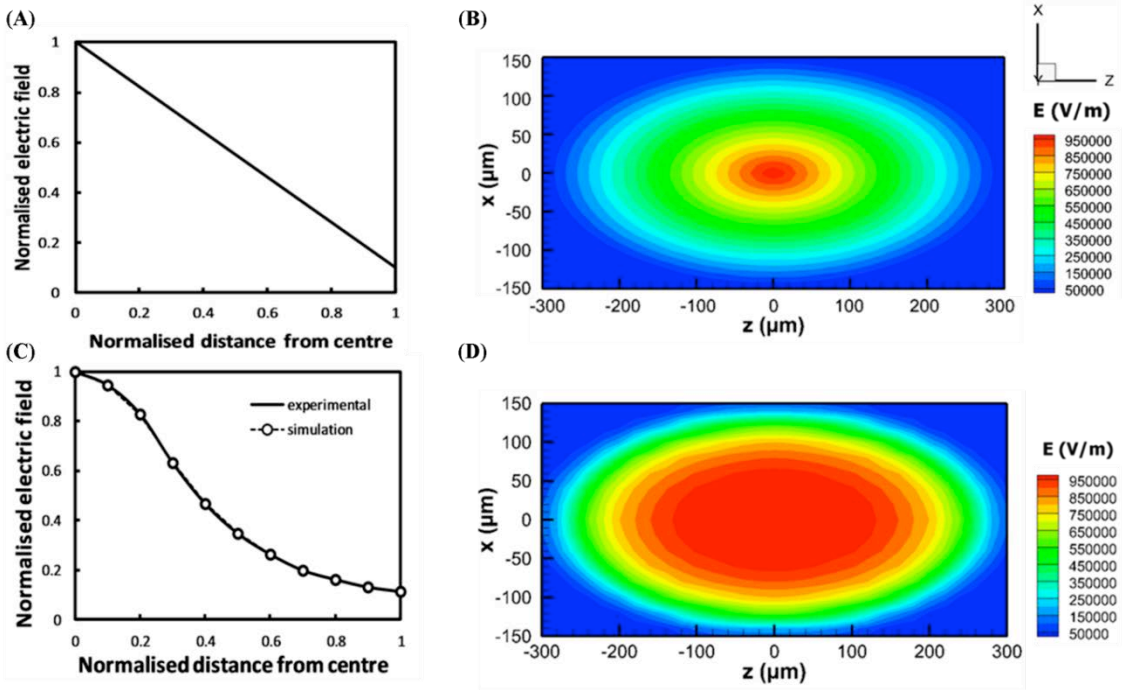

Figure 4.2: Spatial distributions of two electric fields in elliptical shape. (a) Linear variations and (b) the corresponding electric field contour. (c) The variations commonly

experimentally determined in electrostatic precipitation processes and (d) the corresponding electric field contour.

To simulate the electrical conditions of electrostatic precipitation processes, the arrangement of multiple electric fields is also important. It has been observed in practical experiments that individually the non-uniform electric fields can be considered as elliptical, and the arrangement of the multiple elliptical electric fields may also impacts on the resultant structural profiles [12]. The arrangement of the multiple electric fields can be described by a parameter k:

$$k = \frac{a}{A} = \frac{b}{B} \tag{4.4}$$

where A and B are the defined box width and length. Now, we are able to adjust the size of elliptical shaped electric fields by changing k. Lastly, an additional quarter of the electric field at the centre of the box was added to each corner in order to account for the influence of the neighbouring elliptical-shaped electric fields. Along with periodic boundary conditions, the electrical conditions in electrostatic precipitation processes can be readily simulated (see Figure 4.3).

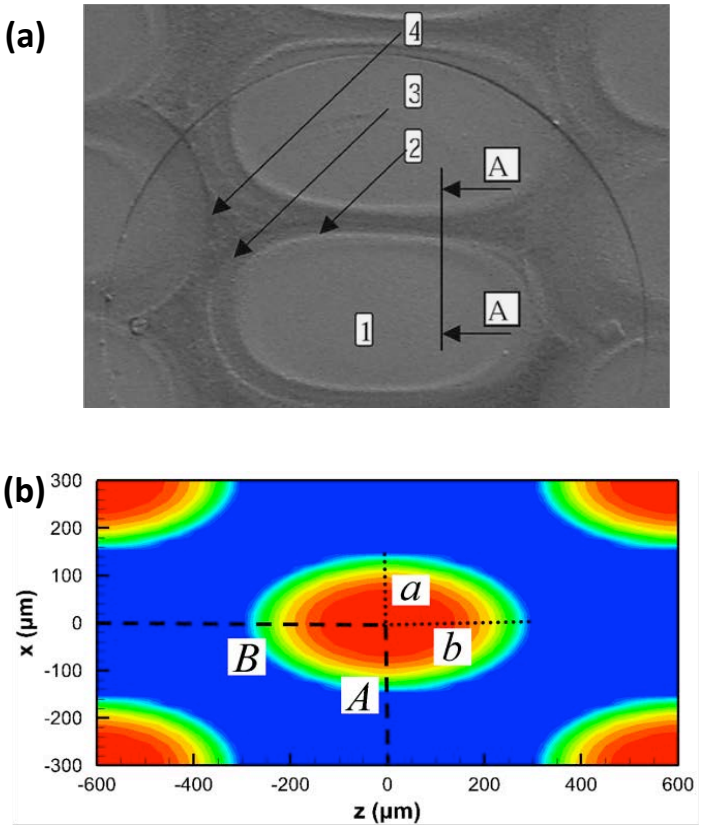

Figure 4.3: (a) The structural profile of the packings observed in electrostatic precipitation processes, and (b) the electric field contour used in the simulation.

So far, we have demonstrated that the electrical condition of a non-uniform electric field is defined by its shape, spatial distribution and the multiple field arrangement. In fact, we are now capable of simulating any non-uniform electric field as long as its non-uniform property can be properly defined. A typical simulation starts with a random generation of particles with zero velocity, and their acceleration depends on the corresponding electric field at their positions according to Eq.4.3. The translational and rotational motions of particles are given by Eq.4.1 and Eq.4.2. In particular, the collective electric-field-induced electrostatic interactions include both the Coulomb's interactions and the boundary image force between the particle and the imaginary collection plate. The simulation finishes when all particles are settled on the bottom plane at y=0 with zero velocity again. As expected, the shape of the final packing structure is related to the shape of the imposed electric field (see Figure 4.4). The packing appears thin at the centres where the electric field is strong and thick at the edges where the electric field is weak. These results are qualitatively in agreement with

the previous visual observations of the packing structures found in electrostatic precipitation processes [12].

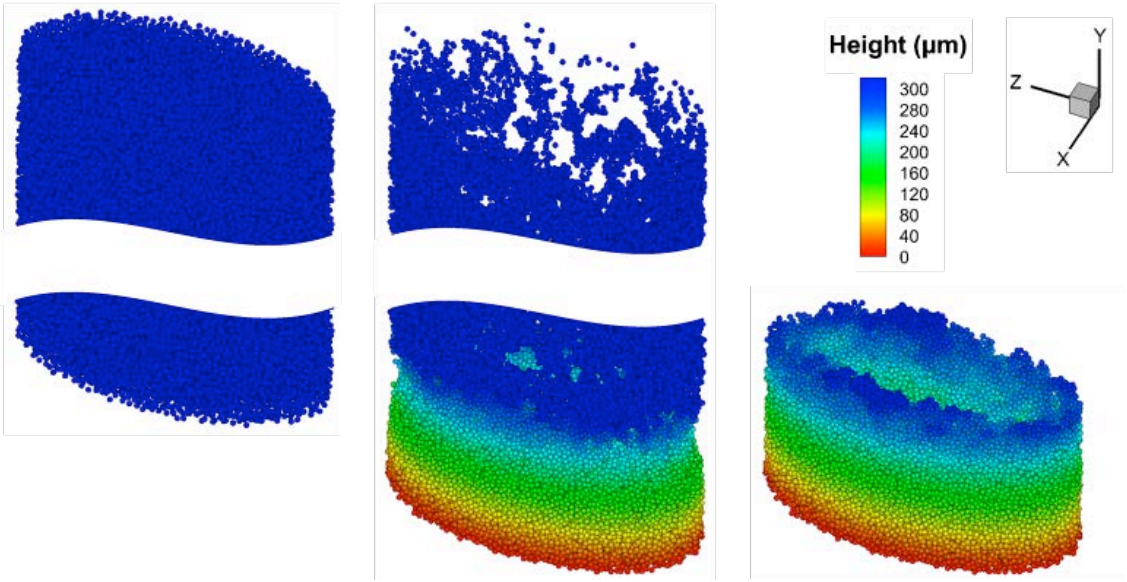

Figure 4.4: The formation process of a packing made of 10μm particles under an imposed elliptical shaped electric field.

4.3. Results and discussion

4.3.1. Effect of the shape of non-uniform electric fields

To investigate the effect of electric field distributions on the resultant packing structure, we have applied the electric field in three shapes, which are circular, rectangular and elliptical. The pre-defined electric field contours are shown in Figure 4.5a. The spatial distribution of the electric fields is kept linear from the centre to the perimeter for all three cases so that the results can be compared (see Figure 4.2). Firstly, the final structural profile of the resultant packings is characterised by the particle heights as illustrated in Figure 4.5b. Our results reveal that the structural profile of the resultant packings has the same shape as the corresponding electric fields. The structure is thin at the centre where the electric field is strong, and the other way around at the periphery where the electric field is weak. Next, we analyse the packing fraction distribution of

the packing structures in order to understand the observed packing structural profile. The results indicate that packing fraction is high at the centre and low at the periphery (see Figure 4.5c). This explains the packing structural profile being thin at the centre and thick at the periphery despite the fact that the particles are initially randomly and evenly generated. Thus, the results confirm that the structure of a packing under a non-uniform electric field depends on the distribution of the imposed electric field.

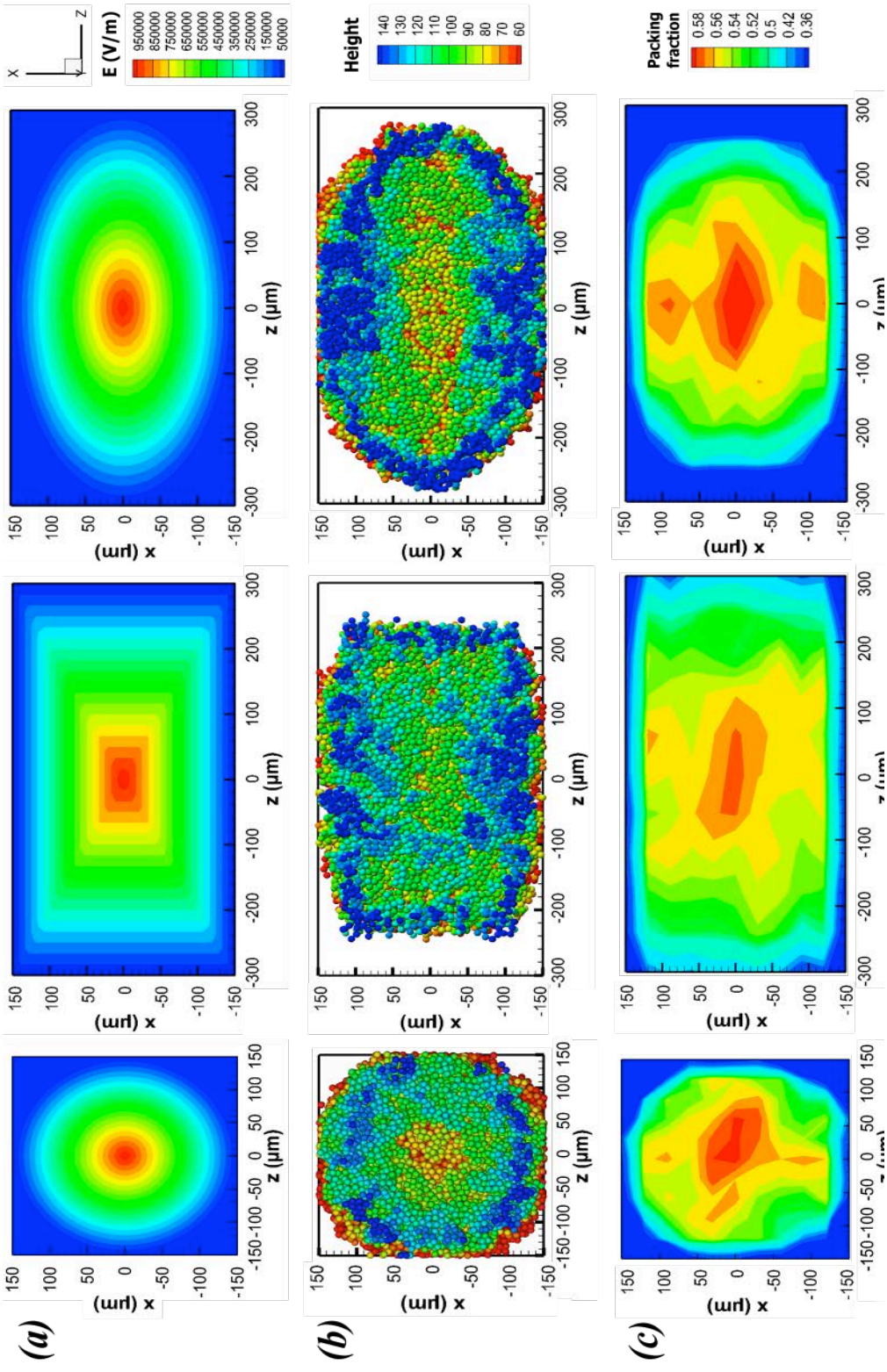

Figure 4.5: The formed packings under non-uniform electric fields with (a) the electric field contours; (b) the resultant packing structural profiles; and (c) the corresponding packing fraction contours.

4.3.2. Effects of the arrangement of multiple non-uniform electric fields

Secondly, comparisons are made between the simulated packings and the experimentally observed packings from conventional electrostatic precipitation processes. Early experimental studies on packings of fine particles in this process show that the structure profile of the packing is indeed elliptical as illustrated in Figure 4.6 [12, 16]. However, there is no direct evidence on the exact mechanisms of how this structural profile is formed in the precipitation processes. Lack of experimental measured data for the electric quantities and packing structures makes it impossible to study such observations [17]. It has been suggested that the packing structure is dense at the centre where the electric field is strong, whilst a loose structure is formed at the perimeter where the electric field is weak. Consequently, there is a strong correlation between the imposed electric field and packing structure. In contrast, the newly developed discrete element method has offered an alternative way to study the formed packings under electric fields.

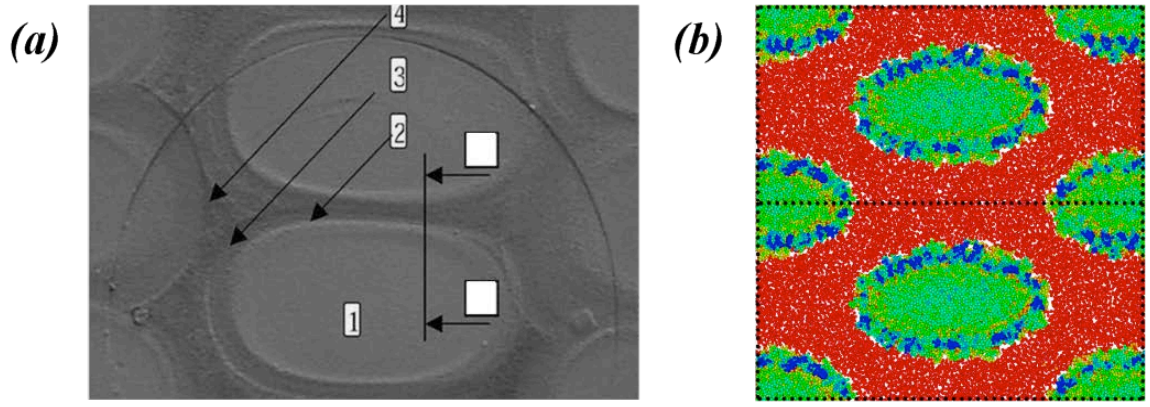

Figure 4.6: (a) The structural profile of the packings found in electrostatic precipitation processes are compared with (b) the structural profile of the simulated packings.

The simulation results demonstrate that the final structure of the formed packings under non-uniformed electric fields are certainly organised in interesting structural profiles (see Figure 4.7b). In general, the packing structures are thin at the centre where the electric field is strong, while the thick perimeter is formed in weak electric fields. Outside these elliptical electric fields, the structure is porous and thin, because the particles in these regions settle at an extremely slow velocity, and therefore, they are

carried on with flue gases before they can reach the bottom. This is justified by the fact that most particles are collected in the regions where the electric field is strong, while other forces such as fluid force in the flue gases are dominant if the electric field is too weak.

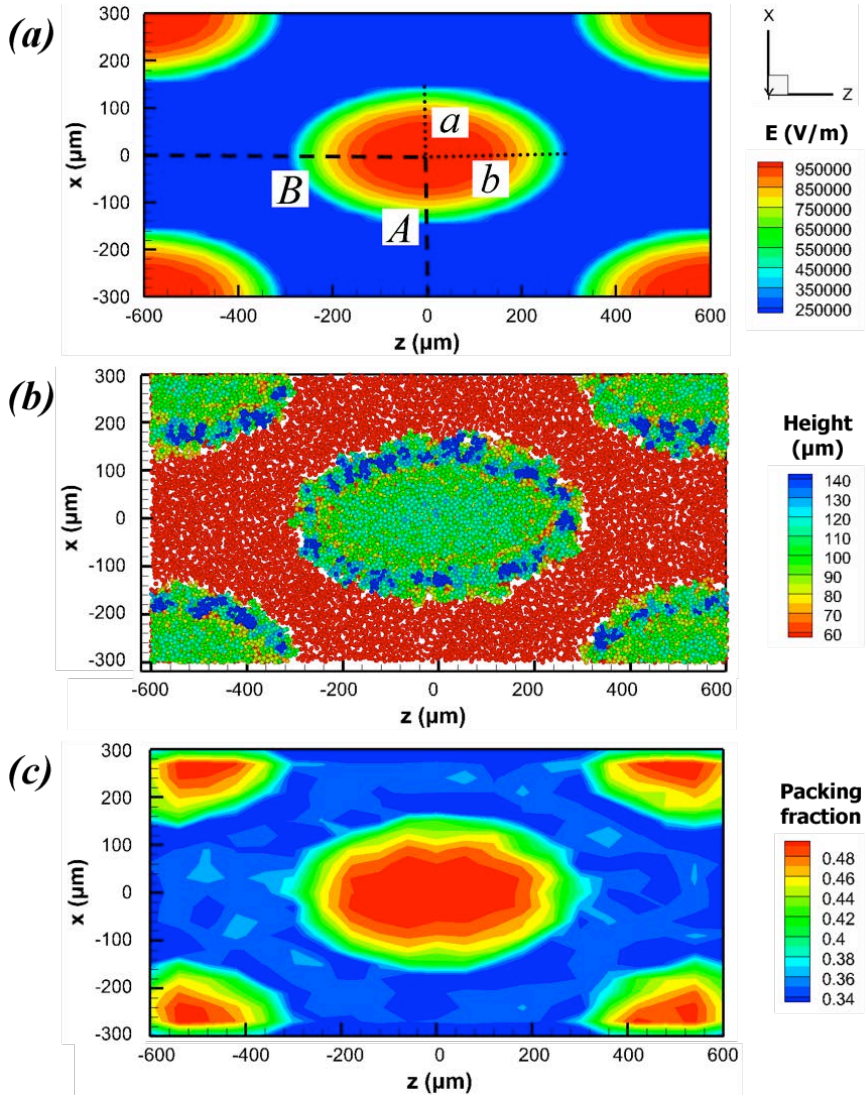

Figure 4.7: (a) The electric field contour with (b) the resultant packing structural profile and (c) packing fraction contour.

To understand the observed packing structural profile in the simulation, we further examine the packing fraction contours of the structure (see Figure 4.7c). The packing fraction contours are produced by examining the packing fraction in a localised region of 30μm×60μm, and an averaged packing fraction is assigned to the corresponding region. As expected, the packing fraction of the structure at the centre of the ellipse is

dense and therefore it is thin. The packing fraction decreases when approaching to the perimeter. Our simulations obtained by considering periodic boundaries demonstrate that the packing structural profiles are comparable to the observations made in the experiments (see Figure 4.6b). In short, we have successfully demonstrated that the experimentally observed packing structure profile can be reproduced by the developed discrete element method.

4.3.3. Overall structural characterisations

This work is focused on elliptical shaped non-uniform electric fields, and therefore, we firstly examine the entire structure of the formed packings using the averaged electric field $\overline{\mathbf{E}}$ and the averaged packing fraction. $\overline{\mathbf{E}}$ is scaled according to the distance from the elliptical centre S_i as more area is covered the farther the distance from the centre. As a result, $\mathbf{E}_i$ value away from the centre would weigh more in the calculation of $\overline{\mathbf{E}}$:

$$\overline{\mathbf{E}} = \sum_{i=0} \mathbf{E}_i S_i \Big/ \sum_{i=0} S_i \tag{4.5}$$

The averaged packing fraction $\overline{\rho}$ is calculated in a similar way as follows, but the top and bottom layers are excluded to eliminate the effect of uneven packing surface:

$$\overline{\rho} = \sum_{i=0} \rho_i S_i \Big/ \sum_{i=0} S_i \tag{4.6}$$

The results of the analysis are depicted in Figure 4.8. The packing fraction increases with the electric field, and the trend of the increase is comparable with the findings in the study of the packing of fine particles under uniform electric fields [13]. However, the use of the averaged packing structure is not so meaningful, because the formed structure under non-uniform electric fields are highly non-uniform. Thus, more insightful structural information is needed to elucidate the detailed packing structures.

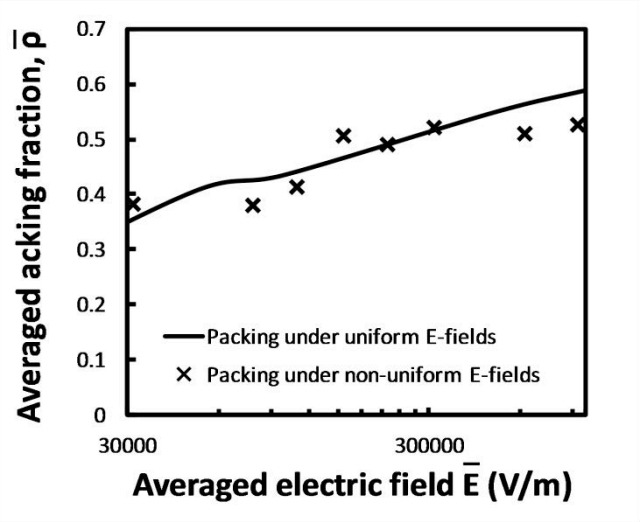

Figure 4.8: Variations of the packing fraction against the electric field in local regions.

To further understand the non-uniform packing structural profile, we investigate the detailed spatial distributions of the packing fraction and electric field. A typical packing structure is divided into smaller regions of 20μm width in z-axis direction as depicted in Figure 4.9b. Due to the uneven packing structural profile, the top and bottom portions of the packing are disregarded to eliminate the boundary effects. The region outside the defined elliptical shape is also not considered when estimating the packing fraction in the divided regions. Then, we use the averaged electric field and the averaged packing fraction within the divided regions to represent the electric field and packing fraction of such a region. In this way, variations of packing fraction as well as electric field along z-axis can be quantitatively plotted as shown in Figure 4.9c. The packing fraction is high in the regions where the electric field is strong, and vice versa in the regions where the electric field is weak. Clearly, the averaged packing fraction is affected by the averaged electric field within each divided region.

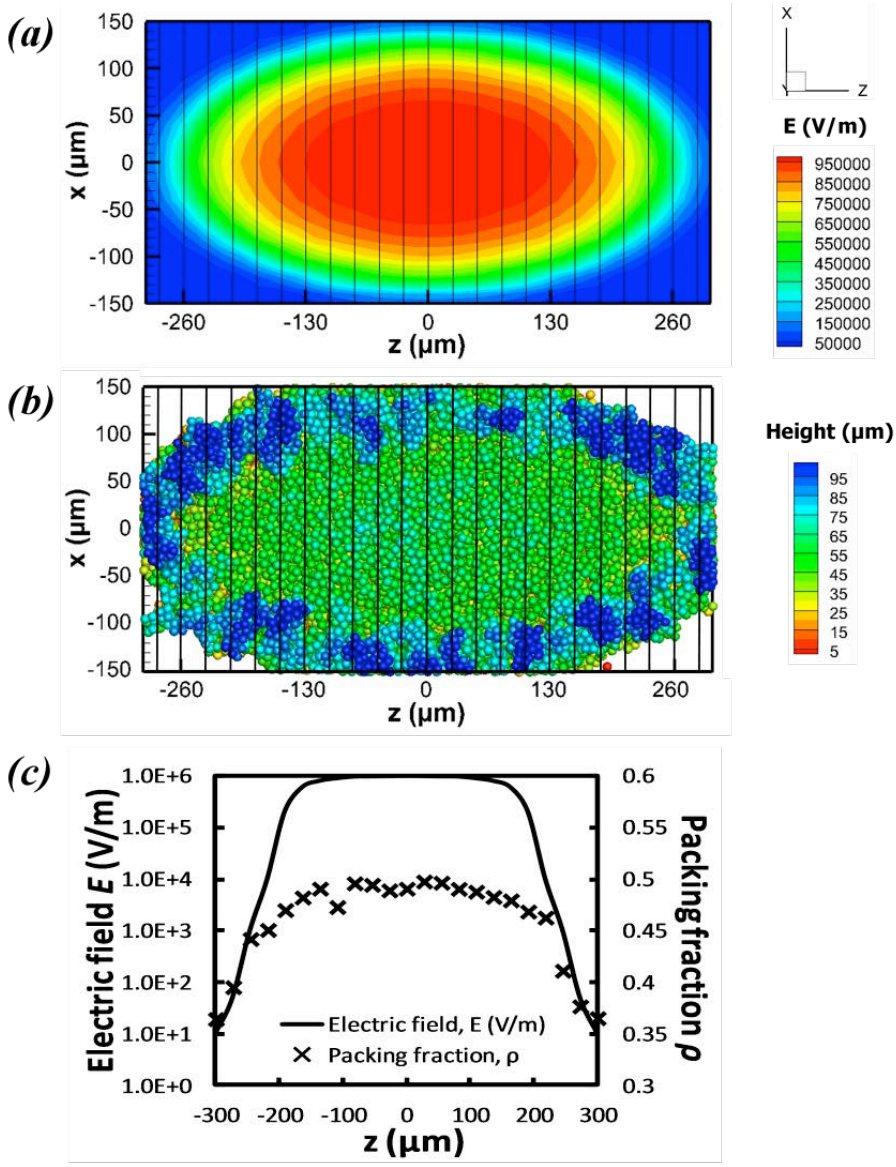

Figure 4.9: (a) The electric field distribution and (b) the packing structure are divided along *z*-axis; and (c) the resultant variations of electric field and packing fraction along *z*-axis.

4.3.4. Local structural characterisations

Next, we attempt to use the averaged structural properties in a local region to represent the local packing structure. When the local region is small enough, the local electric field and structure can be assumed to be quasi-uniform. Such requirements are fulfilled

when a spherical local region with a radius of 20μm is applied during the analysis. Therefore, from now on, when we discuss packing properties, we are referring to the local properties of packing. So far, we have proven that the structure of the packing under non-uniform electric fields depends on the electric field distributions. Due to the non-uniformity of the final structure, it is necessary to characterise the structure in localised small regions.

To begin with, we examine the local packing fraction of the simulated packings in order to understand the observed packing structural profile. The results indicate that the packing fraction of the local structure increases with the local electric field. These results are in agreement with the previously established relation between packing fraction and electric field for the packings under uniform electric fields [13]. The difference is that the packing fraction is much more scattered for the packings under non-uniform electric fields comparing to the uniform electric field cases. This is probably due to the non-uniformity of the electric fields and consequently the non-uniformity of the resultant structures in local regions. Nevertheless, it appears that the previously established relationship between the packing fraction and electric field is still applicable to the packings under non-uniform electric fields.

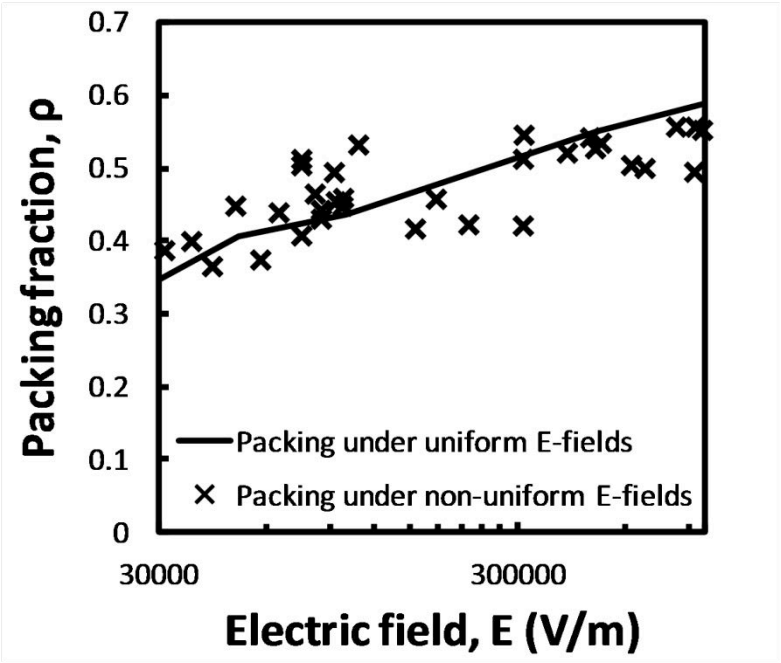

Figure 4.10: The local packing fraction is expressed as a function of the local electric field. The solid line shows the previously established correlation between packing fraction and electric field.

In addition, the coordination number of the formed packings in local regions also depends on the local electric fields. The coordination number of a particle represents the number of contacting neighbouring particles. The coordination number is an important structural parameter, because it represents how the particles are connected, which determines the transport properties of packing [9]. Obviously, it is impossible for all particles in a random packing to have the same coordination number. Hence, we examine the coordination number distribution in the defined local regions. Figure 4.11 reveals the coordination number distribution of the formed packings under non-uniform electric fields. Our results suggest that the coordination number distributions of the formed packings under uniform and non-uniform electric fields are similar when their averaged coordination numbers are similar. Thus, we can use the averaged coordination number to characterize the structure of packings.

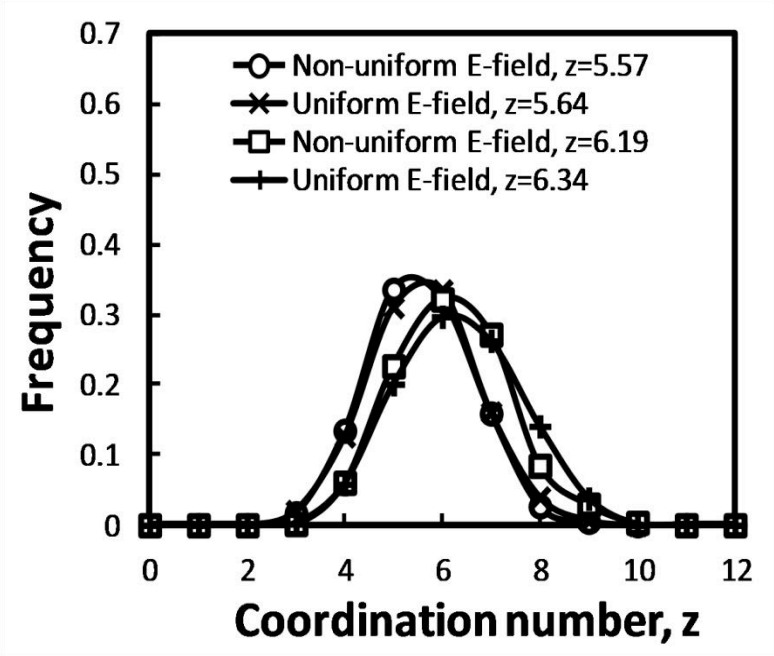

Figure 4.11: Comparison of the coordination number distributions of the packings under uniform and non-uniform electric fields.

Furthermore, the non-uniform electric field distribution also has a significant impact on the averaged coordination number of the packing. In the past, it has been proven that there is a universal relationship between coordination number and packing fraction for the packings under gravity or uniform electric fields [13, 18]. In this study, our results indicate this relation is still applicable for packings under non-uniform electric fields, and the averaged coordination number increases with the increasing packing fraction for all the simulated packings (see Figure 4.12). As depicted in Figure 4.9, the local structures of the packing in local electric field are more or less similar to the formed structure under a uniform electric field with the same strength. Above all, the results demonstrate that the packings under different electrical conditions have similar packing structures if they have similar packing fractions. Thus, these findings enable us to use a single macroscopic parameter, i.e., packing fraction, to characterise the formed packings under non-uniform electric fields.

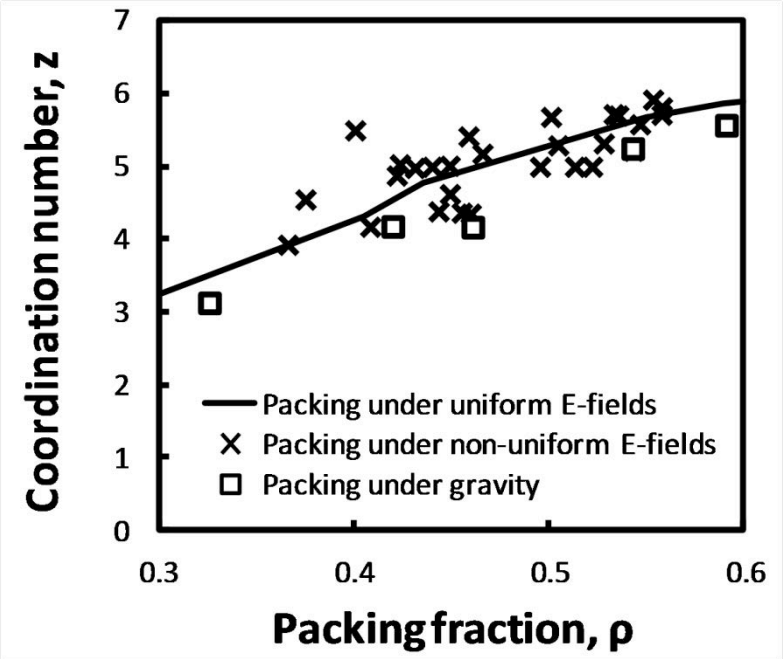

Figure 4.12: Variations of coordination number against packing fraction for the packings under non-uniform electric fields are compared with those of the packings under uniform electric fields or gravity.

Lastly, the strong correlation between the electric field distribution and the resultant packing structure has suggested the significance of the electric-field-induced electrostatic interactions. Traditionally, packings of coarse, fine and wet particles is controlled by the constant gravitational force, the van der Waals interactions and fluid-related forces, respectively [4, 5]. For fine and electrically charged particles, we focus on the electrostatic interactions, in particular its effect on the packing structures. In our simulation, the electric-field-induced electrostatic interactions increase with the imposed electric field, while the short-range van der Waals interactions that are only related to the material properties of particle, are independent of the electric field. Thus, strong electrostatic interactions dominate over other forces in the presence of a strong electric field, which, in turn, promotes the rearrangement of particles during packing formations. As a result, the centre regions of packing under strong electric fields are dense and thin (see Figure 4.9). Conversely, a weak electric field reduces the magnitude of electrostatic interactions, and thus the particle movements upon settlement are reduced. Thus, loose and thick edges are formed (see Figure 4.9). These findings suggest that the structure of packings under electric fields may be manipulated by

controlling the applied electric field and consequently the electrostatic interactions, which may lead to achieving desirable electrical properties of the packings.

Quantitatively, the competing forces involved in the formation of a packing can be characterized in terms of a force ratio. For instance, the force ratio has been defined as the ratio of the van der Waals interactions and the gravity in the study of particle packing under gravity [18]. It has been proven that the packing fraction can be expressed in terms of the force ratio, and the packing fraction decreases with the increasing force ratio. In a previous study of the packing of fine particle under uniform electric fields, the force ratio χ_i is defined as the ratio between the interparticle van der Waals interactions $\mathbf{F}_{ij}^{vdw}$ and the electric-field-induced electrostatic interactions $\mathbf{F}_i^e$ as given below [13]:

$$\chi_i = \sum_j \left|\mathbf{F}_{ij}^{vdw}\right| \Big/ \mathbf{F}_i^e \tag{4.7}$$

Here, we define the force ratio for a packing under a non-uniform electric field as the averaged force ratio between the two competing forces in a local region. The relationship between packing fraction and force ratio is depicted in Figure 4.13. In general, the packing fraction decreases as the force ratio increases. This is consistent with the observations in the studies of the packing of fine particles under gravity and uniform electric fields [13, 18]. Again, the scatter of the data is caused by the non-uniformity of the local electric field. Nevertheless, the results confirm that the previously established relation between packing fraction and force ratio still applies to packings of fine particles under non-uniform electric fields.

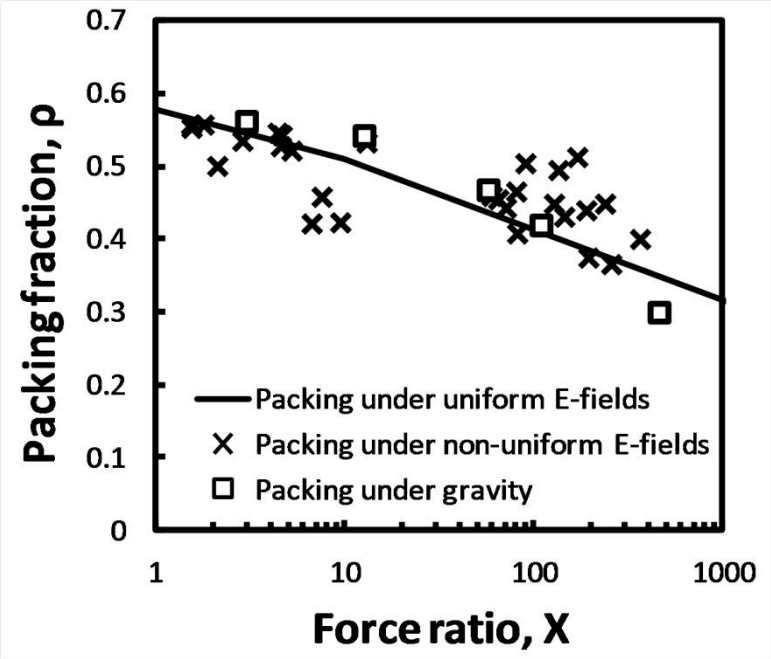

Figure 4.13: The dependence of the packing fraction on the force ratio between the interparticle van der Waals interactions and the electric-field-induced electrostatic interactions.

4.4. Conclusions

In summary, we have used the discrete element simulation to investigate packings of fine particles under non-uniform electric fields. Both the electric-field-induced electrostatic interactions and the interparticle van der Waals interactions have been taken into account in the packing processes. The results reveal a strong dependence of the structure of the packings on the imposed non-uniform electric field. The elliptical shaped packing structural profile generally observed in electrostatic precipitation processes has been reproduced by the newly developed model. Based on the simulation results, a detailed structural characterisation of the non-uniform structure is conducted, which is difficult if not impossible, to achieve in practical experiments. Despite the non-uniformity of the overall structural profile, our results indicate that local packing structures, in terms of packing fraction and coordination number, are determined by the local electric fields. The local packing fraction increases with the local electric field,

and such results are consistent with the previous findings in studies of particle packing under gravity or uniform electric fields. Furthermore, we have demonstrated that the structural change in formed packings can be rationalized by the competition between the electric-field-induced electrostatic interactions and interparticle forces on particles. These findings highlight the importance of the electrostatic interactions during the process of packings under non-uniform electric fields. In addition, our results have demonstrated that the discrete element method provides an effective way to investigate particle packing, even for packings under non-uniform electric fields.

Nomenclature

m = mass

$\mathbf{v}$ = velocity

t = time

I = moment of inertia

$\mathbf{R}$ = particle radius

$\mathbf{F}$ = force

$\mathbf{T}$ = torque

L = normalised distance

a = major axis of an ellipse

b = minor axis of an ellipse

$\mathbf{E}$ = electric field

Y = Young's modulus

H_a = Hamaker constant

k_p = dielectric constant

k = multiplication parameter

S_i = distance from elliptical centre

z = coordination number

Greek Letters

$\boldsymbol{\omega}$ = angular velocity

ρ_m = mass density

v = Poisson's ratio

μ = friction

χ = force ratio

Subscript

i, j = ith particle, jth particle

n = normal direction

s = tangential direction

r = rolling friction

e = electrical

vdw = van der Waals

References

[1] H. M. Jaeger, *et al.*, "Granular solids, liquids, and gases," *Reviews of Modern Physics,* vol. 68, p. 1259, 1996.

[2] W. Strauss, *Air pollution control, part I*: Wiley-Interscience, 1971.

[3] P. G. de Gennes, "Granular matter: a tentative view," *Reviews of Modern Physics,* vol. 71, pp. S374-S382, 1999.

[4] K. J. Dong, *et al.*, "Role of Interparticle Forces in the Formation of Random Loose Packing," *Physical Review Letters,* vol. 96, p. 145505, 2006.

[5] R. Y. Yang, *et al.*, "Characterization of interparticle forces in the packing of cohesive fine particles," *Physical Review E,* vol. 78, p. 031302, 2008.

[6] S. H. Kim and K. W. Lee, "Experimental study of electrostatic precipitator performance and comparison with existing theoretical prediction models," *Journal of Electrostatics,* vol. 48, pp. 3-25, 1999.

[7] A. Jaworek, *et al.*, "Modern electrostatic devices and methods for exhaust gas cleaning: A brief review," *Journal of Electrostatics,* vol. 65, pp. 133-155, 2007.

[8] C. Calle, *et al.*, "An electrostatic precipitator system for the Martian environment," *Journal of Electrostatics*, vol. 71, pp. 254-256, 2013.

[9] G. K. Batchelor and R. W. O'Brien, "Thermal or electrical conduction through a granular material," *Proceedings of the Royal Society of London. Series A, Mathematical and Physical Sciences*, vol. 355, pp. 313-333, 1977.

[10] V. Mourzenko, *et al.*, "Geometrical and transport properties of random packings of polydisperse spheres," *Physical Review E*, vol. 77, p. 066306, 2008.

[11] M. Sahimi, "Flow phenomena in rocks: from continuum models to fractals, percolation, cellular automata, and simulated annealing," *Reviews of Modern Physics*, vol. 65, p. 1393, 1993.

[12] D. Blanchard, *et al.*, "Correlation between current density and layer structure for fine particle deposition in a laboratory electrostatic precipitator," *Ieee Transactions on Industry Applications*, vol. 38, pp. 832-839, 2002.

[13] S. Yang, *et al.*, "Packing of fine particles in an electrical field," *Granular Matter*, vol. 15, pp. 467-476, 2013.

[14] T. E. Allibone, *et al.*, "Spatial characteristics of electric current and field in large direct-current coronas," *Proceedings of the Royal Society of London. Series A: Mathematical and Physical Sciences*, vol. 441, pp. 125-146, 1993.

[15] O. J. Tassicker, "Aspects of forces of charged particles in electrostatic precipitators," *Ph.D. Thesis, The University of New South Wales*, pp. 156-166, 1972.

[16] J. Miller, *et al.*, "Local deposition of particles in a laboratory scale electrostatic precipitator with barbed discharge electrodes," in *Sixth International Conference on Electrostatic Precipitation*, Budapest, 1996, pp. 325-334.

[17] E. Schmidt and F. Loffler, "Preparation of dust cakes for microscopic examination," *Powder Technology*, vol. 60, pp. 173-177, 1990.

[18] R. Y. Yang, *et al.*, "Computer simulation of the packing of fine particles," *Physical Review E*, vol. 62, p. 3900, 2000.

CHAPTER 5. NUMERICAL EVALUATION OF THE EFFECTIVE ELECTRICAL CONDUCTIVITY OF PACKINGS UNDER ELECTRIC FIELDS

Abstract

We present a novel numerical method to evaluate the effective electrical conductivity of the formed packings under electric fields. In particular, we focus on the electrical conduction between the contacting solid particles, which is important to electrostatic precipitation processes. The packings with a wide range of porosities are simulated using the discrete element method. The effective conductivity of the simulated packings is calculated from nodal analysis commonly applied to solve electrical network problems in the field of electrical engineering. The nodal analysis involves explicitly solving electrical network equations under an applied voltage across the boundaries of the packings. Our results reveal that the effective conductivity is influenced by several factors, such as the material properties of particles, the contact area between particles and certainly the packing structure. Also, we have shown that the electric current network of a packing resembles its contact force network. The findings suggest that the electric current flow is determined by the contact force distribution. The results may lead to better understanding of the electrical transport in random packings and thus to better design strategies in electrostatic precipitation processes.

5.1. Introduction

Random packings consisting of suspended solids embedded in a liquid or gas phase are frequently encountered in process of pharmaceutical, petroleum, food and chemical industries. Evaluation of the effective electrical conductivity of the random packing is essential for improving these processes. Theoretical evaluation of the effective conductivity involves solving the corresponding Laplace's and continuity equations [1]. For a random packing, such an approach is rather difficult due to the complexity of the packing structure [2]. There are several different approaches to solving this problem: for instance, the effective medium theory, coherent potential approach, and percolation theory [3-8]. Here, we are interested in finding the effective electrical conductivity of packing, in which electrical conduction exists only in the solid phase. This problem is particularly difficult to solve because of the failure of the continuity equation at the

interface between solid and other phases in the packings. Early studies on this problem have focused on cases of regular packings or random packings in a narrow porosity range [9, 10]. As for the studies based on laboratory experiments, the challenge exists in the characterization of the packing structure in most cases [11, 12]. For instance, the packing of fine particles in electrostatic precipitation processes are too vulnerable for practical examinations. [13] Another example is packings of ore particles in electric arc furnaces are subject to extremely high temperatures [14]. Thus, it is difficult, if not impossible to experimentally characterise the packing structures. This problem can be readily overcome by numerical simulations. In the past decades, the discrete element method has been increasingly applied to solve various problems concerning particle packing [15-18]. Here, we extend such an approach to the evaluation of the effective electrical conductivity of packings.

In this paper, a novel approach to solve the effective electrical conductivity of a random packing is presented with the specific focus on the packings found in typical electrostatic precipitation processes. The packings under electric fields with porosities ranging from 0.380 to 0.884 are generated by varying either the particle diameter or electric field using the discrete element method. Also, we examine the effect of material properties of particles, contact area between particles and the structure of a packing on its effective conductivity. Finally, we compare the similarities between contact force networks and electric current networks of the packings to reveal the effect of the interparticle forces on the contact area diameter, and consequently the effective electrical conductivity. The findings may help to advance understanding of the electrical transport through random packing.

5.2. Model descriptions

5.2.1. Generation of random packings

In this work, the random packings of particles under various electric fields are simulated using the discrete element method. Both the interparticle van der Waals interactions and the electrostatic interactions induced by the imposed electric field have been

incorporated in the simulation codes. In the discrete element method, the translational and rotational motions of particles are described following the Newton's second law of motion as,

$$m_i \frac{d\mathbf{v}_i}{dt} = \sum \left(\mathbf{F}_{ij}^{n} + \mathbf{F}_{ij}^{t} + \mathbf{F}_{ij}^{vdw} \right) + \mathbf{F}_i^{e} \tag{5.1}$$

and

$$I_{c,i} \frac{d\boldsymbol{\omega}_i}{dt} = \sum \left(\mathbf{r}_i \times \mathbf{F}_{ij}^{s} + \mathbf{T}_{ij}^{r} \right) \tag{5.2}$$

where m_i is the particle mass; $\mathbf{v}_i$ is the translational velocity; t is time; $I_{c,i}$ is the moment of inertia; $\boldsymbol{\omega}_i$ is the angular velocity; $\mathbf{r}_i$ is the particle radius; $\mathbf{T}_{ij}^{r}$ is the torque; $\mathbf{F}$ is the force acting on a particle; and the superscripts n, s, vdw, e and r, respectively denote the normal, tangential, and van der Waals interactions, electrostatic interactions and rolling friction. The detailed descriptions of the simulation method can be found in our previous work on the effect of particle diameter and electric field on the formed structures under a range of uniform electric fields [19]. Here, we focus on the effect of the structure of a packing on its electrical transport properties. The different structures of the packings are generated by changing either the particle diameter or electric field. For instance, the porosity of the packing made of 1μm particles decreases from 0.884 to 0.464, when the imposed electric field increases from 10^4V/m to 10^6V/m (see Figure 5.1). The electrical properties are calculated based on the typical structures depicted in Figure 5.1. Periodic boundary conditions are applied along the x-axis and z-axis directions, while the electrical potential difference that drives electric current is set along the y-axis direction. Then, we can define the effective electrical conductivity of a packing as,

$$\langle \mathbf{J} \rangle = \sigma_{eff} \langle \mathbf{E} \rangle \tag{5.3}$$

where σ_{eff} is the effective electrical conductivity, **J** is the current density, **E** is the electric field and the brackets denote the average over the entire structure.

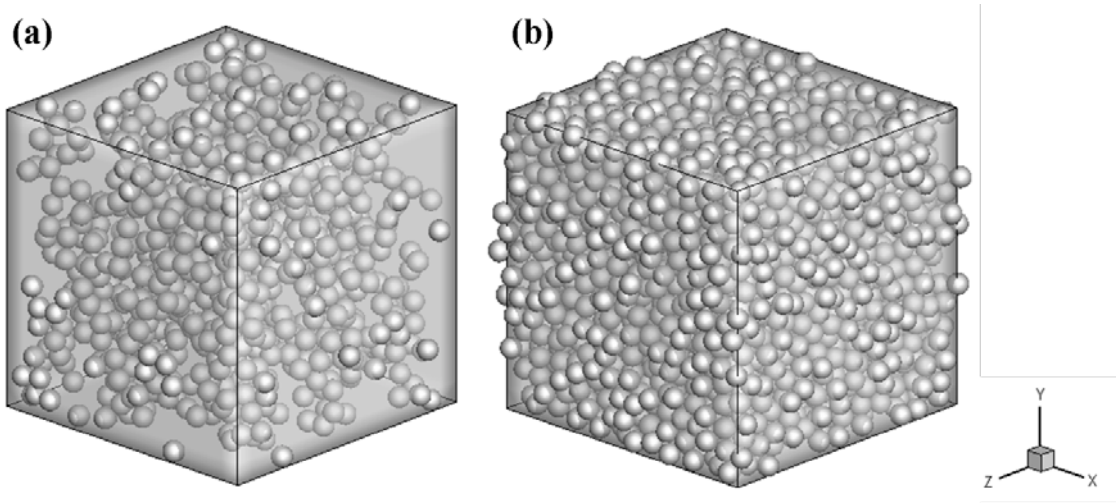

Figure 5.1: Snapshots of the packings made of 1μm particles under an electric field of (a) 10^4V/m and (b) 10^6V/m, and the porosity of the packings respectively are 0.884 and 0.464.

5.2.2. Evaluation of contact area

The effective electrical conductivity of a packing can be found in many ways. Here, we focus on the packings of fine particles precipitated in electrostatic precipitation processes. In these packings, the conductivity of the particles is much greater than the conductivity of the interstitial gases. As a result, the contacts between particles are essential. In fact, the effective conductivity of such packings is determined by the contact diameter between the particles, the packing structure as well as the material properties of the particles.

Firstly, the contact diameter between particles is determined. As described in the last section, we use the soft sphere model originally developed by Cundall and Strack, and this method employs the Hertz contact theory to calculate the interparticle contacts. Thus, the contact diameter can be found as [20],

$$d_c = \left(\frac{10md^2}{Y} \right)^{1/5} v_n^{2/5} \tag{5.4}$$

where d_c is the contact diameter, d is the particle diameter, Y is the Young's modulus and v_n is the relative velocity in the normal direction. It should be noted that the contact diameter between the contacting particles is directly computed in the simulation due to the dynamic nature of the discrete element method. From Eq.5.4, the contact forces between particles influence the contact diameter. However, the force information is difficult to measure in practical experiments. This problem can be easily overcome in our simulation. It should be noted that the simulated Young's modulus is set to be less than the real Young's modulus in order to improve the computational efficiency and reduce the computational time. This treatment is justified since it is well established that the modified Young's modulus does not affect the structure of packings [17]. On the other hand, we find that the contact diameter is nonetheless affected by the small Young's modulus. Thus, we introduce a correction coefficient k, which relates the real contact diameter d_c to the contact diameter used in the simulation d_{co} as [21],

$$d_c = k \cdot d_{c0} = \left(\frac{Y_0}{Y} \right)^{1/5} \left(\frac{5mr^2}{4Y} \right)^{1/5} v_n^{2/5} \tag{5.5}$$

where Y_0 and Y respectively are the simulated and the real Young's modulus. In short, the contact diameter is determined with ease in our simulations.

5.2.3. Electrical conduction methods

Additionally, both the volume and surface conductions influence the effective electrical conductivity. In electrostatic precipitation processes, the operational temperature impacts the electrical conductivity of the packing as depicted in Figure 5.2. When the temperature is low, the precipitation environment is humid, and a large amount of liquid vapour covers the particles. This will increase the surface conductivity, meaning that the

overall effective electrical conductivity increases with decreasing temperature. On the other hand, when the temperature is high, the humidity level is low. However, the volume conductivity increases with rising temperature and dominates over the surface conductivity. Thus, the overall conductivity again increases with the temperature (see Figure 5.2). In short, the changes in the electrical conductivity according to temperature can be expressed by the changes in volume and surface conductivities of particles. Thus, they must both be included in the evaluation of effective electrical conductivity of the simulated packing.

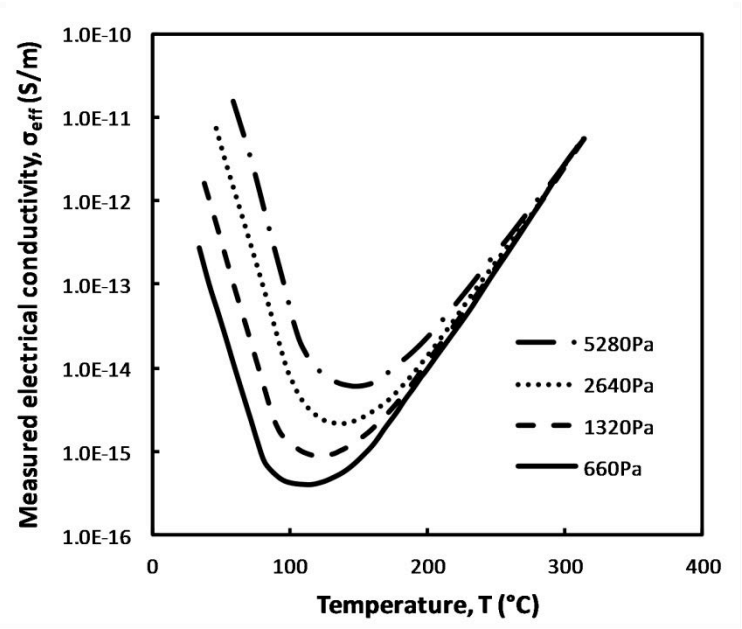

Figure 5.2: Variations of the electrical conductivity of packings with temperature. The different lines were produced by changing the water vapour pressure [22].

To consider the surface and volume conductions, we assume that a uniform electric field is established in the vicinity of the contact between a pair of contacting particles so that an equivalent electrical potential exists inside each particle. Under these conditions, the volume contact conductance G_v between the contacting particles is given by [23],

$$G_v = d_c \cdot \sigma_v \tag{5.6}$$

where σ_v is the bulk volume conductivity and d_c is the contact diameter. Also, the surface contact conductance G_s is given by [23],

$$G_s = \frac{\sigma_s \pi}{\ln\left(\frac{d}{d_c}\right)} \tag{5.7}$$

where σ_s is the bulk surface conductivity. When the volume and surface conductions are considered as if they are connected in parallel, the total contact conductance G is,

$$G = d_c \cdot \sigma_v + \frac{\sigma_s \pi}{\ln\left(\frac{d}{d_c}\right)} \tag{5.8}$$

Now, we can express the temperature effect on the electrical conductivity as changes in the volume and surface conductivities based on Eq.5.8. It is worth noting that the conductivity of the interstitial gases has to be considered to account for the abnormal back corona that may occur during electrostatic precipitation operations [24, 25]. However, this is outside the scope of this paper. The electrical conditions of the back corona will be the subject of a future study. Nevertheless, both the volume and surface conductions are considered here in the evaluation of the effective conductivity.

5.2.4. Evaluation of effective conductivity

Now, the effective electrical conductivity of the simulated packings can be determined knowing the electrical conductance between each pair of particles and the packing structure. Here, we use nodal analysis to characterise the packing structure. The nodal analysis is commonly applied in the field of electrical engineering to examine properties of electrical networks [6]. Applying to particle packing, particles and contacts are regarded as nodes and edges respectively for the electrical network analysis. For instance, nodal analysis of a typical packing in two dimensions is shown in Figure 5.3. In this case, the packing structure is discretized into an equivalent network of conductors. Each pair of contacts is expressed as an equivalent edge. Then, the structure of the packing, or more precisely, the connectivity of the packing is expressed in an

incidence matrix *A*. In this example, an incidence matrix has six rows and seven columns representing a structure with 6 nodes and 7 edges. The direction of an electric current is indicated by the plus and minus signs in the matrix. The electric current flow from particle 2 to 1 is expressed as +1 and -1 in the first and second columns of the first row, and the plus and minus signs indicate the direction of the current flow.

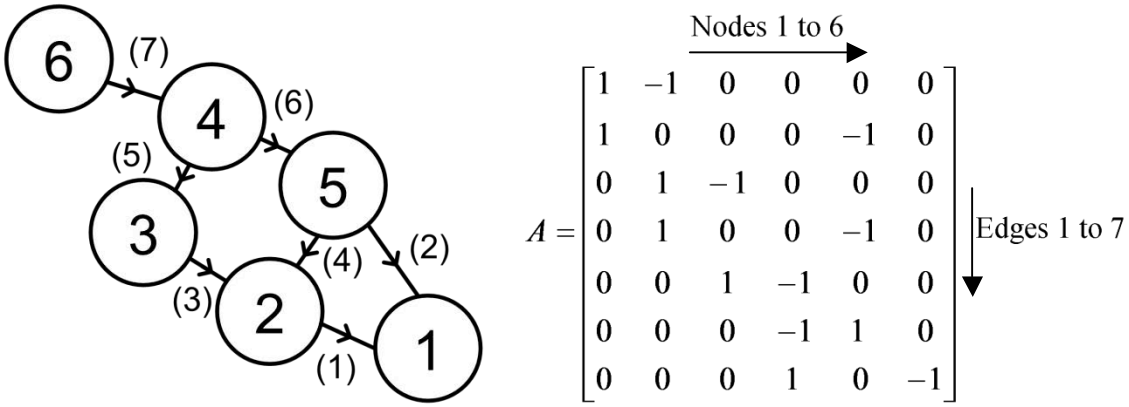

Figure 5.3: Schematic diagram of the formation of an incidence matrix from a typical packing in two dimensions.

Then, the potential difference **e** between every pair of contacting particles is,

$$\mathbf{e} = A\mathbf{u} \tag{5.9}$$

where **u** is a vector containing the voltage on every particle. The electric current **I**, is given by Ohm's law as,

$$\mathbf{I} = g\mathbf{e} = g\left(A\mathbf{u}\right) \tag{5.10}$$

where g is a vector containing all the conductance between particles. Note that the incidence matrix is essential in the nodal analysis, because it allows the expression of the electrical conditions inside a random packing in a matrix form. Moreover, the Kirchhoff's law states that the sum of electric current flows in and out of a particle must equal to zero, which mathematically is,

$$\sum_j I_{ij} = 0 \tag{5.11}$$

The Kirchhoff's law also applies to our cases, and in the matrix form, it is,

$$A^T \mathbf{I} = A^T \left(g \left(A\mathbf{u} \right) \right) = 0 \tag{5.12}$$

Thus, we have established a set of linear equations describing the electrical conditions in a given structure. Together with the boundary conditions, we can explicitly solve Eq. 5.12 for both the potential difference and the electric current between each pair of particles in a given packing. Here, we have found that the Gauss-Seidel method is effective in solving the matrix. In this study, we set the convergence limit to 10^{-12}. Finally, the effective electrical conductivity is found by,

$$\sigma_{eff} = \frac{I \cdot H}{S \cdot \Delta V} \tag{5.13}$$

where I is the total electric current, ΔV is the potential difference applied at the boundaries, H is the depth, and S is the cross-sectional area of a packing.

5.2.5. Corrections to numerical packings

Using the proposed method, we now can explicitly determine the electrical potential on every particle in a random packing. A typical electrical potential range on each particle in a packing is illustrated in Figure 5.4a, which demonstrates a continuous variation of the electrical potential on the particles from the top to the bottom boundaries. As expected, the electrical potential on the particles decreases as their depth increases (see Figure 5.4b). However, the slight non-linearity of the plot suggests that variations of the effective electrical conductivity against the depth are non-linear.

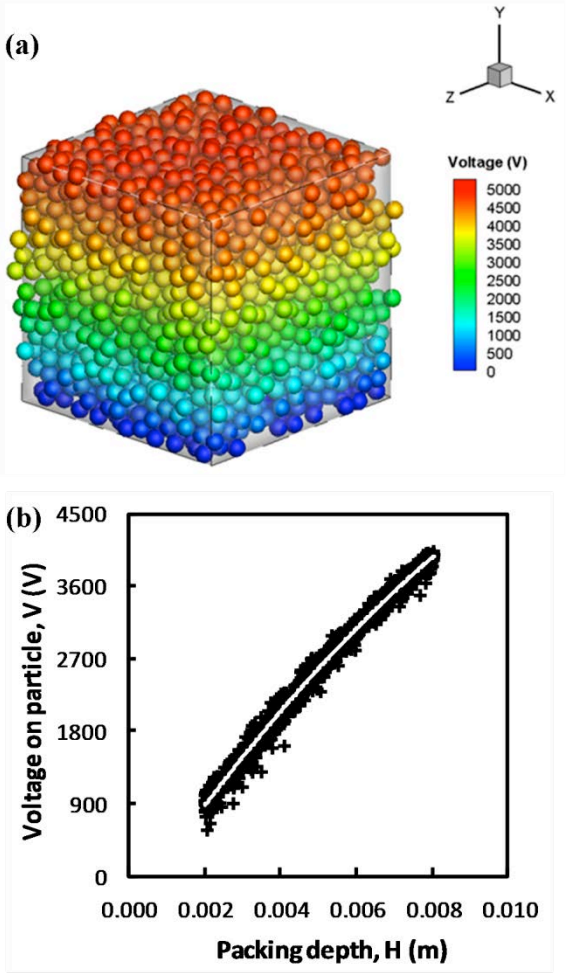

Figure 5.4: (a) Distributions of the voltage on each particle in a packing with a porosity of 0.464, and (b) the corresponding variations of the voltage against the depth of the particle.

To elucidate the depth dependent non-linearity in the simulated packings, we investigate variations of both the structure and contact diameter against the packing depth. Here, we use the averaged porosity, coordination number and contact diameter at a given depth to represent the properties at that packing depth. Firstly, we examine the change of structure with the packing depth (see Figure 5.5a). Our results illustrate that there is no obvious structural change, in terms of porosity and coordination number, with the packing depth. On the other hand, the contact diameter is found to change with the depth (see Figure 5.5b). As a consequence, the effective conductivity varies correspondingly with the depth. The depth dependent contact diameter can be explained by the depth dependent forces between contacting particles in the packing. Early studies

have demonstrated that the contact force between particles increases with the packing depth, because of the weight of the subsequent particles impacting on the existing ones during the formation of packing [26]. This, in turn, will increase the contact diameter between particles at the bottom of packing, resulting in an increase in the effective electrical conductivity.

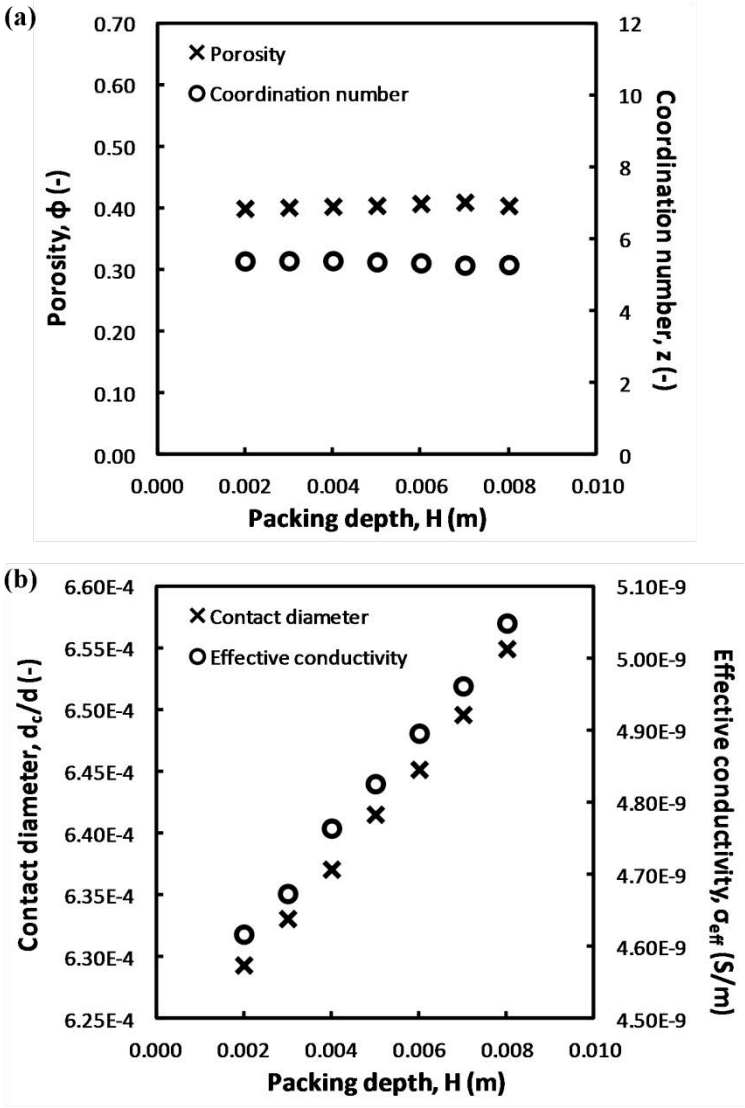

Figure 5.5: (a) Changes in porosity and coordination number against packing depth, and (b) changes in contact diameter and effective conductivity against packing depth of a typical formed packing using 1mm particles under an electric field of 50000V/m.

To account for the effect of the packing depth on the effective electrical conductivity, we use the depth dependent contact diameter in the calculation of the effective conductivity. The depth dependent contact diameter $\bar{d}_c$ is defined as,

$$\overline{d}_c = \frac{1}{H_{\max}} \int_0^{H_{\max}} d_c(H) \cdot dH \tag{5.14}$$

where 0 and H_{max} represent the top and bottom boundaries. Next, we apply the depth dependent contact diameter to solve for the effective conductivity. The results indicate this treatment effectively eliminates the previously observed depth dependent non-linearity in the packing (see Figure 5.6b). We find that the effective electrical conductivity now is independent of the depth of a packing. Moreover, the scatter in the data points suggests that the electric properties of a random packing, e.g., electrical potential distributions and electric current paths are complicated (see Figure 5.6b). This implies that the structure and the connectivity of a packing is essential to the electrical transfer through the packing. The detailed quantitative analysis will be carried out in the results section. It is worth noting that the gradient of the voltage against the depth of the particle in Figure 5.6b are significantly different from that in Figure 5.4b.

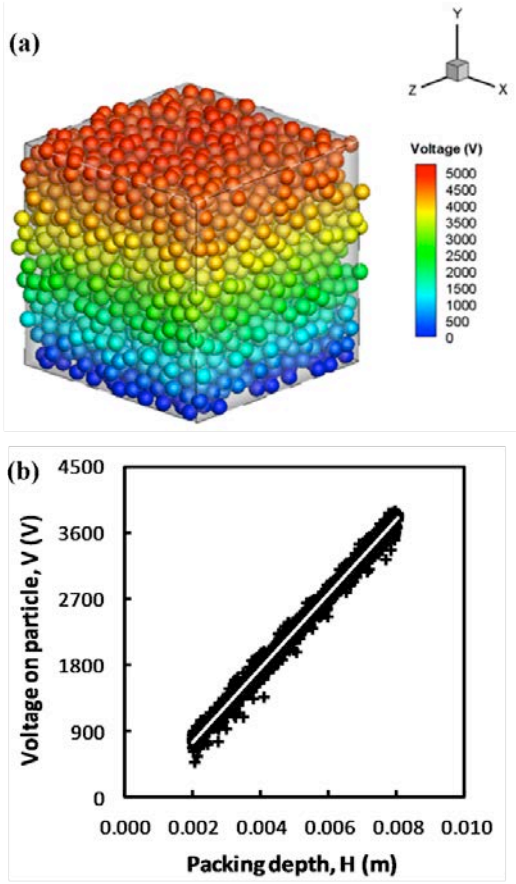

Figure 5.6: (a) Distributions of the voltage on each particle in a packing with a porosity of 0.464 accounting for the depth effect, and (b) the corresponding variations of the voltage against the depth of the particle.

Lastly, the list of simulation parameters used in our model is included in Table 5.1. To examine the effective conductivity of different packings, both the particle diameter and the imposed electric field are varied to generate packings with a range of packing structures (see Table 5.1). The effective conductivity is then found using nodal analysis as described in section 5.2.4. To eliminate the effect of uneven top boundary, ten percent of the top boundary of each packing is excluded in the calculation of the effective conductivity. The effect of bottom boundary is in fact in existence and important to the overall conductivity of the packings, and therefore it is included in all our simulations. Although the cross-sectional area of the simulated packings is varied greatly, the resultant effective conductivity should not be affected because periodic boundaries are applied in the two directions perpendicular to the imaginary collection plate. The comparison of the effective conductivity of the packings formed using a

range of particle diameter and under a range of imposed electric fields will be included in the results section.

Table 5.1: Simulation parameters and their values.

Particle diameter, d	1×10^{-6} to 1×10^{-3} m
Electric field, **E**	10^4 to 10^6 V/m
Packing porosity, Φ	0.380 to 0.884
Material density, ρ_m	2500 kg/m^3
Young's modulus, Y	6x10^{10}
Volume conductivity, σ_v	1×10^{-5} S/m
Surface conductivity, σ_s	1×10^{-9} S/m
Cross-sectional area, S	2.25×10^{-10} to 2.25×10^{-4} m^2
Potential difference, ΔV	0 to 5000V
Packing depth, H	1×10^{-5} to 1×10^{-2} m

5.3. Results and discussion

5.3.1. Model validation

To start with, the model predicted effective electrical conductivity of the simulated packings are compared with the experimentally measured ones to verify the developed model [22]. The material properties of particles in the simulated packings are set to match the properties of soda glass beads in the experiments. The experimental results have demonstrated that the effective conductivity of packings decreases with the increasing particle diameter. The simulation results show that the numerical predictions are in good agreement with the experimental data (see Figure 5.7). Furthermore, the effective electrical conductivity decreases with increasing particle diameter at all three humidity levels considered. Thus, it is effective to control the volume and surface

conductivity of particles to account for the humidity effects on the effective conductivity. These findings have successful proven the validity of the newly proposed model for the predictions of the effective electrical conductivity of various packings.

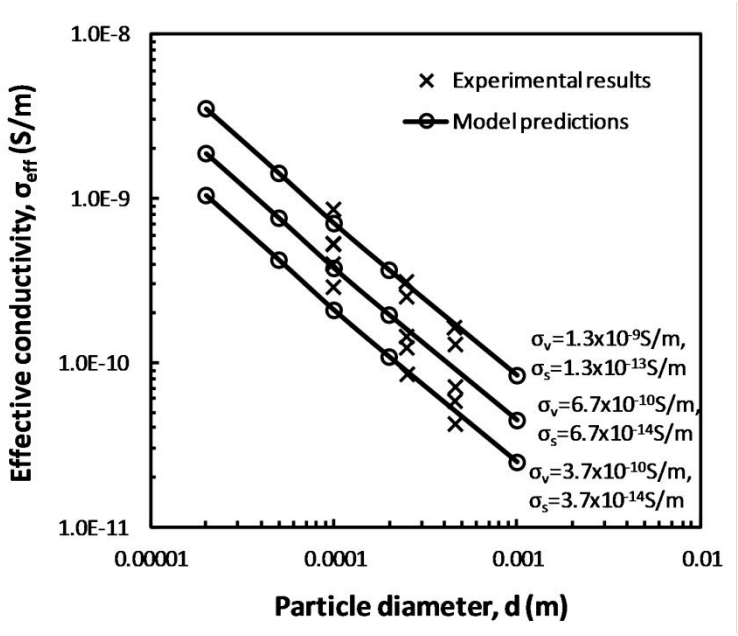

Figure 5.7: The comparison of the numerical results with the existing experimental measurements.

5.3.2. Effect of material properties

As mentioned earlier, the material properties of particles in a random packing impact the effective electrical conductivity. Here, we study effects of factors related to material and physical properties of particles, such as the volume conductivity, surface conductivities and particle diameter. To begin with, we study the effect of the volume and surface conductivities. For a given surface conductivity, the effective conductivity is found to increase with the volume conductivity (see Figure 5.8a). The results are intuitive. When volume conductivity of particles increases, the conduction at the point of contact between the particles improves and this leads to an increase in the effective conductivity of the packing. The similar trends are observed by varying the surface conductivity while keeping the volume conductivity unchanged (see Figure 5.8b). Thus,

the findings confirm that the electrical properties of particles are parts of the influencing factors that determine the effective electrical conductivity of the packings under electric fields.

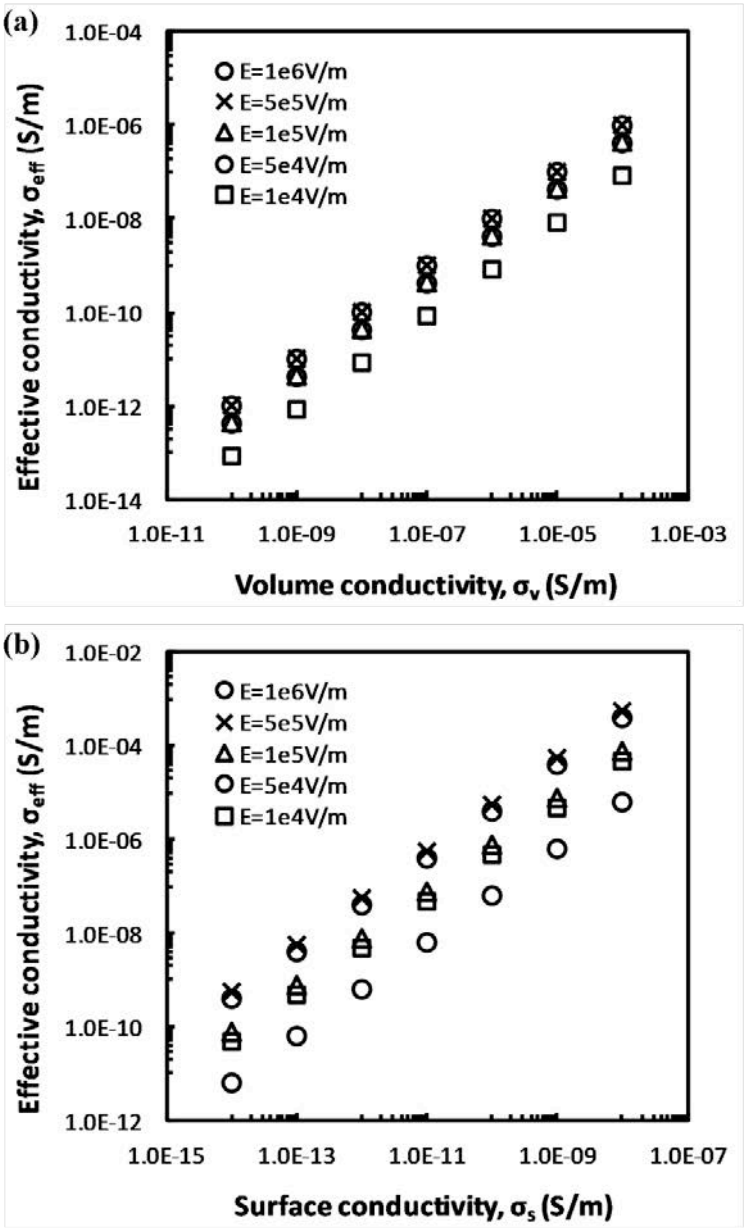

Figure 5.8: Variations of the effective electrical conductivity of the simulated packings against (a) the volume conductivity and (b) the surface conductivity of the particle. The particle diameter is in range of 5μm to 1000μm and the electric field varies from 10^4V/m to 10^6V/m .

In addition, the particle diameter is another important material property that influences the effective conductivity of packings. In general, we find that the effective conductivity

decreases with the increasing diameter of particles in a packing (see Figure 5.9). Here, all data are obtained from the packings formed under electric fields. The observed trend is consistent with experimental observations on electrostatic precipitation processes [22]. Moreover, the effective conductivity of the formed packings under strong electric fields varies with the particle diameter more significantly than that of the formed packings under weak electric fields (see Figure 5.9). This implies that there are factors other than material properties influencing the effective electrical conductivity. In fact, we find that the effective conductivity changes with both the contact diameter and packing structure. As the particle diameter increases, these two factors will cause the effective conductivity to decrease, which will result in the trends observed in Figure 5.9. Unlike the particle diameter that is easily measurable, the contact or structural information is difficult to determine in conventional practical experiments. In contrast, these characteristics of packings are readily available in our simulations.

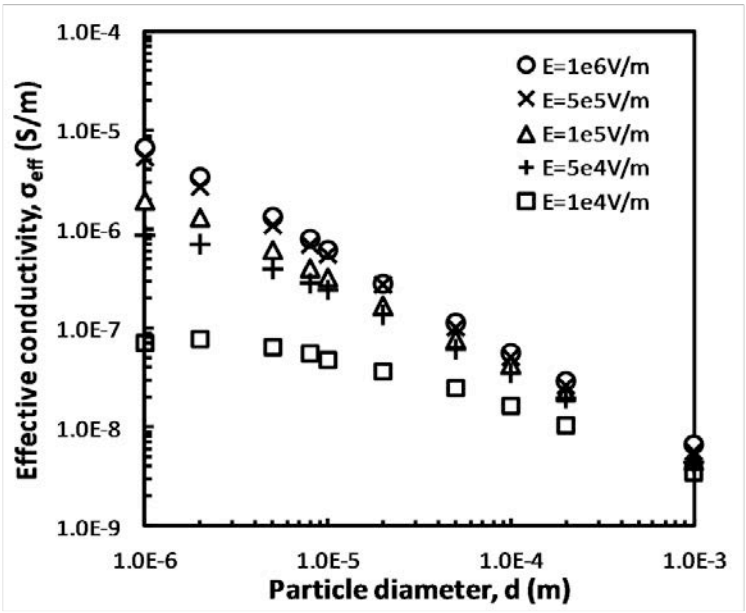

Figure 5.9: Variations of effective electrical conductivity against particle diameter.

5.3.3. Effect of contact diameter

To elucidate the effect of contact diameter on the effective electrical conductivity, we firstly examine the impact of particle diameter on the contact diameter between particles.

Here, we focus on the averaged contact diameter between particles in packings. Our results indicate that the averaged contact diameter increases with particle diameter for all simulation cases (see Figure 5.10a). Note that the results from our simulation are highly reproducible. To compare the results from the packings made of the different sizes of particles, we use the dimensionless contact diameter that is the contact diameter divided by the particle diameter. The results demonstrate that the dimensionless contact diameter actually decreases with the increasing particle diameter (see Figure 5.10b). These counterintuitive findings can be explained by the changes in the forces at the contact points between particles as the particle diameter changes. It is generally accepted that when the particle diameter is small, the attractive interparticle van der Waals interactions are more significant compared to other forces, that are gravitational force or electrostatic interactions [19, 27]. Consequently, the dimensionless contact diameter increases with decreasing particle diameter. This improves the electrical transport in the packing and the effective conductivity increases. In short, the contact diameter between particles is shown to vary with the diameter of the particles under given imposed electric fields.

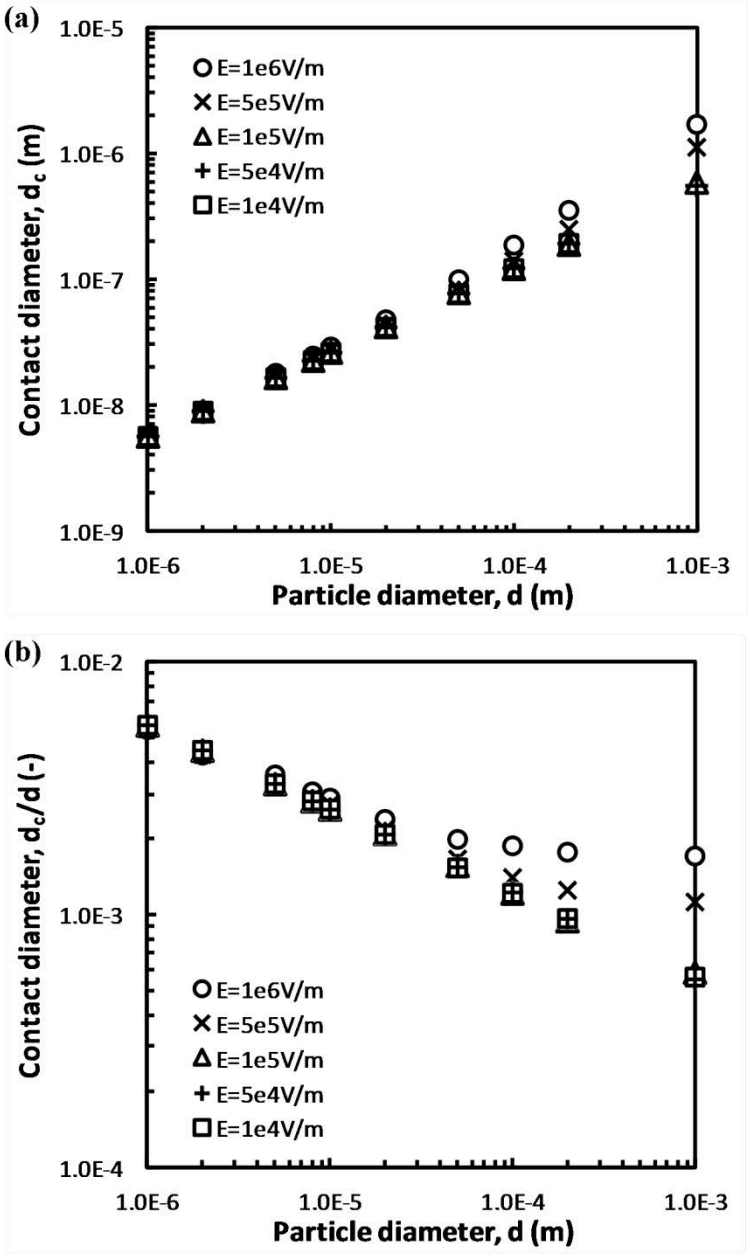

Figure 5.10: Effect of the particle diameter on (a) the absolute contact diameter and (b) the dimensionless contact diameter between particles.

Next, we examine the effect of contact diameter on the effective electrical conductivity of the simulated packings. The results reveal that the effective conductivity always increases with the contact diameter between particles (see Figure 5.11). As what we expected, the increasing contact diameter improves the electrical conduction between the contact particles and consequently the effective electrical conductivity. These findings support the previously observed relationship between the effective conductivity

and the particle diameter (see Figure 5.9). The increasing particle diameter in a packing decreases the dimensionless contact diameter between particles. This leads to a reduction in the effective conductivity of the packing. In summary, it is evident that the effective electrical conductivity of a packing increases with the contact diameter between the particles in the packing. It should be noted that varying particle diameter not only changes the contact area but also causes structural variations in a packing. In the next section, we will study the effect of packing structure on the effective electrical conductivity.

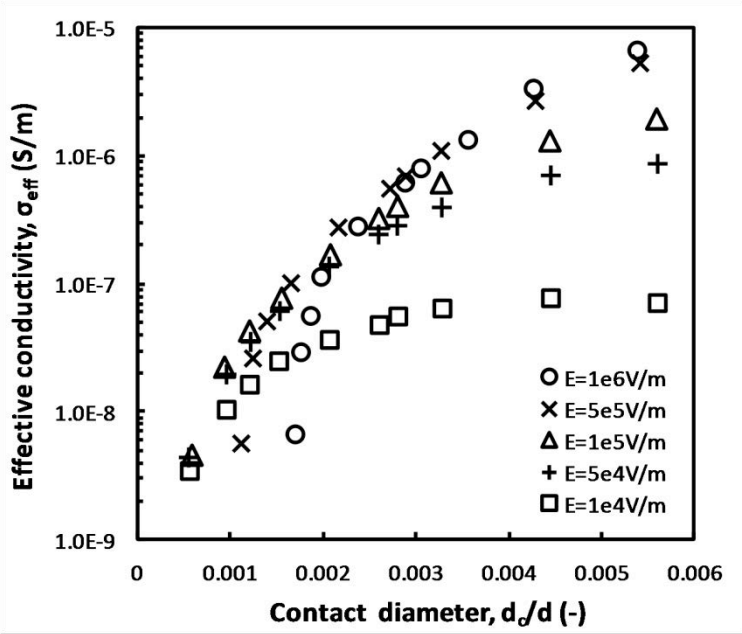

Figure 5.11: Variations of effective electrical conductivity against contact diameter.

5.3.4. Effect of structural properties

There are many ways to characterise the structure of a random packing. In this study, we focus on the porosity and the coordination number, because they are the most relevant in the evaluation of the effective electrical conductivity. To examine the effect of the porosity of a packing on its effective electrical conductivity, we firstly generate the packings in the porosity range of 0.380 to 0.884 by adjusting the particle diameter or electric field. Then the effective conductivity of the simulated packings is determined

using the proposed numerical model. Our results has indicated that the effective conductivity increases with the porosity as depicted in Figure 5.12a. The degree of the change in effective conductivity according to the porosity is evidently influenced by the imposed electric fields. The effective conductivity increases more sharply with the porosity for the formed packing under stronger electric fields. Furthermore, to compare the formed packing under various electric fields, the effective conductivity is normalised by the square of the corresponding electric field. After normalisation, almost all of our data collapse into a single curve showing that the effective conductivity indeed increases with the porosity of a packing (see Figure 5.12b). One might expect that the effective conductivity of a more porous structure is smaller because there is less particles to conduct electric current in a given volume. However, it is generally accepted that the average number of contacts is also smaller in a more porous structure [27, 28]. A reduction in the number of contacts results in a small resistance to the electric current that flows through a packing. This explains the observed increasing in the effective conductivity as the porosity increases. The number of contacts in a packing can be characterised by the coordination number of a packing. Hence, the relationship between coordination number and effective electrical conductivity should be studied.

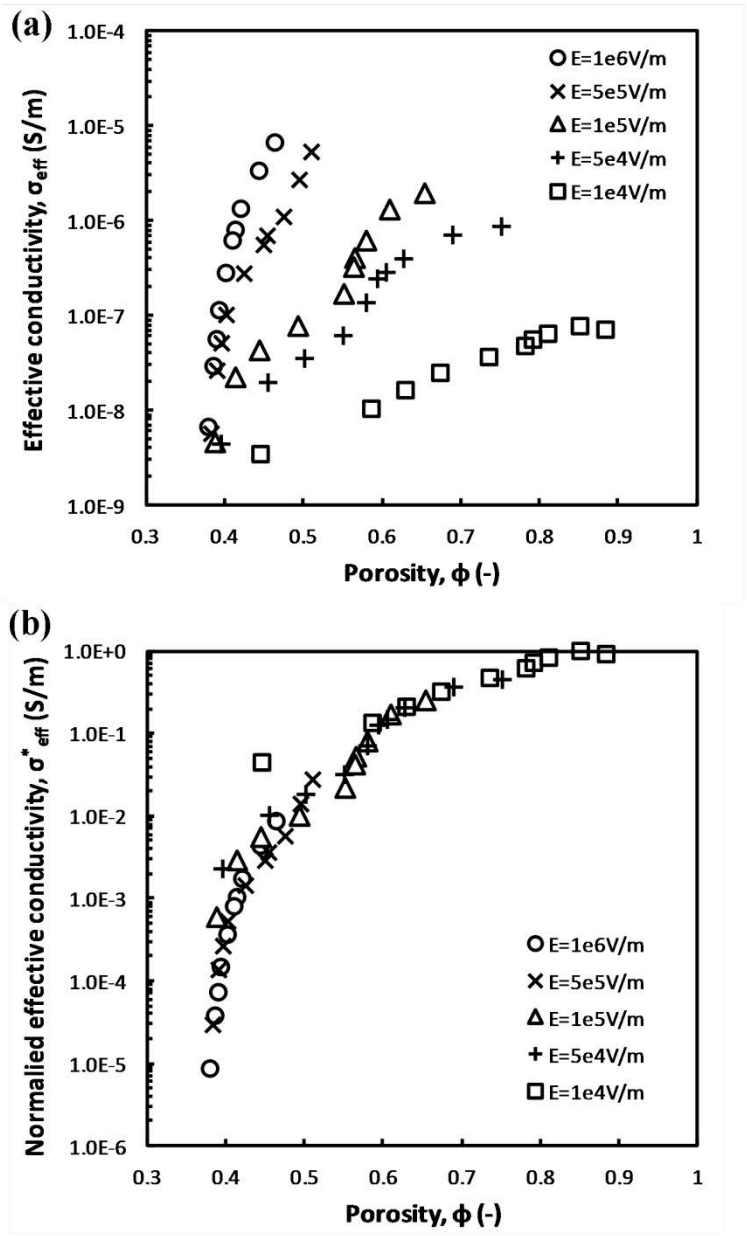

Figure 5.12: (a) The relationship between the porosity of the simulated packings and their effective conductivity, and (b) the effective conductivity has been normalised by the square of the electric field.

To investigate the effect of coordination number on the effective conductivity of packings, we characterise the packings using the average coordination number. The coordination number represents the number of contacts a particle has with the surrounding particles. Here, we define two particles are in contact when the centre distance between them is smaller than 1.01 times of the sum of their diameters. Our results reveal that the effective conductivity decreases with the increasing coordination

number for most cases, and the degree of change is dependent on the imposed electric field (see Figure 5.13a). Similar to the porosity, it is clearly that the effective conductivity of packings needs to be normalised according to the electric fields. The results after the normalisation indicate a single relation between the effective conductivity and the coordination number (see Figure 5.13b). As expected, increasing coordination number provides more resistance to the electric current flowing across a packing. As a result, the effective conductivity is lowered. In addition, the force at each contact point increases with the decreasing number of contacts per unit volume when the total stress on a packing is always kept constant. The impact of the interparticle force on the effective conductivity will be discussed later. In summary, we have successfully demonstrated the importance of the structure of a packing on its effective electrical conductivity. Both porosity and coordination number have significant effects on the effective conductivity of a packing.

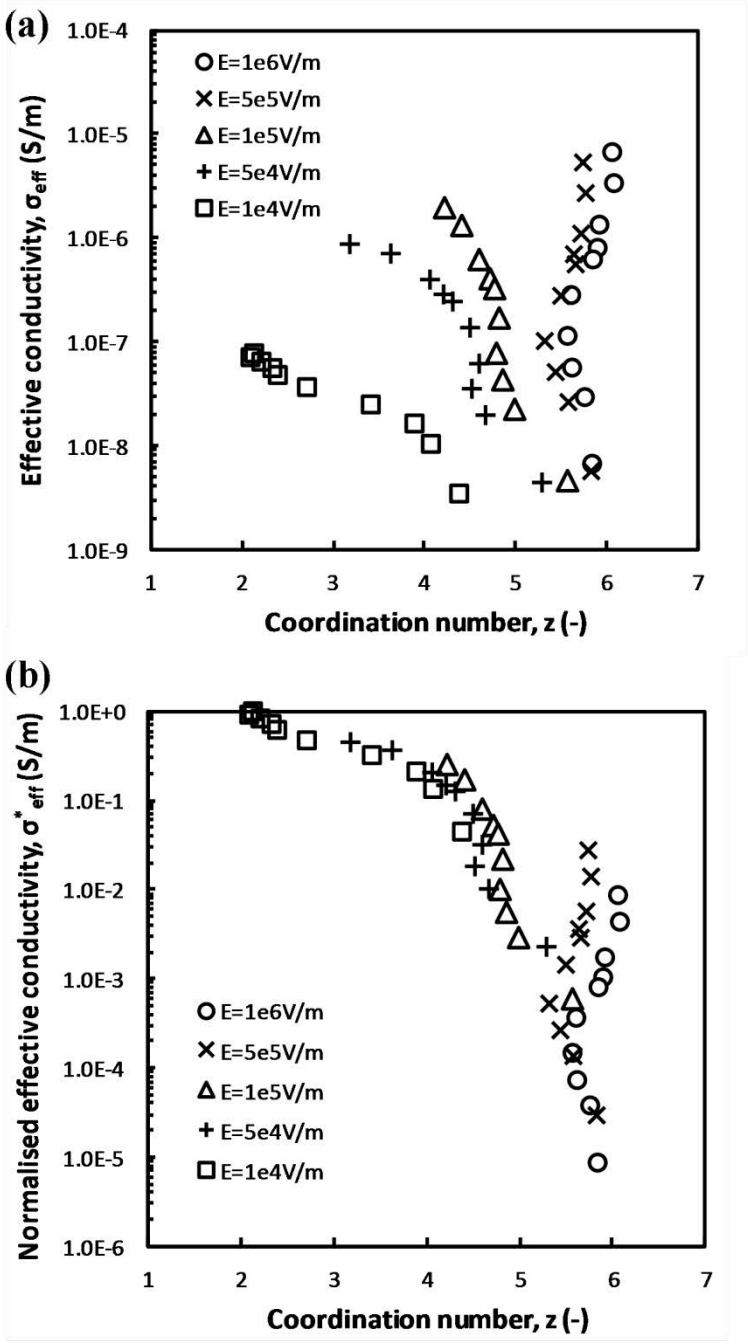

Figure 5.13: (a) The relationship between the averaged coordination number of the simulated packings and their effective electrical conductivity, and (b) the effective conductivity has been normalised by the square of the electric field.

5.3.5. Correlation between contact force and electric current

To this point, we have demonstrated the importance of the interparticle forces between particles in the determination of the contact area and the coordination number and subsequently the effective conductivity of random packings. Analysing the microscopic forces in a random packing always is a challenge in practice. The most effective way to experimentally characterise the interparticle forces is to use photoelastic particles, and yet such a method is generally limited to two-dimensional packings [29]. On the contrary, the interparticle forces can be obtained from our simulations with ease. For example, the interparticle contact force networks of typical packings are depicted in Figure 5.14a and Figure 5.14b. The contact forces between particles are represented by bonds, and the thickness of a bond represents the magnitude of the inter-particle force. The thicker bond represents the stronger force between particles. Also, the results demonstrate the contact force network varies according to the porosity of the packings. For a dense packing, the contact force is concentrated at the bottom of the packing (see Figure 5.14a). The anisotropy due to the stress from the subsequently-dropped particles has been extensively studied in literature [26]. As the packing becomes less dense, the non-uniform contact network disappears (see Figure 5.14b). It is expected that these changes in the contact force will have an impact on the contact area, and therefore, the electric current between particles. This, in turn, leads to changes in the effective electrical conductivity of packings.

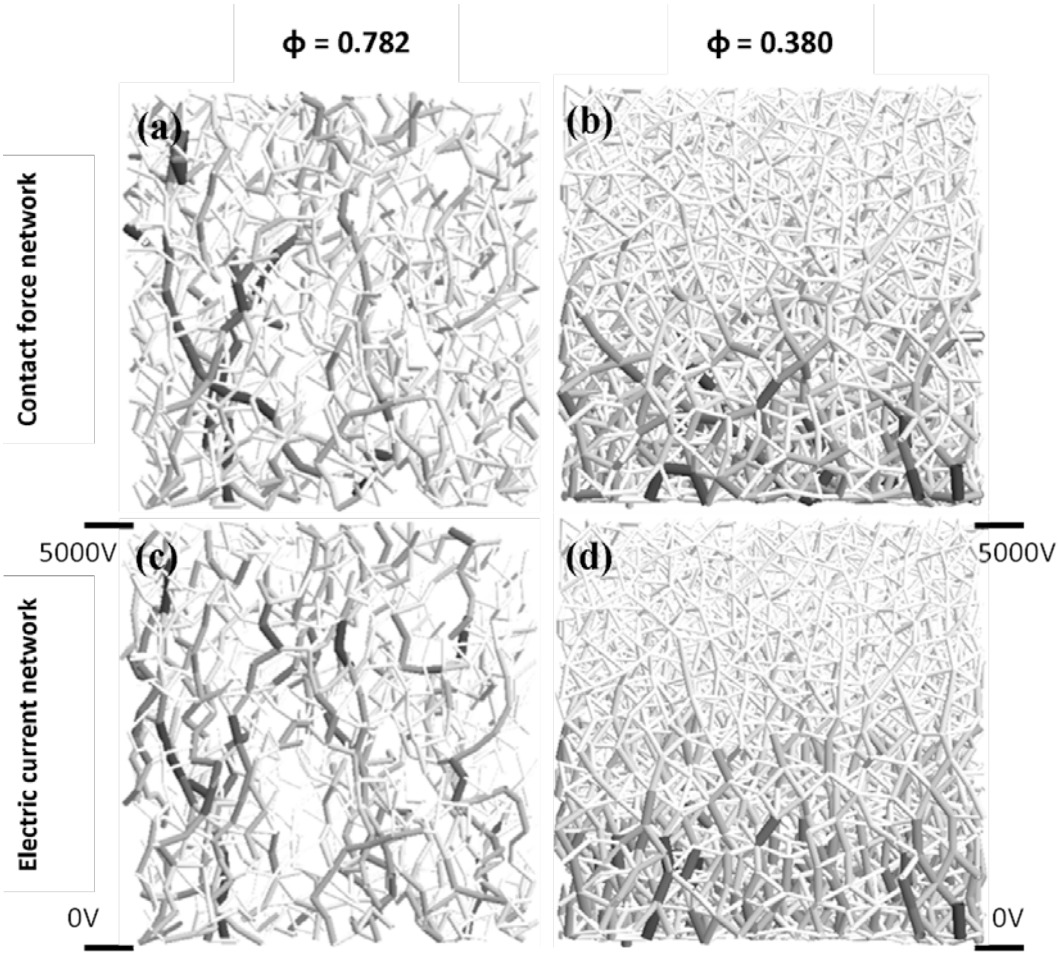

Figure 5.14: Contact force network for a section of a packing with (a) a porosity of 0.782, and (b) a porosity of 0.380; and the corresponding electric current network for the packing with (c) a porosity of 0.782 and (d) a porosity of 0.380.

As the electric current between each pair of particles is solved explicitly in our approach, we can also study the electric current flow among particles in a packing. The electric current networks of the packings with different porosities are illustrated in Figure 5.14c and Figure 5.14d. For both cases, a potential difference of 5000V is applied across the boundaries as described earlier. Here, a bond represents the electric current between particles, and the thickness of the bond represents the amount of the current flow. The results reveal that the electric current network of a packing varies with the porosity of the packing. It is evident that the electric current network resembles the contact force network because both depend on the contact point network. These findings indicate that the inter-particle force network of a packing is a determining factor of the effective conductivity of the packing. Moreover, it should be noted that the difference between

the contact force and electric current network is that the electric current preferentially flows along the direction that the electrical potential is applied. Noticeably, many bonds in the contact force network have disappeared in the electric current network in the direction perpendicular to the applied electrical potentials at the boundaries. In conclusion, the interparticle forces between particles have an undeniable effect on the electric current flow and consequently the effective conductivity of packings. The larger the inter-particle force between a pair of particles, the larger the contact area and subsequently the larger current flow between them. The detailed study on the impact of the interparticle force on the contact diameter and consequently the effective conductivity will be provided in the following chapter.

5.4. Conclusions

In summary, we have presented a novel approach to evaluate the effective electrical conductivity of random packings that is applicable to electrostatic precipitation processes. Packings with a wide range of porosities are generated using the discrete element method. Our results indicate that the material properties of particles, contact area between particles and structure of a packing all have significant effects on the effective electrical conductivity. Also, the contact force and electric current network of packings can be readily analysed using the developed simulation method. The force analysis is difficult if not impossible for experimental studies. The results reveal that the interparticle contact force determines the contact area and current flow between particles, and therefore the effective conductivity of a packing. This method can easily be applied to calculate the effective thermal conductivity of a packed bed when only solid-solid thermal conduction is significant.

Nomenclature

m = mass

$\mathbf{v}$ = velocity

t = time

F = force

I_c = moment of inertia

r = particle radius

d_c = contact diameter

d = particle diameter

Y = Young's modulus

k = correction coefficient

G, g = electrical conductance

e, ΔV = potential difference

A = incidence matrix

u = electrical potenial

I = electric current

H = packing depth

S = cross-sectional area

Greek Letters

ω = angular velocity

σ = electrical conductivity

Φ = porosity

ρ_m = mass density

Subscript

i, j = ith particle, jth particle

n = normal direction

t = tangential direction

vdw = van der Waals

e = electrical

r = rolling friction

eff = effective conductivity

v = volume

s = surface

References

[1] S. Torquato, *Random heterogeneous materials: microstructure and macroscopic properties* vol. 16: Springer, 2001.

[2] D. Bruggeman, "Calculation of various physics constants in heterogenous substances I Dielectricity constants and conductivity of mixed bodies from isotropic substances," *Annalen Der Physik,* vol. 24, pp. 636-664, 1935.

[3] J. C. Maxwell, *A treatise on electricity and magnetism* vol. 1: Clarendon Press, 1881.

[4] S. Kirkpatrick, "Percolation and conduction," *Reviews of Modern Physics,* vol. 45, p. 574, 1973.

[5] D. J. Jeffrey, "Conduction through a random suspension of spheres," *Proceedings of the Royal Society of London. A. Mathematical and Physical Sciences,* vol. 335, pp. 355-367, 1973.

[6] G. Milton, "The coherent potential approximation is a realizable effective medium scheme," *Communications in Mathematical Physics,* vol. 99, pp. 463-500, 1985.

[7] G. W. Milton, *The theory of composites* vol. 6: Cambridge University Press, 2002.

[8] Q. To, *et al.*, "Closed-form solutions for the effective conductivity of two-phase periodic composites with spherical inclusions," *Proceedings of the Royal Society A: Mathematical, Physical and Engineering Science,* vol. 469, p. 20120339, 2013.

[9] G. K. Batchelor and R. W. O'Brien, "Thermal or electrical conduction through a granular material," *Proceedings of the Royal Society of London. Series A, Mathematical and Physical Sciences,* vol. 355, pp. 313-333, 1977.

[10] J. C. R. Turner, "Two-phase conductivity : The electrical conductance of liquid-fluidized beds of spheres," *Chemical Engineering Science,* vol. 31, pp. 487-492, 1976.

[11] K. McLean, "Factors affecting the resistivity of a particulate layer in electrostatic precipitators," *Air Pollution Control Association, Journal,* vol. 26, pp. 866-870, 1976.

[12] P. Eidem, *et al.*, "Effect of contact resistance on bulk resistivity of dry coke beds," *Metallurgical and Materials Transactions B,* vol. 40, pp. 388-396, 2009.

[13] E. Schmidt and F. Loffler, "Preparation of dust cakes for microscopic examination," *Powder Technology,* vol. 60, pp. 173-177, 1990.

[14] P. Eidem, *et al.*, "Determination of electrical resistivity of dry coke beds," *Metallurgical and Materials Transactions B,* vol. 39, pp. 7-15, 2008.

[15] H. Zhu, *et al.*, "Discrete particle simulation of particulate systems: A review of major applications and findings," *Chemical Engineering Science,* vol. 63, pp. 5728-5770, 2008.

[16] K. J. Dong, *et al.*, "DEM simulation of cake formation in sedimentation and filtration," *Minerals Engineering,* vol. 22, pp. 921-930, 2009.

[17] H. P. Zhu, *et al.*, "Discrete particle simulation of particulate systems: Theoretical developments," *Chemical Engineering Science,* vol. 62, pp. 3378-3396, 2007.

[18] K. Bourbatache, *et al.*, "Discrete modelling of electrical transfer in multi-contact systems," *Granular Matter,* vol. 14, pp. 1-10, 2012.

[19] S. Yang, *et al.*, "Packing of fine particles in an electrical field," *Granular Matter,* vol. 15, pp. 467-476, 2013.

[20] P. Cundall and O. Strack, "A discrete numerical model for granular assemblies," ed: Dames and Moore London, England, 1979.

[21] Z. Y. Zhou, *et al.*, "A new computational method for studying heat transfer in fluid bed reactors," *Powder Technology,* vol. 197, pp. 102-110, 2010.

[22] S. Masuda, "Effects of temperature and humidity on the apparent conductivity of high resistivity dust," *Electrotech journal, Japan,* vol. 7, p. 108, 1962.

[23] R. Holm, *Electric contacts theory and application*. New York: Springer-Verlag, 1967.

[24] A. Mizuno, "Electrostatic precipitation," *Dielectrics and Electrical Insulation, IEEE Transactions on,* vol. 7, pp. 615-624, 2000.

[25] K. J. McLean, "Electrostatic precipitators," *Iee Proceedings-a-Science Measurement and Technology,* vol. 135, pp. 347-361, 1988.

[26] R. Y. Yang, *et al.*, "Characterization of interparticle forces in the packing of cohesive fine particles," *Physical Review E,* vol. 78, p. 031302, 2008.

[27] R. Y. Yang, *et al.*, "Computer simulation of the packing of fine particles," *Physical Review E,* vol. 62, p. 3900, 2000.

[28] J. D. Bernal and J. Mason, "Coordination of randomly packed spheres," *Nature,* vol. 188, pp. 910-911, 1960.

[29] T. S. Majmudar and R. P. Behringer, "Contact force measurements and stress-induced anisotropy in granular materials," *Nature,* vol. 435, pp. 1079-1082, 2005.

CHAPTER 6. MODELLING OF THE EFFECTIVE ELECTRICAL CONDUCTIVITY OF PACKINGS UNDER ELECTRIC FIELDS

Abstract

In this study, we present two novel models to predict the effective conductivity of the formed packings under various electric fields. The specific focus is on the precipitated packings in electrostatic precipitation processes, where the conductivity of the solid constituents is much greater than the conductivity of the interstitial gases. The previously established models predicting the effective conductivity employ the packing characteristics, such as packing fraction, coordination number and contact diameter, which are difficult to measure in practical experiments. In this work, we firstly model these characteristics in terms of the controllable parameters, e.g., the particle diameter, electric field and packing depth. Then by implementing these models into a previously established model for effective conductivity, we have established an explicit form of the previous model using only the controllable parameters. Our results indicate that the previous model is inadequate when the formed packing structures are loose. There exist some isolated chain-like structures that are not contributing to the overall electrical transport in loose packings. Thus, to account for this effect, we have proposed an empirical model and a modified model. The results demonstrate that the predictions made by these models are much better than the previous model. Furthermore, the proposed models can be readily applied in practical experiments since the only parameters needed are the particle diameter, electric field and packing depth. Hence, the desirable electrical properties of a packing are achievable by adjusting the controllable parameters. The results may lead to improvements on the design and control of electrostatic precipitation processes.

6.1. Introduction

The need for finding the effective electrical conductivity of random packings is encountered in many areas of science and engineering, ranging from agricultural, environmental, material science to metallurgical, chemical, and electrical engineering [1-7]. Generally, the models to model the effective conductivity can be divided into two categories, the continuum and the discrete approach. The continuum models involve

solving the governing classic transport and continuity equations describing the electrical conditions of packing. Alternatively, in the discrete models, the effective conductivity of a random packing is evaluated by discretization of the packing structure. Here, we focus on determining the effective conductivity of the formed packings under electric fields, in particular, of the packings found in electrostatic precipitation processes, where the conduction of the solid constituents is much greater than the conduction of the interstitial gases. This problem is technically challenging because of the continuity equations fail at the boundaries between the solid and gas constituents. In addition, practical experiments on the packing of fine particles found in electrostatic precipitation processes are difficult, if not impossible, because of the fragility of the packing [8, 9].

Conversely, computer simulations are being increasingly applied in the studies of particle packing due to advancing computer technologies and programming know-hows over the last few decades. From these simulations, macroscopic characters along with microscopic structural information of packing can be readily extracted. For instance, packings of fine, wet or charged particles have been successfully studied using the discrete element method [10-12]. It has been revealed that the structural characteristics of a packing depends on the controllable parameters, such as the particle diameter and electric field for the formed packings under various electric fields [12]. Furthermore, the characteristics of the simulated packings are readily available, and therefore, solving for the electrical properties of every single particle and consequently the effective conductivity is achievable. The numerical method to find the effective conductivity of packings has been developed in the last chapter, which has demonstrated that the packing depth influences the contact area diameter and therefore the effective electrical conductivity [13]. The packing depth is practically controlled by mechanical rappings in conventional electrostatic precipitation processes. In summary, the particle diameter, electric field and packing depth are the main controllable parameters that impact the effective conductivity.

In this work, we use the discrete element method to simulate the packings under electric fields, and the effective conductivity of the simulated packings is numerically determined. The previously established model to predict the effective conductivity is based on the packing variables, such as the contact diameter, the packing fraction, the

coordination number, that are difficult to obtain in practical experiments [14]. Thus, we aim to develop a model for predicting the effective conductivity directly using these parameters. The results of the model are then compared with the numerical measurements in order to verify the model and identify its limitations. Lastly, empirical and modified models are proposed to predict the effective conductivity of the packings beyond the limitation of the previous model. These models for the effective electrical conductivity are particularly desirable in industrial applications, because the electrical properties of a formed packing can then be adjusted by changing the controllable quantities. This, in turn, may lead to the better designs and the optimisation of electrostatic precipitation processes.

6.2. Model descriptions

The discrete element method is used to simulate packings of fine particles under electric fields. The discrete element method was first proposed to study rock mechanics by Cundall and Strack [15]. Here, we take into account the electric-field-induced electrostatic interactions. Then, the translational and rotational motions of a particle can be described by the Newton's second law of motion as follows:

$$m_i \frac{d\mathbf{v}_i}{dt} = \sum \left(\mathbf{F}_{ij}^{n} + \mathbf{F}_{ij}^{s} + \mathbf{F}_{ij}^{vdw} \right) + \mathbf{F}_i^{e} \tag{6.1}$$

and

$$I_i \frac{d\boldsymbol{\omega}_i}{dt} = \sum \left(\mathbf{R}_{ij} \times \mathbf{F}_{ij}^{s} - \mu_r \mathbf{R}_i \left| \mathbf{F}_{ij}^{n} \right| \hat{\boldsymbol{\omega}}_i \right) \tag{6.2}$$

Where m_i is the mass, $\mathbf{v}_i$ is the translational velocity, t is the time, I_i is the moment of inertia, $\boldsymbol{\omega}_i$ is the angular velocity, μ_r is the rolling friction and $\mathbf{R}_{ij}$ is a vector running from the centre of the particle to the point of contact on the surface and has a magnitude equalling the particle radius. $\mathbf{F}_{ij}^{n}, \mathbf{F}_{ij}^{s}, \mathbf{F}_{ij}^{vdw}$ and $\mathbf{F}_i^{e}$ respectively represent the normal

contact force, tangential contact force, van der Waals interaction and the electric-field-induced electrostatic interactions. The detailed equations used to calculate these forces and torques are well established and reported in our early studies [12, 16]. The simulation parameters are listed in Table 6.1.

Table 6.1: Simulation parameters of the developed model.

Parameters	Values
Particle diameter, d	1×10^{-6} to 1×10^{-4} m
Electric field, **E**	1×10^{4} to 1×10^{6} V/m
Material conductivity, σ_m	1×10^{-7} S/m
Dielectric constant, k_p	2.0
Time step, δt	1×10^{-20} s
Packing fraction, ρ	0.103 to 0.619
Young's modulus, Y	1 x 10^{7} Pa
Poisson's ratio, v	0.29
Sliding friction coefficient, μ_s	0.4
Rolling friction coefficient, μ_r	0.02

A typical simulation starts with random generation of the particles with an initial velocity of zero under a per-defined electric field as depicted in Figure 5.1. The electric field is imposed along the *y*-axis direction, and periodic boundaries are applied along the *x* and *z* axes directions. Under the influence of the electric field, the particles start to move downwards toward the bottom. On each particle in the packing, the exerting forces are updated after each time step. The time step is set to be small enough so that the forces can only be transmitted from the particle to its intermediate neighbours. When the forces are updated, the motions of the particles are also updated according to

the Newton's second law of motion (see Eq.6.1 and Eq.6.2). This applies to every particle in the packing. Eventually, the simulation ends with all particles settled and a stable packing is formed.

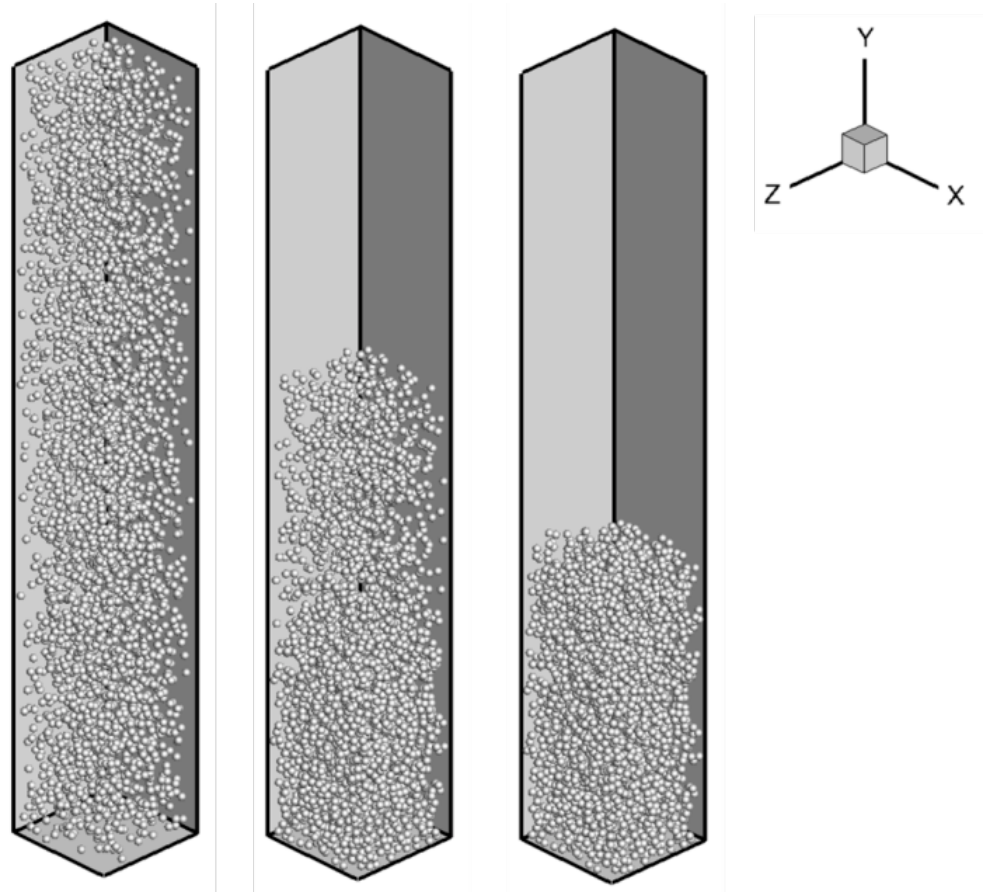

Figure 6.1: Snapshots of the formation of a packing under an imposed electric field using the discrete element method. The particle diameter is 10^{-5}m and the electric field is 10^{5}V/m.

To produce packings with various structures, we change the particle diameter and the electric field used in the simulations. The typical packings with a wide range of packing fractions are illustrated in Figure 6.2. In the case of a packing made of small particles under a weak electric field, a loose packing structure is formed, because the dominant interparticle van der Waals interactions restrict the rearrangement of the particles that consolidate the packing (see Figure 6.2a). In contrast, a strong electric field promotes the rearrangement of the particles and consequently the packing densification. Hence, a dense structure made of large particles is formed under a strong electric field (see Figure 6.2c). The effects of the particle diameter and electric field are well established in the

early chapters [10, 12]. Nevertheless, the effective conductivity is determined based on the packing structures produced using a range of particle diameters and electric fields (see Table 6.1).

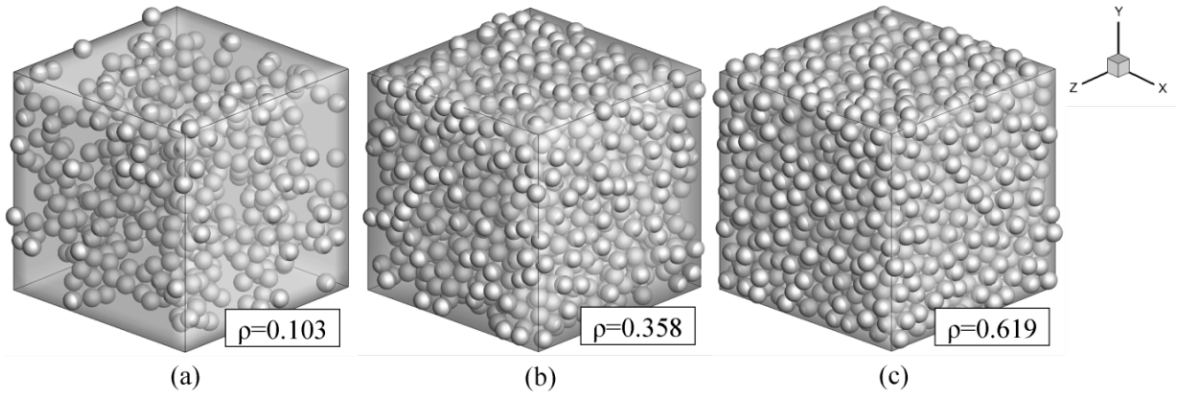

Figure 6.2: Illustrations of the formed packings with a range of packing fractions. The particle diameter is (a) 10^{-6}m, (b) 2×10^{-5}m, (c) 10^{-3}m, and the packings are formed under electric fields of (a) 10^{4}V/m, (b) 5×10^{4}V/m, and (b) 10^{6}V/m.

In this study, we use nodal analysis to evaluate the effective conductivity of packing. The nodal analysis is commonly applied in the studies of electrical network [17]. In the last chapter, we have demonstrated that this method is effective in determining the effective conductivity of the random packing in which the electric current is only carried by the interconnected particles. Under normal operational conditions of electrostatic precipitation processes, the conduction through the connecting particles dominates over the conduction through interstitial gases [18, 19]. Thus, it is appropriate to apply the nodal analysis to our simulated packings.

To apply nodal analysis, the structure of packing must be firstly discretized into an equivalent network of nodes and edges. In a formed packing under an electric field, the most of the resistance to electric current is offered by the interparticle contacts. This character of a packing is frequently discussed using the percolation theory. However, the particles in the simulated packings are always connected. The lack of percolation threshold makes it difficult to apply the percolation theory to these packings. Here, the interparticle contacts are represented by equivalent edges, and the conductance of the edges depends on the contact area between particles. Here, the Hertz's theory of contact

is applied to the contact between particles so that the corresponding contact conductance G is [20],

$$G = d_c \sigma_m \tag{6.3}$$

where d_c is the contact diameter and σ_m is the material conductivity. Also, the electrical potential is treated as uniform inside every single particle because of the relatively high conductivity of the particles. Then, the centres of the particles in packings can be treated as the nodes in electrical networks, and contacts between particles as the edges in the electrical networks.

As seen from Eq.6.3, the conductance between the contacting particles is dependent on the contact diameter. It has been demonstrated in the last chapter that the average contact diameter of particles in a formed packing under electric fields increases with the packing depth. As a result, the effective conductivity of the packing is also affected. The solution to this problem could be found by normalising the contact diameter according to the packing depth as mentioned in the last chapter. Therefore, every contact could be treated as if there were no other particles above the contact. Here too, we apply the same treatment to contact diameters in the evaluation of the effective conductivity, because the packings under electric fields are depth dependent. To apply the results of this study to industrial electrostatic precipitation processes, the effect of packing depth must be considered. However, it has been shown that the packing depth has no effect on the packing structure. Thus, the contact diameter is normalised by packing depth unless when studying the effect of packing depth on the contact diameter and consequently the effective conductivity.

Now, to find the effective electrical conductivity of a packing, the packing structure is discretised by using the electrical network concept, and a set of linear independent equations describing the structure is formulated using Kirchhoff's law. The Kirchhoff's law states that the sum of the electric current flow in and out of a node is zero. The set of equations for the discretized packing can be described in the matrix form:

$$A^T \mathbf{I} = A^T \left(g \left(A \mathbf{u} \right) \right) \tag{6.4}$$

where A is the incidence matrix, $\mathbf{I}$ and g are the vectors representing the electric current and conductance between each pair of particles respectively, and $\mathbf{u}$ is the vector representing the voltage on each particle. The incidence matrix is one of the most essential components of the nodal analysis, because it allows expression of the structure of packings in a matrix form. In an incidence matrix, every edge is recorded in the rows, and the connecting nodes by an edge are recorded in the columns of the corresponding row. Therefore, the number of rows and columns in an incidence matrix are determined by the number of conductors and nodes in the packing. The method of establishing an incidence matrix based on the structure of a random packing can be found in the last chapter.

In our study, the Gauss-Seidel method with appropriate boundary conditions was applied to numerically solve the established linearly independent equations describing the structure of packings. The convergence limit is set to 10^{-12}S/m. Thus, we now can solve the voltage on each particle and electric current between each pair of the contacting particles in packing. Then, the effective conductivity of the packing is given by:

$$\sigma_{eff} = \frac{I \cdot H}{S \cdot \Delta V} \tag{6.5}$$

where I is the total electric current, H is the packing depth, S is the packing area and the ΔV is the total voltage applied across the packing. In summary, the effective electrical conductivity of a packing is determined by explicitly solving the electrical potential and electric current on every single particle in the packing.

6.3. Results and discussion

The electrical quantities in Eq.6.5 are almost always difficult to obtain in practical experiments, especially for packings of fine particles. For the packings with the electric current is only conducted through the interconnecting particles, early studied have demonstrated that the effective conductivity is influenced by the packing fraction, coordination number, contact diameter and particle diameter [14]. The equation describing the effective conductivity has been summarised as,

$$\sigma_{eff} = \sigma_m \cdot \rho \cdot z \cdot \frac{d_c}{d} \tag{6.6}$$

where σ_m is the material conductivity of particles. The challenge in the application of this equation in industrial applications such as electrostatic precipitation processes is the determination of the micro-scale parameters of the packings, namely, the coordination number and contact diameter of particles. In contrast, the particle diameter and electric field are highly controllable in electrostatic precipitation processes. It is known from previous studies that the particle diameter and electric field impact on the structure of the packings under electric fields [12]. Consequently, it is expected that these parameters should also affect the effective conductivity of packings. In addition, it has been proven that the packing depth has an effect on the contact diameter of the formed packings under electric fields as discussed in the last chapter. Thus, the establishment of a relationship between the effective conductivity and the controllable parameters, e.g., the particle diameter, the electric field and the packing depth, is of paramount significance in the design and modelling of electrostatic precipitation processes. In the following sections, we firstly attempt to study the effect of the particle diameter, electric field and packing depth on the structure and contact diameter of packings, and the ultimate goal is to model the effective electrical conductivity using these controllable parameters.

6.3.1. Quantification of packing fraction

First of all, the packing fraction of a formed packing affects its effective electrical conductivity. Packing fraction represents the number of particles in a unit volume of packings. Experimental measurement of the packing fraction can be challenging, especially for the packings made of micro-scale particles in electrostatic precipitation processes. Our previous study indicates that the particle diameter and electric field are the most important parameters determining the packing fraction of packings [12]. These parameters are easy to quantify in practical experiments. Hence, we attempt to model the packing fraction using the particle diameter and electric field.

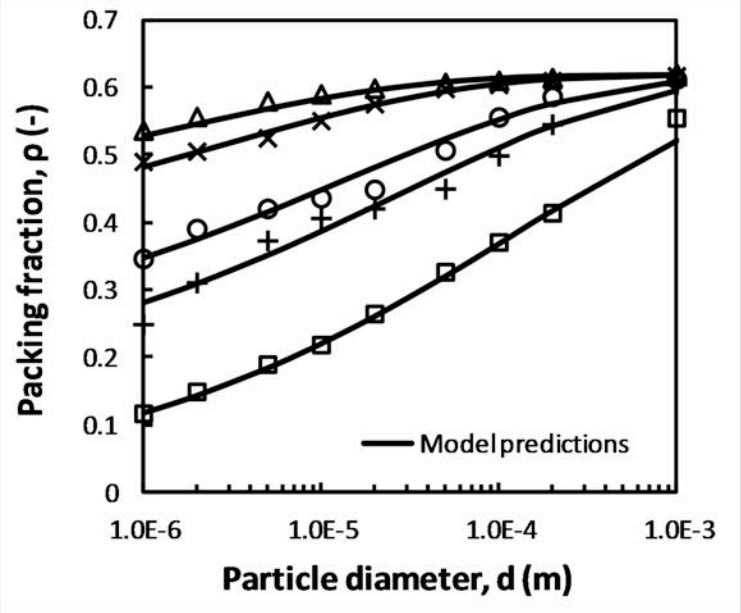

Figure 6.3: Dependence of the packing fraction on particle diameter of packings. The packings are formed under an imposed electric field of 10^6V/m (Δ), 5×10^5V/m (×), 10^5V/m (o), 5×10^4V/m (+) and 10^4V/m (□).

To study the effect of particle diameter and electric field on the packing fraction of packings, we fix the particle diameter and vary the electric field or vice versa. Here, the averaged packing fraction of packings excluding the boundary effects is determined for the simulated packings. Our results shown in Figure 6.3 and Figure **6.4** demonstrate that the packing fraction of packings increases with either the increasing particle diameter or increasing electric field. These observations are reasonable due to competing changes in the interparticle and field forces as the electric field or the particle diameter changes.

When the packings are formed under weaker electric fields, the interparticle van der Waals interactions are more dominant. As a result, the particle rearrangement and subsequent packing densification are delayed during the packing formation. The same applies to the case of decreasing the particle diameter. The quantification of the force competition is discussed elsewhere [12]. In this study, we aim at quantifying the packing fraction. An early study indicates that the packing fraction can be explicitly expressed as a function of the particles diameter as [21],

$$\rho = \rho_0 \left(1 + \exp\left(ad^b\right)\right) \tag{6.7}$$

where a and b are empirical parameters and ρ_0 refers to the initial packing fraction of the packing with negligible cohesion between particles. Despite different methods of packing formation, the packing fraction of packings under electric fields is still determined by the particle diameter (see Figure 6.3). However, the electric field obviously affects the relationship between the packing fraction and particle diameter. It appears that the empirical parameters in Eq.6.7 will change with the electric field. By fitting with existing data, Eq.6.7 reduces to Eq.6.8, and thus the packing fraction can be modelled in terms of particle diameter and electric field as,

$$\rho = \rho_0 \left(1 + \left(i \ln E - j\right)\exp\left(k\left(E \cdot d\right)^l\right)\right) \tag{6.8}$$

where values of ρ_0, i, j, k and l are respectively 0.619, 0.140, 2.307, -0.919 and 0.306. We find that our model offers excellent predictions for the range of the electric fields and particle diameters considered. Quantitatively, the discrepancies of the model predictions are well within ±10% margins (see Figure 6.5).

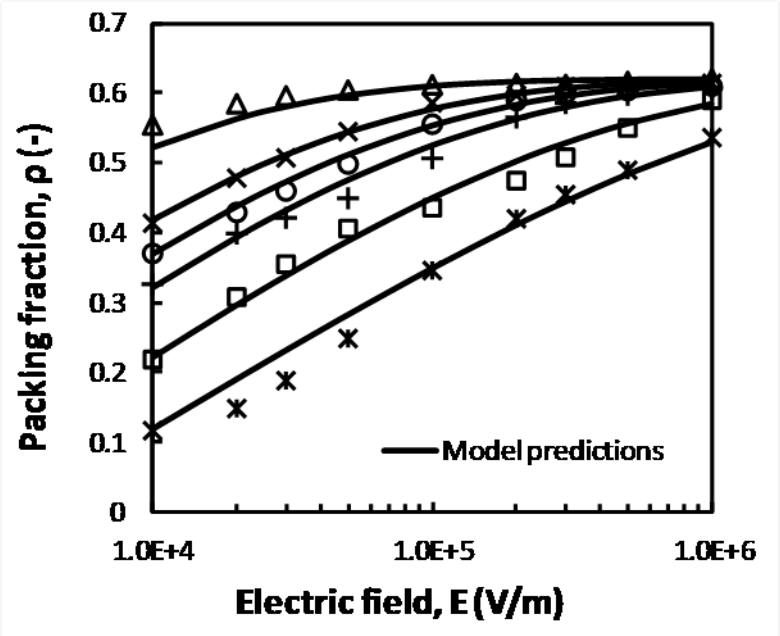

Figure 6.4: Dependence of the packing fraction on the imposed electric field, The particle diameter is 10^{-3}m (∆), 2×10^{-4}m (×), 10^{-4}m (o), 5×10^{-5}m (+), 10^{-5}m (□) and 10^{-6}m (∗).

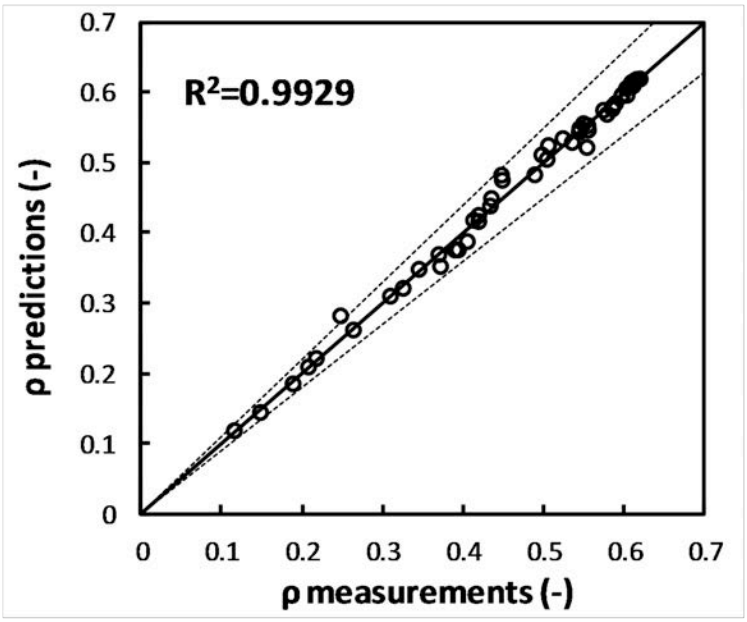

Figure 6.5: Comparisons of the proposed model predicted packing fractions with the existing measurements: the dotted-lines are the error margins of ±10%.

6.3.2. Quantification of coordination number

Secondly, coordination number is also important in determining the effective conductivity of a packing. The coordination number of a particle denotes the number of contacts the particle has with its neighbours. Now, electric current is carried through the contacting particles. The averaged coordination number of the particles in packing, which represents the connectivity of the packing, should affect the electrical transport phenomenon. It is worth noting that the coordination number of a precipitated packing in electrostatic precipitation processes is difficult to measure in practical experiments. On the contrary, such information is readily available in numerical simulations. Here, we aim to model the coordination number using particle diameter and electric field.

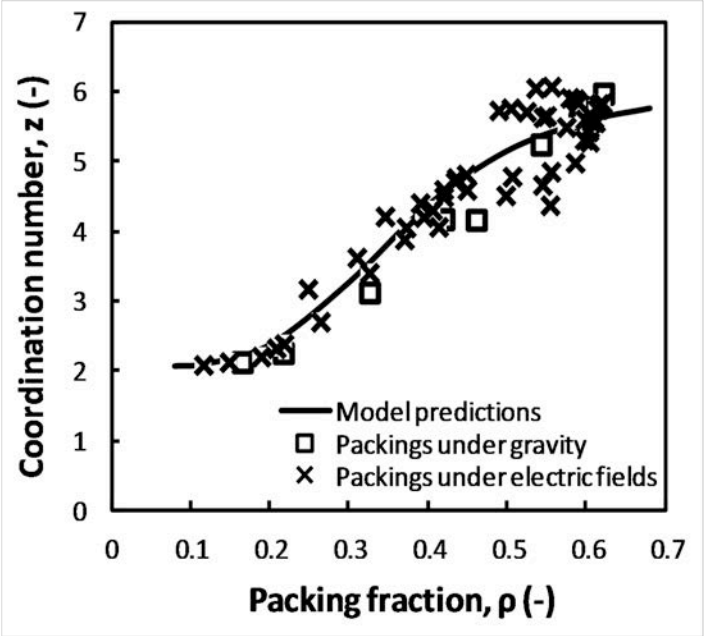

Figure 6.6: Variations of the averaged coordination number with the packing fraction of the packings.

Here, we use the averaged coordination number because it has been proven that the distributions of the coordination number of packings under electric fields are similar as long as they have similar averaged coordination numbers [12]. It is generally accepted that there is a universal relation between the averaged coordination number and the packing fraction for random packings (see Figure 6.6) [10, 12]. Mathematically, this relation is,

$$z = z_0 \frac{1 + a' \rho^4}{1 + b' \rho^4} \tag{6.9}$$

where z_0, a' and b' are empirical parameters. The term z_0 is sometimes referred to as the limiting coordination number that is required to support a stable structure in a packing, and the value of z_0 is usually close to two. Together with the previously developed model for packing fraction (see Eq.6.8), we can now model the averaged coordination number of packings in terms of the particle diameter and the electric field as,

$$z = z_0 \frac{1 + m\left(1 - \left(i \ln E + j\right)\exp\left(k\left(E \cdot d\right)^l\right)\right)^4}{1 + n\left(1 - \left(i \ln E + j\right)\exp\left(k\left(E \cdot d\right)^l\right)\right)^4} \tag{6.10}$$

where z_0, m and n are the empirical parameters. As depicted in Figure 6.6, the model predictions are in good agreement with the existing data, and the values of z_0, m and n are respectively 2.056, 156.609 and 52.802. Quantitatively, the coefficient of determination for the predictions is 0.9027 (see Figure 6.7). The discrepancy between the predictions and the measurements is mostly within ±10% margins.

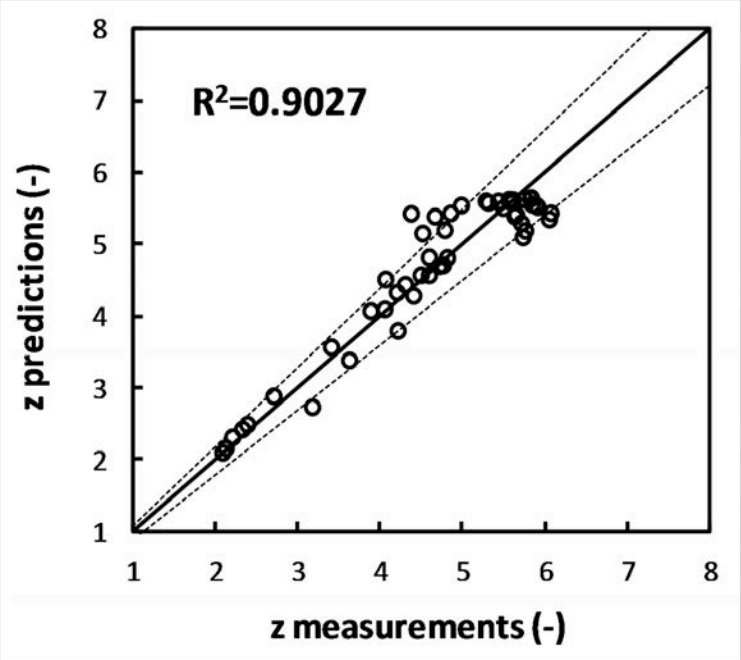

Figure 6.7: Comparisons of the proposed model's predictions for the averaged coordination number with the measurements: dotted lines are error margins of ±10%.

6.3.3. Quantification of contact diameter

The effective electrical conductivity of a formed packing is determined not only by the number of contacts between particles but also by the particle contact areas. The resistance to electric current at the interparticle contact equals to the reciprocal of the product of the contact conductivity and the contact area. Hence, the conduction between a pair of contacting particles in a packing improves with the increasing contact area. This, in turn, leads to an increase in the effective conductivity of the packing. Thus, we must include the effect of contact area in modelling the effective conductivity. Yet again, such contact information of the formed packings under electric fields is impossible to determine in practical experiments, and our simulations provides a remedy to this problem. Our aim is to model the contact diameter using particle diameter and electric field.

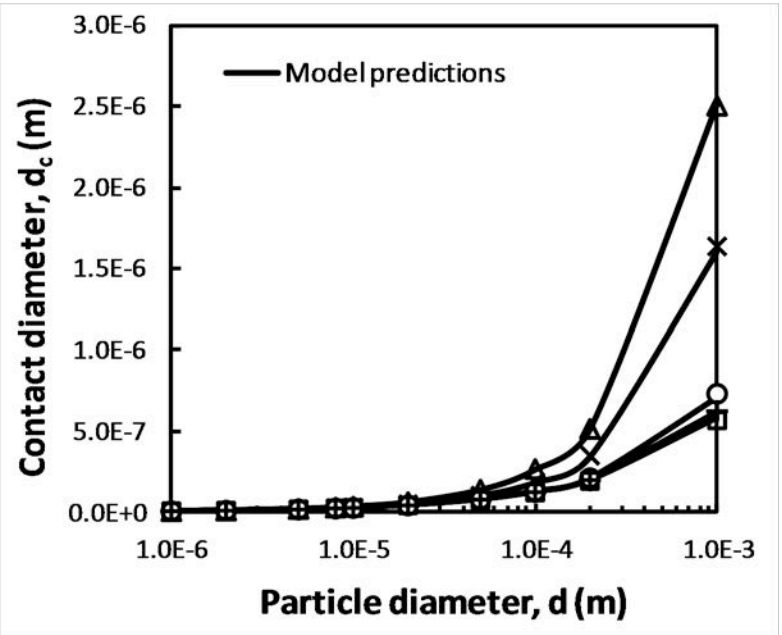

Figure 6.8: Variations of the contact diameter between particles with the particle diameter under the imposed electric field of 10^6V/m (Δ), 5×10^5V/m (×), 10^5V/m (o), 5×10^4V/m (+) and 10^4V/m (□).

In this study, we use the averaged contact diameter to characterise the contact area between particles in the packings, because the contact diameter shows similar distributions as long as the average contact diameters of packings are the same. Our results show that the contact diameter increases with the particle diameter as depicted in Figure 6.8. To elucidate the observed changes, we firstly consider the contact between a pair of particles. Hertz contact theory states that the contact diameter d_c between particles is given by [22],

$$d_c = 2 \cdot \left(\frac{3Pd}{8Y'} \right)^{1/3} \tag{6.11}$$

where P is the pressure at the contact and Y' is the effective Young's modulus. From this formula, we can see that the contact diameter is proportional to the particle diameter. This is consistent with our observations. Moreover, Eq.6.11 shows that the contact diameter increases with the contact pressure according to the Hertz theory. In our cases, the electrostatic interactions must also be considered to account for the contact pressure completely. It is evident that the contact diameter between particles increases with the

electric field for the formed packings under electric fields (see Figure 6.9). The applied electric field determines the magnitude of the electrostatic interactions between particles and subsequently the contact diameter. In addition to the electrostatic interactions, the interparticle van der Waals interactions also become important when the particle diameter is small. It should be noted that the contact force is a passive force, which is only reactive when other forces, such as electrostatic interactions and van der Waals interactions, have "dragged" two particles together. Thus, the contact pressure between particles in packings under an electric field should be proportional to the electrostatic interactions and van der Waals interactions, namely,

$$P \propto a'' F^{e} + b'' F^{vdw} \tag{6.12}$$

Considering the effects of particle diameter and electric field on these forces gives us,

$$P \propto a'' F^{e} + b'' F^{vdw} \propto a'' \cdot E^{2} d^{2} + b'' \cdot d \tag{6.13}$$

Now, when substituting Eq 12 into Eq 11, we now can express the contact diameter in terms of particle diameter and electric field as,

$$d_{c} = u \cdot d^{1/3} \left(v \cdot E^{2} d^{2} + w \cdot d \right)^{1/3} \tag{6.14}$$

where u, v and w are empirical parameters. The predictions by the developed model are shown in Figure 6.8 and Figure 6.9 and seen to be in excellent agreement with the existing measurements. The values of u, v and w are respectively 3.734×10^{-7}, 0.305 and 3.776×10^{6}. Quantitative error analysis suggests that the coefficient of determination is 0.9998 (see Figure 6.10).

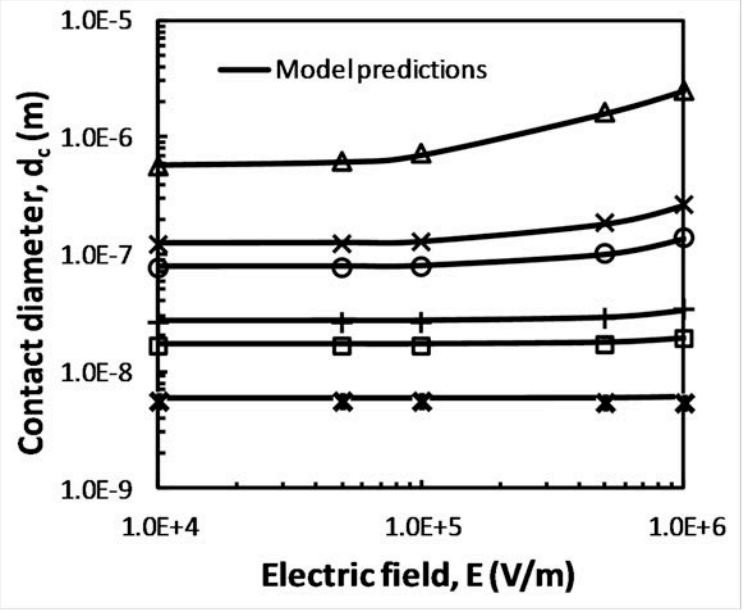

Figure 6.9: Variations of the contact diameter with the strength of imposed electric fields. The packing particle diameters used are: 10^{-3}m (Δ), 10^{-4}m (×), 5×10^{-5}m (o), 10^{-5}m (+), 5×10^{-6}m (□) and 10^{-6}m (∗).

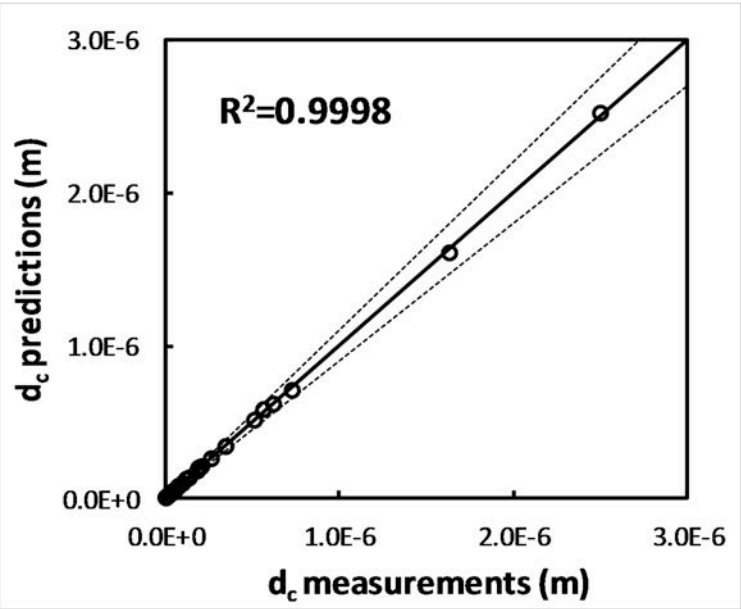

Figure 6.10: Comparisons of the model predicted and measured contact diameters: the dotted lines are error margins of ±10%.

6.3.4. Effect of packing depth

Lastly, we investigate the effect of packing depth on the effective electrical conductivity. In the previous chapter, it has been suggested that the depth of a packing has no effect on the packing structures, but the contact diameter between particles increases with the packing depth. To eliminate the packing depth effect, we have proposed to normalise the contact diameter between particles in the packing by its packing depth. Based on the normalisation, we have modelled the packing fraction, coordination number and contact diameter of packings using the particle diameter and electric field. Figure 6.11 demonstrates that there is no structural change with the packing depth in the simulated packings. Hence, the previously established models of packing fraction and coordination number are still applicable here. However, it should be noted that the contact diameter between particles has to be corrected to incorporate the effect of the packing depth in the contact diameter. Thus, we now derive the expression for the contact diameter that includes the effect of packing depth. The model for contact diameter derived in the previous section is still valid when all the particles in packing are treated as if they are located on the surface of the packing. The theoretical contact diameter independent of the packing depth is denoted as d_{c0}, which is,

$$d_{c0} = u \cdot d^{1/3} \left(v \cdot E^2 d^2 + w \cdot d \right)^{1/3} \tag{6.15}$$

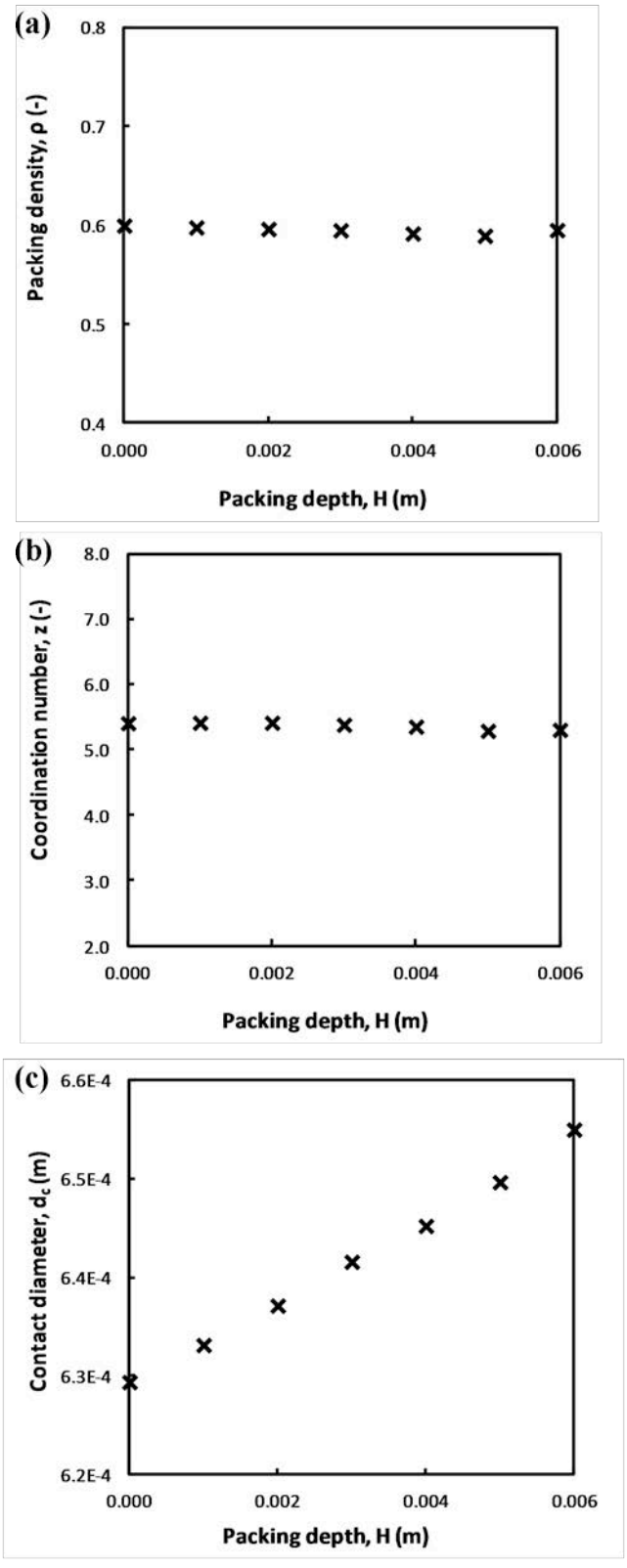

Figure 6.11: Variations of the (a) packing fraction, (b) coordination number and (c) contact diameter with the packing depth. Note that the packing has been formed using 10^{-5}m diameter particles under an imposed electric field of 10^{5}V/m.

To elucidate the effect of packing depth on the contact diameter between particles, we firstly consider the pressure change at the particle contact. To a certain extent, the hydrostatic pressure in fluids is analogous to the effect of packing depth in packings (see Figure 6.12). In a fluid, the hydrostatic pressure is,

$$P = \rho_f gH \tag{6.16}$$

where ρ_f is the density of the fluid and g is the gravitational constant. As seen from this equation, the depth dependent pressure at a point in a fluid is caused by the weight of the fluids above the point. The same applies to the formed packings under electric fields. The contact diameter between a pair of particles should increases with the packing depth, because the number of particles above the contact increases with the packing depth. Despite the similarity, the evaluation of the effect of packing depth on the contact diameter is still difficult, largely due to the uncertainty in the pressure applied at the contacts. The hydrostatic pressure is evenly distributed by the fluid molecules in a fluid. On the other hand, the pressure in a packing is in no way evenly distributed. This is because the contacts between particles in a packing are randomly distributed, and the pressure can only be transmitted through the contacts between particles. Nevertheless, the depth dependent contact diameter is caused by the increasing electrostatic interactions from the subsequently-laid particles on top of the existing particles during the packing process. In our simulations, the periodic boundaries are applied instead of side walls. As a result, the friction between particle and wall is negligible. The use of periodic boundaries can also reduce the Janssen effect commonly observed in granular materials. It should also be noted that the hydrostatic pressure distribution in the fluids is usually not the same as that in granular packing mainly due to the contribution of particle-wall friction. However, in our simulations, the periodic boundaries are applied instead of side walls, which contribute to the observed hydrostatic pressure distribution. The use of periodic boundaries can also reduce the Janssen effect commonly observed in granular materials.

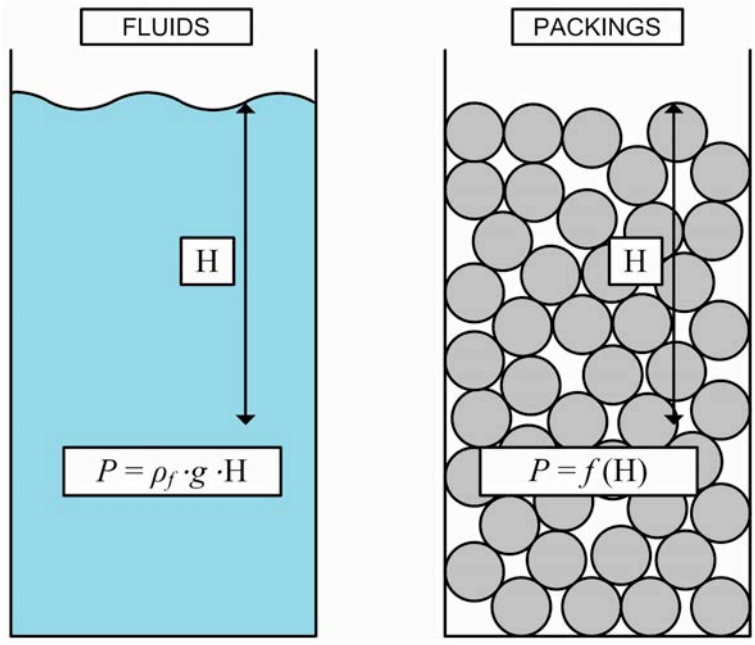

Figure 6.12: Schematic comparisons between the hydrostatic pressure in fluids and the depth dependent contact pressure in packings (Not to scale).

After understanding the origin of the depth dependence contact diameter in the formed packings, we now can formulate the contact diameter considering the effect of packing depth. Here, the particle diameter and the electric field are kept constant when examining the changes in the contact diameter with the packing depth. Once again, we focus on the averaged contact diameter. In this situation, we define the contact diameter at a packing depth as the averaged contact diameter within three particle diameter range at that depth. To compare the packings with different particle diameters, the contact diameter and the packing depth are normalised according to the particle diameter,

$$H^* = \frac{H}{d} \tag{6.17}$$

and

$$d_c^* = \frac{d_c}{d} \tag{6.18}$$

where H^* and d_c^* are the normalised packing depth and contact diameter respectively. The results demonstrate that the contact diameter indeed increases with the packing depth (see Figure 6.13). Moreover, the degree of change in contact diameter with packing depth increases with either the increasing particle diameter or the increasing electric field. Thus, both the particle diameter and the electric field must be included in the formulation of the contact diameter using the packing depth. Using the existing measurements, we say that the contact diameter is related to the packing depth as,

$$d_c = d_{c0}\left(xd^{2/3}E^{3/2}H + 1\right) \tag{6.19}$$

where x is an empirical parameter, which in our study is 4.382×10^{-11}. Quantitative error analysis shows that the model predictions are in reasonable agreement with the existing measurements with a coefficient of determination of 0.9853. In summary, we have incorporated the effect of packing depth in the estimation of contact diameter for the formed packings under electric fields. This relation will be applied in the evaluation of the effective electrical conductivity of packings.

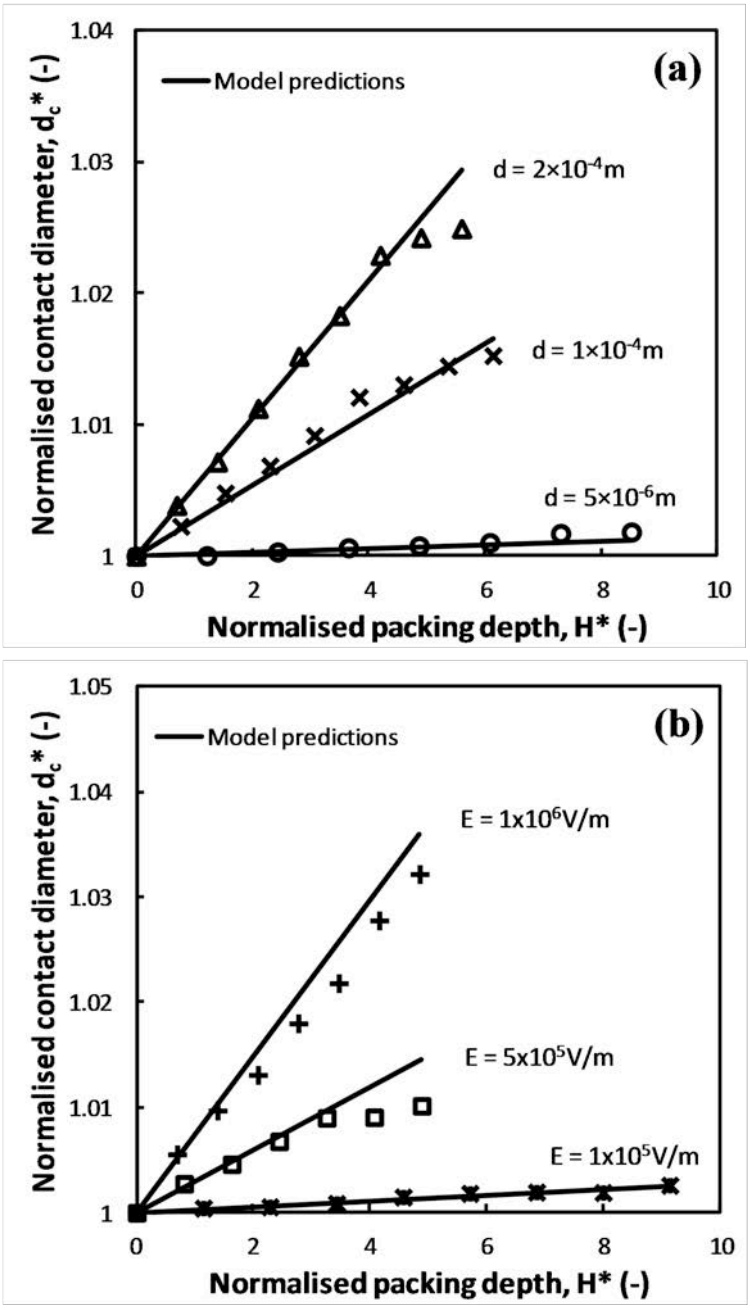

Figure 6.13: Variations of the normalised contact diameter with the normalised packing depth for the formed packings (a) under an electric field of 10^5V/m; (b) with 10^{-5}m diameter particles.

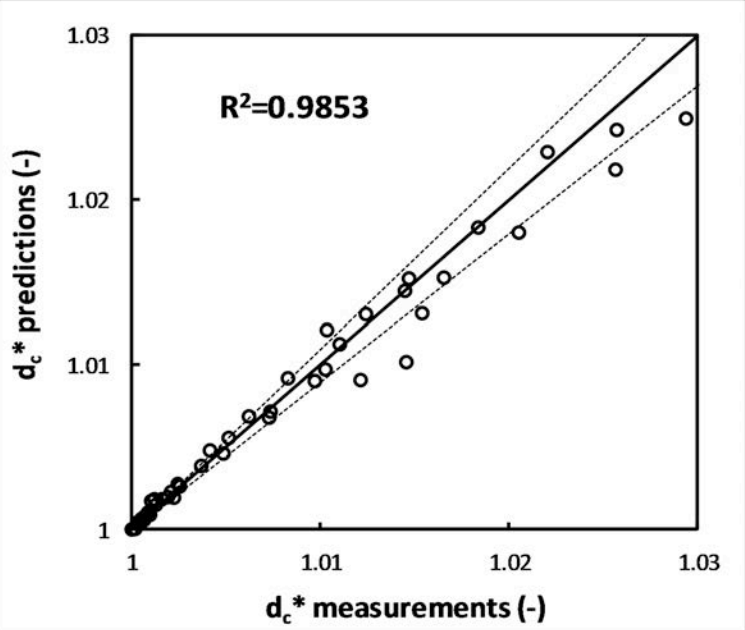

Figure 6.14: Error analysis on the predicted contact diameter; dotted lines are error margins of ±10%.

6.3.5. Modelling of effective electrical conductivity

So far, we have successfully modelled the packing fraction, coordination number and contact diameter of random packings using only the particle diameter and electric field. In addition, it has been shown that the packing depth is an important parameter for the formed packings under electric fields as it affects the contact diameter. Therefore, the contact diameter is corrected to include the effect of the packing depth. As mentioned earlier, the previously established model predicting the effective conductivity is given by [14],

$$\sigma_{eff} = \sigma_m \cdot \rho \cdot z \cdot \frac{d_c}{d} \tag{6.20}$$

So now if we replace the variables in Eq.6.20 with the expressions for particle diameter, electric field and packing depth, the explicit form of the previous model becomes:

$$\sigma_{eff} = \sigma_m \cdot C_0 \cdot \varphi \cdot d^{-\frac{1}{3}} \frac{1+m\varphi^4}{1+n\varphi^4} \left(vE^2 d + w\right)^{\frac{1}{3}} \left(xd^{\frac{2}{3}} E^{\frac{3}{2}} H + 1 \right) \tag{6.21}$$

where,

$$\varphi = 1 + \left(i \ln E - j\right) \exp\left(k \left(E \cdot d\right)^l\right)$$

Using this model, the effective conductivity of packings can be determined in terms of the three variables, particle diameter, electric field and packing depth, which are all measurable and controllable in practical experiments. Here, we keep the packing depth constant at ten particle diameters when calculating the effective conductivity, because the effective conductivity measurements from the numerical simulations are obtained based on this condition. The predicted effective conductivities from the previously established model are compared in Figure 6.15 with the numerical measurements. The results indicate that the previous model reasonably predicts the effective conductivity of the formed packings made of large particles or under strong electric field. However, the predictions significantly deviate from the measurements for the packings made of small particles under weak electric fields. As the numerical measurements are made based on the actual packing structures, there is no doubt that the previous model is inadequate to predict the effective conductivity of packings of various structures. Thus, improvements must be made to the previously established model.

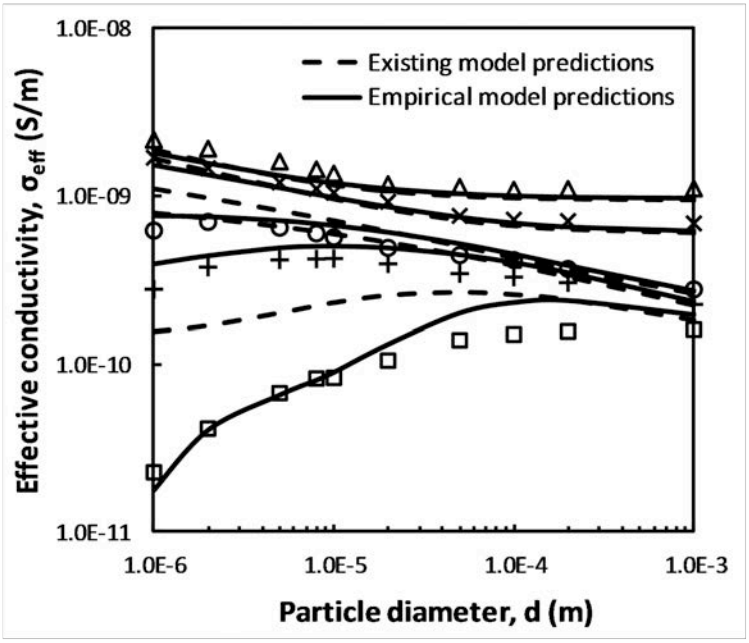

Figure 6.15: Comparisons of the effective conductivity predictions between the previously established model and the proposed empirical model. Note that the packings have been formed under electric fields of 10^6V/m (Δ), 5×10^5V/m (×), 10^5V/m (o), 5×10^4V/m (+) and 10^4V/m (□).

6.3.5.1. Empirical approach

The simplest approach to improve the previously established model for the effective conductivity is empirically fitting. There are several empirical parameters in Eq.6.21 that can be adjusted. We find that changing the parameters related to the packing fraction, i.e., *i*, *j*, *k* and *l*, is the most helpful way to fit the previous model with the measurements. Based on the existing measurements, the empirical parameters are empirically determined and listed in Table 6.2. Figure 6.15 demonstrates that the empirical model produces excellent predictions of the effective conductivity of the formed packings using a range of particle diameters and under various electric fields. In this study, the packing fraction varies from 0.103 to 0.619. Therefore, the empirical model is applicable to packings with a wide range of packing fractions. Quantitative error analysis shows a coefficient of determination of 0.9967, and the predicted effective conductivity of packings are well within error margins of ±20% (see Figure 6.16).

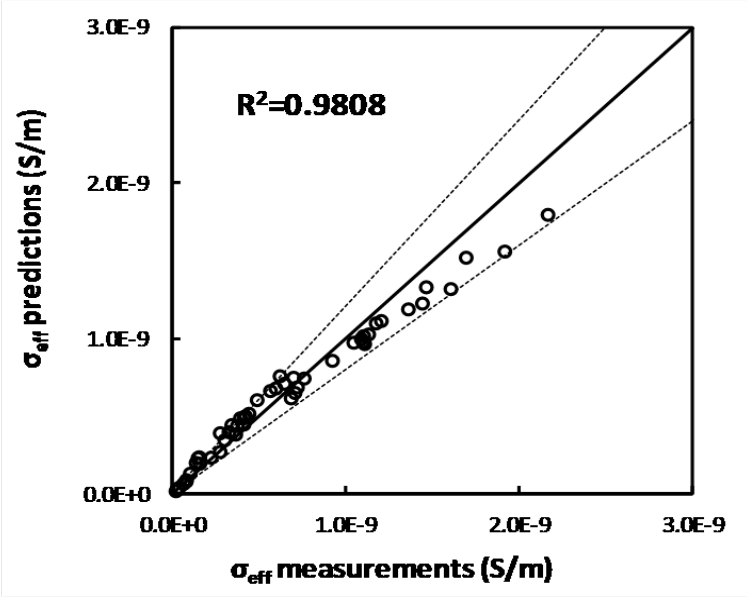

Figure 6.16: Comparisons of the effective conductivities predicted by the empirical model with the existing measurements; dotted-lines arfe error margins of ±20%.

Table 6.2: Empirical parameters of the proposed models.

Parameters	Empirical model	Modified model
C_o	4.870×10^{-7}	5.881×10^{-7}
i	0.139	0.140
j	2.408	2.307
k	-0.896	-0.919
l	0.398	0.306
m	156.609	156.609
n	52.802	52.802
v	0.305	0.305
w	3.776×10^{6}	3.776×10^{6}
x	4.382×10^{-11}	4.382×10^{-11}

The problem with the empirical model is that the parameters relating to the packing fractions are modified in order to predict the correct effective conductivity. In other words, the model uses the packing fractions that are different from the actual packing fractions. These findings imply that the previously established model for the effective conductivity does not follow physics of the packing process. Thus, a modification to the existing theoretical model is necessary.

6.3.5.2. Modified model

To modify the previously established model to predict the effective conductivity of a packing, we must first understand its shortcomings. Firstly, all the adjusted empirical parameters in the empirical model are related to the packing fraction as stated in the previous section. This suggests that the packing fraction may be responsible for the breakdown of the previous model. Secondly, the model successfully predicts the effective conductivity of the formed packings under strong electric fields, while it fails for the loose packing structures that are formed when the particle diameter is small and the electric field is weak. Thus, it is most likely that the previously established model does not work for the loose packing structures. Lastly, the limitation of the previous model has been discussed in the early studies using the percolation theory of transport [23, 24]. In the percolation theory, there exists a percolation threshold, below which the electrical transport through the packing drops to zero. This is because there is not a single continuous electric current conduction path in the packing with a low packing fraction. However, this does not apply to the formed packings under electric fields.

To elucidate the failure of the previously established model, the loose packings are examined. We find that there are many particles that are connected in chain-like structures in the loose packings because of the dominant interparticle forces (see Figure 6.17). It is evident by the averaged coordination number of the packings is close to two (see Figure 6.6). In a loose packing structure, some chain-like structures are not contributing to the overall electrical transfer (see Figure 6.17a), and therefore, the effective conductivity of such a packing is equivalent to that of a packing without the loose chain-like structures (see Figure 6.17b). In essence, the use of packing fraction in

the previously established model for the effective conductivity is problematic. Instead, the packing fraction should be adjusted to exclude the non-essential particles in loose packings.

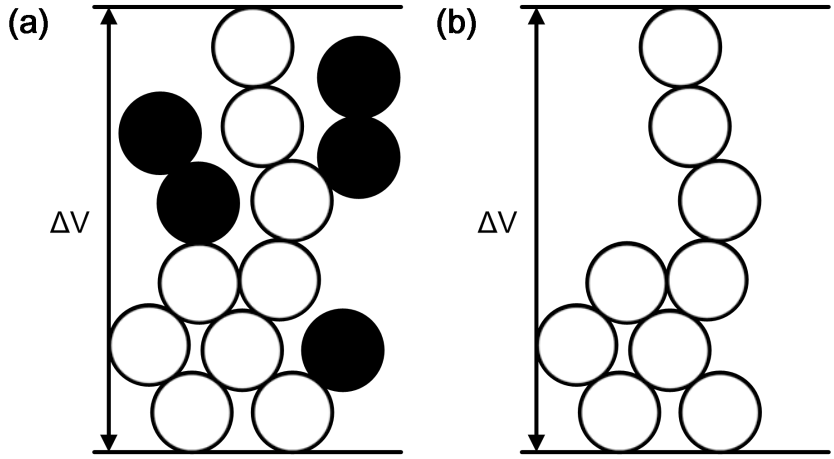

Figure 6.17: Schematic diagram of a packing structure in two dimensions. (a), the particles marked black do not contribute to the electrical transfers; (b), the equivalent packing having only the particles that contribute to the electrical transfer.

Using the numerical measurements, we determine that the modified model for the effective conductivity is,

$$\sigma_{eff} = \sigma_{mat} \cdot \rho^2 \cdot z \cdot \frac{d_c}{d} \tag{6.22}$$

The explicit form of the modified model is,

$$\sigma_{eff} = \sigma_m \cdot C_0 \cdot \varphi^2 \cdot d^{-\frac{1}{3}} \frac{1+m\varphi^4}{1+n\varphi^4} \left(v\mathbf{E}^2 d + w\right)^{\frac{1}{3}} \left(xd^{\frac{2}{3}}\mathbf{E}^{\frac{3}{2}} H + 1 \right) \tag{6.23}$$

where

$$\varphi = 1 + \left(i \ln \mathbf{E} - j\right) \exp\left(k\left(\mathbf{E} \cdot d\right)^l\right)$$

ρ is reduced by squaring to account for the structure without any chain-like structures that are not contributing to the electrical conduction as ρ is a value between 0 and 1. The parameters used in the modified model and their values are summarised in Table 6.2. Our results indicate that the modified model predictions for the effective conductivity of packings are significantly improved comparing to the previous model, especially for the formed packings under weak electric fields (see Figure 6.18). The coefficient of determination between the predicted and the measured effective conductivity is 0.9882 (see Figure 6.19). For the loose packings, the use of the packing fraction of the entire packings is obviously inappropriate in the previous model, because some non-essential chain-like structures should be disregarded in the calculation of the effective conductivity. To solve this problem, the packing fraction is reduced in both the modified and the empirical model proposed in this paper. As a result, the predictions made by these models are significantly improved comparing to the previously established model.

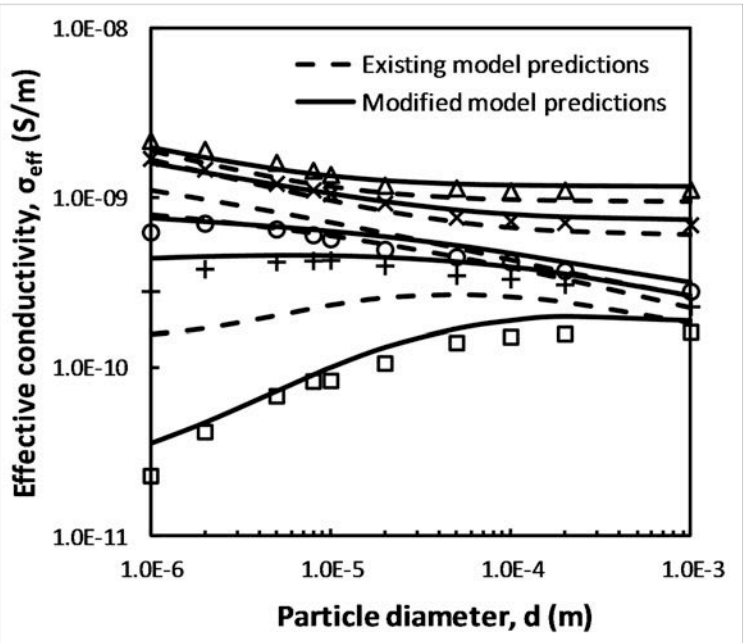

Figure 6.18: Comparisons of the effective conductivity predictions between the previously established model and the proposed modified model. The measurements are made based on the formed packings under electric fields of 10^6V/m (Δ), 5×10^5V/m (×), 10^5V/m (o), 5×10^4V/m (+) and 10^4V/m (□).

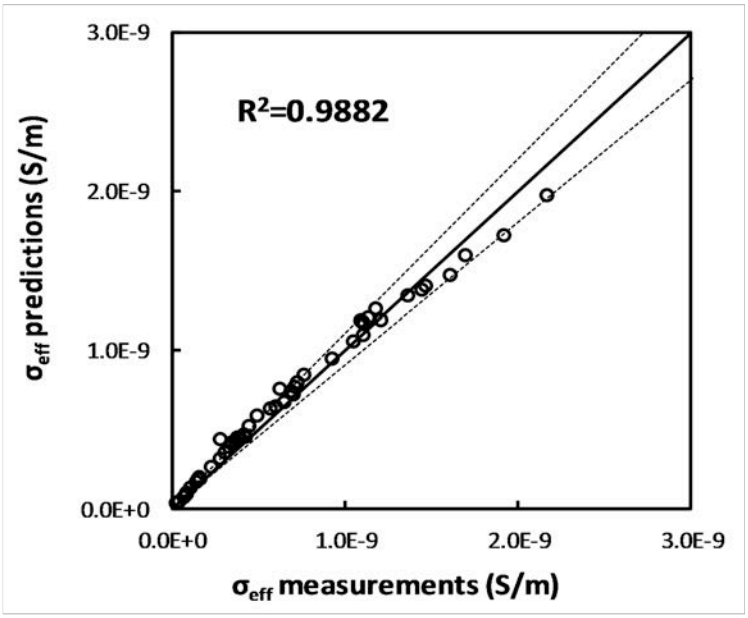

Figure 6.19: Comparisons of the effective conductivity predicitons by the modified model with the existing measurements: the dotted-lines are error margins of ±10%.

6.3.6. Effect of particle packing on electric fields

The newly developed models can be readily applied to industrial electrostatic precipitation processes. For instance, the typical electrical conditions of the precipitation process are depicted in Figure 6.20a. To account for the effect of particle packing on the electrical conditions in the system, the total voltage applied across the discharging electrode and the collection wall is divided into the voltage applied on the ionised gases and the voltage applied on the precipitated packing. Such a representation has been proposed in early studies, and the equivalent electric circuit diagram is illustrated in Figure 6.20b [25, 26]. During normal operations, the voltage across a precipitated packing increases as the growth of the packing with time. The total applied voltage is usually optimised to a set value. As a result, the voltage applied across the ionised gases decreases with the increasing voltage across the precipitated packing. Now, the electric field is given by,

$$\mathbf{E} = -\nabla V \tag{6.24}$$

Thus, the decreasing voltage would directly impact on the imposed electric field in the ionised gases. When the imposed electric field is uniform, the effect of a precipitated packing on the electric field can be expressed as,

$$\mathbf{E}^* = \frac{1}{H_{total} - H_{packing}} \left(\mathbf{E} H_{total} - \frac{\sigma_{gas} \mathbf{E}}{\sigma_{eff}} H_{packing} \right) \tag{6.25}$$

where, H_{total} is the distance between the discharging electrode and the collection wall, $H_{packing}$ is the packing depth, σ_{gas} is the conductivity of the ionized gases, σ_{eff} is the effective conductivity of the precipitated packing, $\mathbf{E}^*$ and $\mathbf{E}$ are the electric field with and without the precipitated packing on the collection wall. Clearly, the effective conductivity of the packing plays an important role in determining the electric field across the ionised gases.

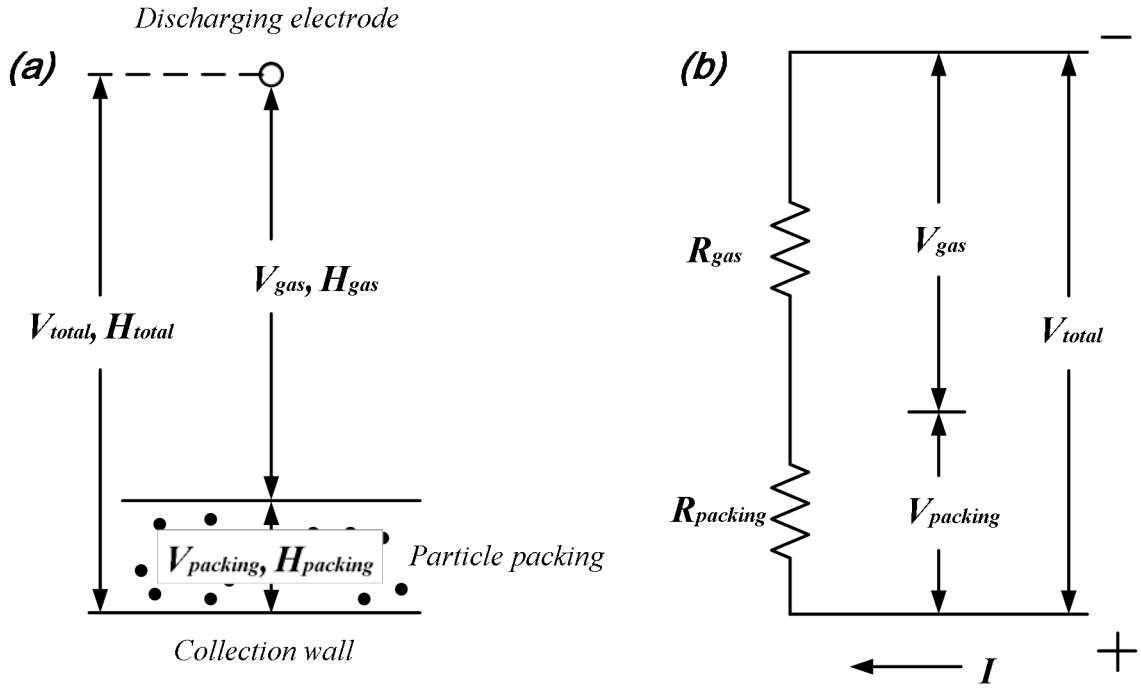

Figure 6.20: (a) Schematic diagram of the typical electrical conditions in electrostatic precipitation processes, and (b) the equivalent electric circuit diagram.

Finding the effective electrical conductivity of a packing usually requires the microscopic information of the packing structure as mentioned earlier. It is particularly

difficult to quantify these microscopic quantities for random packings. It must be pointed out that the only variables required for the developed models, i.e., the empirical and modified model, are the material conductivity, particle diameter, electric field and packing depth, which are all measurable macroscopic quantities. Essentially, we have developed a method to model microscopic characteristics of a formed packing using its macroscopic quantities. Therefore, the proposed empirical and modified models are especially useful in the modelling of the effect of particle packing in electrostatic precipitation processes. An example of a packing grows at a constant rate of 1.56×10^{7}particles/cm^{2}/min has been demonstrated in Figure 6.21a. Using typical parameters of industrial electrostatic precipitation systems (see Table 6.3), we have successfully modelled the deteriorating electric field with the growth of the packing (see Figure 6.21b).

Table 6.3: Typical parameters of electrostatic precipitation processes.

Parameters	Values
The electrical conductivity of particles	1×10^{-7} S/m
The electrical conductivity of ionised gases	2×10^{-9} S/m
Particle diameter	1×10^{-5} m
Initial imposed electric field	1×10^{6} V/m
Electrode-wall distance	0.01 m
Deposition rate	1.56×10^{7}particles/cm^{2}/min

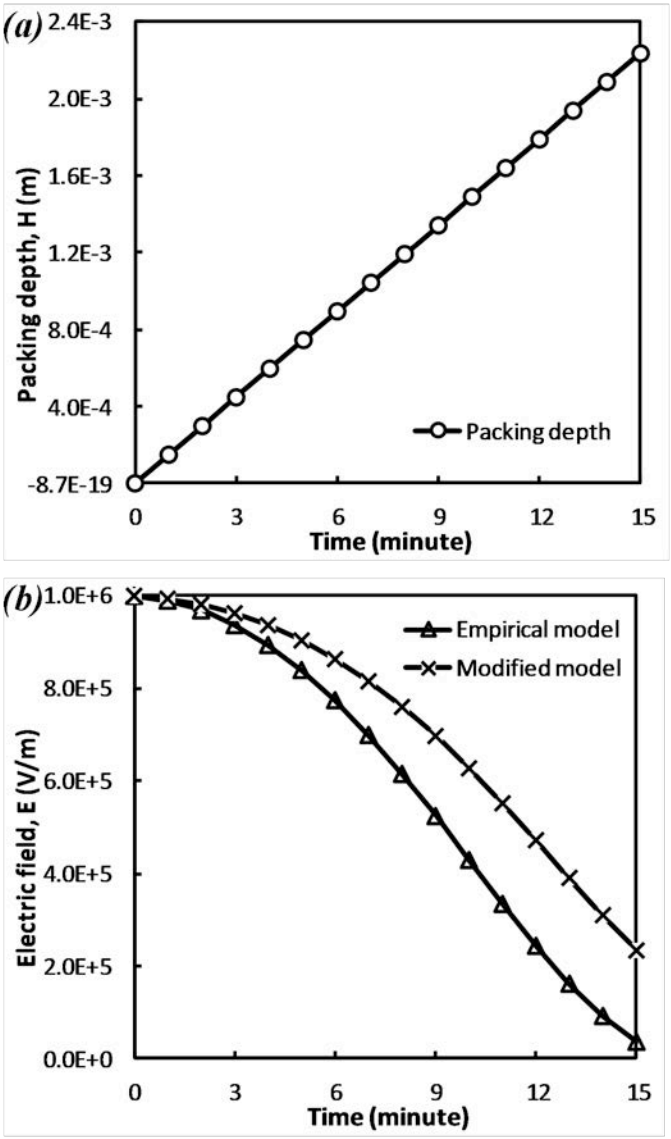

Figure 6.21: (a) The growth of a packing of fine particles with time, and (b) the corresponding deteriorating electric fields with time predicted by the developed models.

6.4. Conclusions

In summary, we have modelled the packing fraction, coordination number, contact diameter using the experimental measurable parameters, e.g., particle diameter and electric field, for the formed packings under electric fields. Using these relationships, we then developed two models to predict the effective conductivity of the packings under electric fields using only the four variables, material conductivity, particle

diameter, electric field and packing depth. The predictions of the developed models are significantly better than the predictions of the previously established model, especially for the packings with a less dense structure. Also, they are applicable to packings with a wide range of packing fractions. The models can be readily applied to optimise the electrical transport through packings by changing the controllable parameters such as the particle diameter, electric field and packing depth. The findings may lead to better designs of industrial electrostatic precipitation processes.

Nomenclature

m = mass

$\mathbf{v}$ = velocity

t = time

$\mathbf{F}$ = force

I = moment of inertia

$\mathbf{R}$ = radius

d = diameter

$\mathbf{E}$ = electric field

k_p = dielectric constant

G, g = electrical conductance

d_c = contact diameter

A = incidence matrix

$\mathbf{I}$ = electric current

$\mathbf{u}$ = electrical potenial

H = packing depth

S = cross-sectional area

ΔV = potential difference

z = coordination number

P = pressure

g = gravitational constant

Greek Letters

$\boldsymbol{\omega}$ = angular velocity

μ = friction

σ = electrical conductivity

ρ = packing fraction

ρ_f = fluid density

Subscript

i, j = *i*th particle, *j*th particle

n = normal direction

s = tangential direction

vdw = van der Waals

e = electrical

r = rolling friction

m = material properties of particle

eff = effective properties

References

[1] G. W. Milton, *The theory of composites* vol. 6: Cambridge University Press, 2002.

[2] P. Eidem, *et al.*, "Determination of electrical resistivity of dry coke beds," *Metallurgical and Materials Transactions B,* vol. 39, pp. 7-15, 2008.

[3] S. P. Friedman, "Soil properties influencing apparent electrical conductivity: a review," *Computers and Electronics in Agriculture,* vol. 46, pp. 45-70, 2005.

[4] K. J. McLean, "Electrostatic precipitators," *Iee Proceedings-a-Science Measurement and Technology,* vol. 135, pp. 347-361, 1988.

[5] V. Mourzenko, *et al.*, "Geometrical and transport properties of random packings of polydisperse spheres," *Physical Review E,* vol. 77, p. 066306, 2008.

[6] M. Sahimi, *Applications of percolation theory*: CRC, 1994.

[7] M. Wang and N. Pan, "Predictions of effective physical properties of complex multiphase materials," *Materials Science and Engineering: R: Reports,* vol. 63, pp. 1-30, 2008.

[8] D. Blanchard, *et al.*, "Correlation between current density and layer structure for fine particle deposition in a laboratory electrostatic precipitator," *Ieee Transactions on Industry Applications,* vol. 38, pp. 832-839, 2002.

[9] E. Schmidt and F. Loffler, "Preparation of dust cakes for microscopic examination," *Powder Technology,* vol. 60, pp. 173-177, 1990.

[10] R. Y. Yang, *et al.*, "Computer simulation of the packing of fine particles," *Physical Review E,* vol. 62, p. 3900, 2000.

[11] K. J. Dong, *et al.*, "Settling of particles in liquids: Effects of material properties," *AIChE Journal,* vol. 58, pp. 1409-1421, 2012.

[12] S. Yang, *et al.*, "Packing of fine particles in an electrical field," *Granular Matter,* vol. 15, pp. 467-476, 2013.

[13] S. E. Yang, *et al.*, "Evaluation of the effective electrical conductivity of random packings in electric fields," *In press,* 2014.

[14] G. K. Batchelor and R. W. O'Brien, "Thermal or electrical conduction through a granular material," *Proceedings of the Royal Society of London. Series A, Mathematical and Physical Sciences,* vol. 355, pp. 313-333, 1977.

[15] P. A. Cundall and O. D. Strack, "A discrete numerical model for granular assemblies," *Geotechnique,* vol. 29, pp. 47-65, 1979.

[16] S. E. Yang, *et al.*, "Random packing of charged particles in non-uniform electric field," *In press,* 2014.

[17] G. Milton, "The coherent potential approximation is a realizable effective medium scheme," *Communications in Mathematical Physics,* vol. 99, pp. 463-500, 1985.

[18] H. J. White, *Industrial Electrostatic Precipitation*: Addison-Wesley Pub. Co., 1963.

[19] K. R. Parker, *Applied electrostatic precipitation*: Springer, 1997.

[20] R. Holm, *Electric contacts theory and application.* New York: Springer-Verlag, 1967.

[21] A. B. Yu, *et al.*, "On the modelling of the packing of fine particles," *Powder Technology,* vol. 92, pp. 185-194, 1997.

[22] K. L. Johnson, "Contact mechanics," *Cambridge University, Cambridge,* 1995.

[23] D. J. Bergman, "Electrical transport properties near a classical conductivity or percolation threshold," *Physica A: Statistical Mechanics and its Applications,* vol. 157, pp. 72-88, 1989.

[24] M. Sahimi, "Flow phenomena in rocks - from continuum models to fractals, percolation, cellular-automata, and simulated annealing," *Reviews of Modern Physics,* vol. 65, pp. 1393-1534, Oct 1993.

[25] K. McLean and R. Kahane, "Electrical performance diagram for a pilot scale electrostatic precipitator," *Proceedings of the International Clean Air Conference,* p. 207, 1978.

[26] A. M. Yuen, "Collector current density and dust collection in wire-plate electrostatic precipitators," Ph.D thesis, School of Materials Science and Engineering, University of New South Wales, 2006.

CHAPTER 7. CONCLUSIONS AND OUTLOOK

7.1. Conclusions

In summary, we have successfully developed a numerical model based on the discrete element method to simulate packings of fine particles under various electric fields. In our simulations, the electric-field-induced electrostatic interactions are included, and simulation conditions are set to the electrical conditions found in industrial electrostatic precipitation processes. Our results have demonstrated that two key parameters influencing the structure of the formed packings are the particle diameter and electric field. Changes in the structures with these two parameters are analysed in terms of the packing fraction, coordination number, radial distribution function, and Voronoi cell properties. Moreover, the forces exerting on each particle in the packings are analysed in detail, which is usually difficult to measure in practical experiments. The results highlight the importance of both the electric-field-induced electrostatic interactions and the interparticle van der Waals interactions in the formed packings under electric fields.

Furthermore, various packings of particles under a range of non-uniform electric fields have been investigated using the proposed discrete element method. In particular, we focus on the elliptical-shaped non-uniform electric fields commonly found in electrostatic precipitation processes, and for the first time, the elliptical-shaped packing structures observed in this processes have been successfully reproduced in numerical simulations. Our results show that non-uniform electric fields produce the non-uniform packing structures that have the same shape as the imposed electric field. In general, strong electric fields result in dense packing structures, while opposites result in loose structures. Also, the detailed structural analysis in the localised regions of the non-uniform packing structures has revealed that the local structural properties, such as packing fraction and coordination number, are determined by the imposed electric fields in the localised regions. When a localised region is small enough to assume a quasi-uniform electric field is imposed in the region, we are able to use the previously established relations on the packing fraction and coordination number to describe the formed packing structures. The findings may lead to better controls of the structure of a formed packing under an imposed electric field, which, in turn, result in improved electrical transport properties of the packing.

In addition, we have developed a novel numerical approach to evaluate the effective electrical conductivity of the formed packings under electric fields, in which electric current is mainly conducted through the interconnecting solid particles. This is the electrical condition frequently encountered in electrostatic precipitation processes, where the conductivity of the particles is much greater than that of the interstitial gases. In our numerical approach, the electrical potential and current on every single particle in a packing are explicitly solved so that its effective electrical conductivity can be determined. The results have demonstrated that the material properties of particles, the contact area between the particles and packing structure can all influence the effective conductivity. Also, the force analysis on the particles has revealed the similarity between contact force networks and electric current networks. These findings highlights that the electrostatic and van der Waals interactions on particles have particular significance for the formed packings under electric fields.

In the last part of this thesis, two mathematical models predicting the effective electrical conductivity of the formed packings under electric fields are presented. Microscopic characters of a packing, e.g., coordination number, contact diameter, are required in the previously established models for effective conductivity. To apply these models to the packings found in electrostatic precipitation processes is difficult due to the microscopic characters are not available in practical experiments. In this work, we use the controllable parameters of a packing in industrial applications, such as the particle diameter, electric field and packing depth, to express the microscopic characters and subsequently the effective electrical conductivity. Firstly, we have developed an explicit form of the previous established model for effective conductivities in terms of the controllable parameters. The results demonstrate that the previous model is inadequate to predict the effective conductivity of the packing with loose structures. To overcome this problem, we have proposed two models based on the previously established model (see Eq.6.21 and Eq.6.23). Both empirical and modified models give better predictions for the effective conductivity of the formed packings under electric fields. The findings may lead to improvements on the design and operations of electrostatic precipitation processes.

7.2. Future research

The effect of multiple particle size should be explored in future studies on the packing of particles under electric fields. Although the shape of the fine particles is spherical in electrostatic precipitation processes, the size of the particles is not identical. Combustion of coal produces solid residues in pulverised coal-fuel power stations. 20% of the solid residues are bottom ashes that are collected at the bottom of furnace, while the other 80% are emitted in the form of fine particles [1]. Burning process and coal properties determine the size distribution of the fine particles. In practical experiments, lognormal distribution functions are often applied to describe the particle size distribution [2, 3]. Probability density function of lognormal distribution is,

$$P(x) = \frac{1}{x\sigma\sqrt{2\pi}} \exp\left(- \frac{(\ln(x) - \mu)^2}{2\sigma^2} \right)$$

where μ and σ are respectively the mean and standard deviation. For example, a lognormal distribution function and the corresponding formed pakcing made of ten representative components are depicted in Figure 7.1. It is expected that the mean and standard deviation of lognormal distribution functions will affect the packing structures and electrical transport properties of the packings. Also, fly ash particles commonly found in electrostatic precipitation processes are generally spherical, the problem of non-spherical particle packing and electrical conduction could be another important research topic. And in this thesis, because the simulated zone is close to the collection plate where the gas flow is weak, the effect of gas flow is not considered. However, to simulate the particle motion in the industrial electrostatic precipitation processes, the gas flow should be modelled along with the particle dynamics, which is also a recommended future research component. Currently, we have attempted to simulate the gas flow using computational fluid dynamics [4]. The combination of the discrete element method and the computational fluid dynamics could be a very promising direction of research. In this thesis, as the simulated zone is close to the collection plate where the gas flow is weak, the effect of gas flow is not considered in the model.

In addition, the effect of gas flow in electrostatic precipitation processes is another important factor is yet to included in our simulation. Currently, we have attempted to simulate the gas flow using computational fluid dynamics [4]. The combination of the discrete element method and the computational fluid dynamics could be a very promising direction of research.

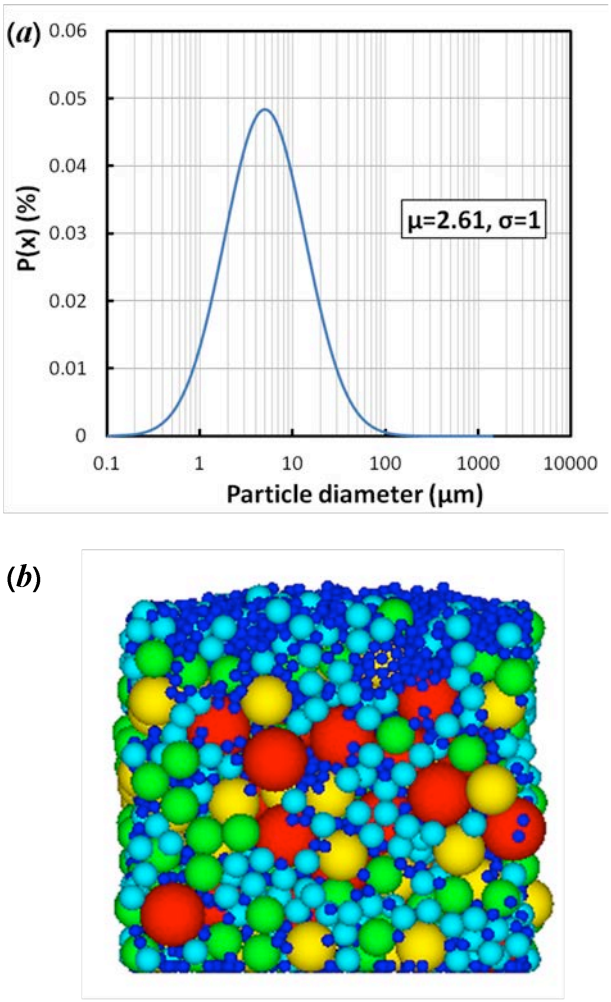

Figure 7.1: (a) A typical lognormal distribution function, and (b) the corresponding formed packing made of multi-sized particles.

References

[1] J. Jankowski, *et al.*, "Mobility of trace elements from selected Australian fly ashes and its potential impact on aquatic ecosystems," *Fuel,* vol. 85, pp. 243-256, 2006.

[2] M. W. McElroy, *et al.*, "Size distribution of fine particles from coal combustion," *Science,* vol. 215, pp. 13-19, 1982.

[3] R. Barranco, *et al.*, "The impact of fly ash resistivity and carbon content on electrostatic precipitator performance," *Fuel,* vol. 86, pp. 2521-2527, 2007.

[4] B. Guo, *et al.*, "Toward the development of an integrated multiscale model for electrostatic precipitation", *Ind. & Eng. Chem. Res.*, vol. 52, pp 11282-11293, 2014.

APPENDIX I. GRAPH THEORY

The graph theory is applied to solve electrical conditions on every particle in a random packing [1]. A graph consists of nodes and edges that respectively represent particle centres and the contacts between particles. The nodes and edges can be expressed in a matrix form **A**, which is referred to an incidence matrix of the graph. We can write the voltage on every node in a column vector **u**, and similar the conductance on every node in **c**. The incidence matrix is particularly useful. For example, the potential difference between each pair of particles **e** is found by **e**=**Au**. Another example is the electric current between each pair of particles is expressed as **w**=**ce**. It should be noted that we need n-1 equations and boundary conditions to solve for the voltage on every node **u**. Here, the Kirchhoff's current law is applied to establish a set of linear equations. Kirchhoff's law states that the sum of electric current into and out of a node must be zero, and mathematically, it is given by,

$$\sum_j I_{ij} = 0$$

Or in a matrix form,

$$\mathbf{A}^{\mathbf{T}}\left(\mathbf{c}\left(\mathbf{Au}\right)\right) = 0$$

We have found that the Gauss-Seidel method is efficient in this case. Consequently, the electric current between each pair of particles is obtained from **w**=**c(Au)**.

References

[1] G. Strang, *Computational science and engineering*: Wellesley-Cambridge Press Wellesley, MA, 2007.